1-1-2018

Tumor Multicomponent Targeting Polymer-Lipid Hybrid Nanoparticles To Overcome Drug Resistance In Renal Cell Carcinoma

Hashem Obaid Alsaab
Wayne State University,

TUMOR MULTICOMPONENT TARGETING POLYMER-LIPID HYBRID NANOPARTICLES TO OVERCOME DRUG RESISTANCE IN RENAL CELL CARCINOMA

by

HASHEM OBAID ALSAAB

DISSERTATION

Submitted to the Graduate School

of Wayne State University,

Detroit, Michigan

in partial fulfillment of the requirements

for the degree of

DOCTOR OF PHILOSOPHY

2018

MAJOR: PHARMACEUTICAL SCIENCES

Approved By:

_____

Advisor Date

_____

_____

_____

DEDICATION

To my beloved parents, wife, children, and all family.

Thanks for being the most important people in my life.

ACKNOWLEDGMENTS

I would like to thank my advisor, my PhD committee members, funding sources, colleagues, friends, and family who have given me support and have helped make this Dissertation possible. First and foremost, I would like to acknowledge the family closest to me: my parents for their unconditional love and support. Their invaluable guidance provided the strength in my life and I hope to continue in their example. My father's wisdom and strict advice will always be remembered, and my mother's love and confidence continue to inspire me. I would like to acknowledge Zekra, my lovely wife, for being my best friend, my love, and my companion. Her words of encouragement and contribution in my life and work cannot be overstated. Without her support and sacrifice, none of this work would be possible. Also, I would like to thank my children, Shaima, Elias, and Bilal for always being there for me. Without your love, motivation and support, I could never have accomplished this work. I love you very much!! Also, I thank my three sisters for their love, support, and tolerance towards their little brother. Also, I wish to thank my brothers: Abdullah, Saad, and Mohammad. Thank you for your encouragement, love and being my support on whom I always can depend. Most of all, I would like to thank my advisor at Eugene Applebaum College of Pharmacy and Pharmaceutical Sciences at Wayne State University, Detroit, MI. I appreciate Dr. Arun K. Iyer for his patience, intellect, passion, and dissertation advice and, for giving me the opportunity to work in his lab and helping me to grow as a researcher; I also appreciate Dr. Iyer for his kindness, consideration, humor, brilliant ideas. I would also like to thank Dr. Arun K. Rishi for being as my external collaborator and mentor and being part of my PhD committee and for their scientific advice. I would also like to thank Dr. Fei Chen and Dr. Randall Commissaries: Thank you for your valuable courses and being in my PhD committee. Your advice and recommendations were helpful. Also, receiving so much support from you as my lab mates

especially Dr. Samaresh Sau, Dr. Rami Alzhrani, and Dr. Vino Cheriyan gives me more incentive to maintain a high personal standard for my academic success. This degree means I had a lot of supporters and I have achieved my goals so far. I would like to thank Eugene Applebaum College of Pharmacy and Pharmaceutical Sciences program members and professors for their help and support. Thank you for Dr. Zhi Mei for the much-needed assistance with the TEM instrument. Thank you for your patience and willingness to help. TEM analysis using JEOL 2010 was supported by an NSF Award#0216084. Also, I would like to acknowledge the Karmanos Cancer Institute and the Molecular Imaging Program for access to its Core facilities. The Biobanking and Correlative Sciences Core is supported, in part, by NIH Center grant P30 CA022453 to the Karmanos Cancer Institute at Wayne State University. I would like to thank Dr. Lisa Polin for her support with animal work and her input in analyzing the results. I would like to thank my funding sources: Saudi Arabian Cultural Mission (SACM), Ministry of Education in Saudi Arabia and College of Pharmacy at Taif University, Saudi Arabia. Thank you for providing me the scholarship and funds to complete my Master's and PhD degrees. I would like also to thank those past and present members of our lab especially, Dr. Prashant Kesharwani, Dr. Rahul Deshmukh, Ketki Bhaise, Duy Luong, Ghazal Nabil, Zhaoxian Wang, Shaimaa M. Yuosef. Kaustubh A. Gawde, Katyayni Tatitparti, and Alex Petrovici who have helped me in my research and for being such great colleagues and friends. I would like to thank all my friends, my classmates for their constant moral support, suggestions, ideas, and their thoughtful discussions. My friends who are really the most important thing in life. Thank you for being there for me and supporting me through all these challenges. I truly have been blessed to have friends like you. I have enjoyed their presence so much during my stay at WSU. I would like to thank all those who made my stay at WSU an unforgettable and rewarding experience.

TABLE OF CONTENTS

LIST OF TABLES

LIST OF FIGURES

LIST OF ABBREVIATIONS

ANOVA, Analysis of Variance

ATCC, American Type Culture Collection

CARP-1/ CCAR1 Cell, cycle and apoptosis regulator 1

CD, Cluster of Differentiation

CTC, Circulating Tumor Cell

CTLA-4, Cytotoxic T Lymphocyte Associated Protein 4

DMEM, Dulbecco's Modified Eagle's Medium

DNA, Dioxyribonucleic Acid

EDTA, Ethylenediaminetetraacetic Acid

ERBB3, Epidermal Growth Factor Receptor Tyrosine Kinase 3

ERBB4, Epidermal Growth Factor Receptor Tyrosine Kinase 4

FBS, Fetal Bovine Serum

FDA, Food and Drug Administration

FFPE, Formalin-Fixed, Paraffin-Embedded

HEPES, 4-(2-Hydroxyethyl)-1-Piperazineethanesulfonic acid

HepG2, Hepatocellular Carcinoma G2 Cells

HPLC, High Performance Liquid Chromatography

IFN-α, Interferon Alpha

IFN-γ, Interferon Gamma

IHC, Immunohistochemistry

IL-10, Interleukin 10

IL-2, Interleukin 2

IU, International Unit

LC/MS, Liquid Chromatography/Mass Spectrometry

LPS, Lipopolysaccharide

MAPK, Mitogen-Activated Protein Kinase

MeOH, Methanol

MHC, Major Histocompatibility Complex

mRNA, Messenger Ribonucleic Acid

mTOR, Mammalian Target of Rapamycin

NK, Natural Killer

PARP, Poly ADP-Ribose Polymerase

PBL, Peripheral Blood Lymphocyte

PBS, Phosphate-Buffered Saline

PD-1, Programmed Death Protein 1

PD-L1, Programmed Death Ligand 1

PI3K, Phosphoinositide 3-Kinase

P/S, Penicillin/Streptomycin

PCR, Polymerase Chain Reaction

RCC, Renal Cell Carcinoma

RNA, Ribonucleic Acid

RPMI, Roswell Park Memorial Institute Medium

TAM, Tumor Associated Macrophage

TBS-T, Tris-Buffered Saline Tween-20

TGF-β, Transforming Growth Factor Beta

TNBC, Triple Negative Breast Cancer

TNF-α, Tumor Necrosis Factor Alpha

Treg, T Regulatory

UHPLC-MS, Ultra-High-Performance Liquid Chromatography Tandem

Mass-Spectrometry

1. CHAPTER 1: LITERATURE REVIEW

1.1.Renal Cell Carcinoma (RCC)

Urologic malignancies of the kidney are responsible for 1.62 % of all cancer deaths in the United States [2]. Also, an age-adjusted incidence rates have elevated approximately 2-3% annually over the past 30 years [3–6]. In 2018, there will be an estimated 65,340 new cases of RCC and over 14,970 deaths [7]. Kidney cancer incidence increased from 1997 to 2008 before leveling off [8]. The increase in incidence since late 1990s reflects a rapid increase in early stage disease that has been associated in part with incidental diagnosis during abdominal imaging and may not represent a real increase in cancer occurrence [9]. The overall mortality rate has fallen an average of 0.6 percent each year since 2001 as shown in Figure 1.1. The expected RCC incidence and mortality rates in 2018 are double as high in men (42,680 cases) versus women (22,660 cases) [7]. Kidney cancer is now the 6th highest occurring cancer in the US and has been continually increasing with over 14,970 patients expected to die from this disease in 2018 [7]. The fivefold rise in incidence is because of many factors, such as smoking, obesity, exposure to some environmental agents, renal failure, and hypertension. The advances in detection technology are likely a result of the widespread utilization of sensitive imaging such as ultrasonography and computed tomography (CT) for diagnosis of abdominal or gastrointestinal complaints[8].

The most common cancer of the kidney with 72% of all cases is the renal cell carcinoma (RCC). RCC is heterogeneous in nature and progression of the disease has been difficult to monitor despite the existence of prognostic scoring systems based on conventional clinical and pathological indices [10]. RCC is derived from renal tubular epithelial cells and considered as one of the ten highest common cancers worldwide [11,12]. RCC is lethal urologic malignancy as approximately third of patients would have developed visceral metastasis during the diagnosis and half of the

remaining patients would eventually progress to distant metastases [13]. Survival data of a population-based cancer indicated that more than 40% of patients with RCC would die from the disease [14–16], in comparison with bladder and prostate cancers which have approximately half the mortality rates [17–20].

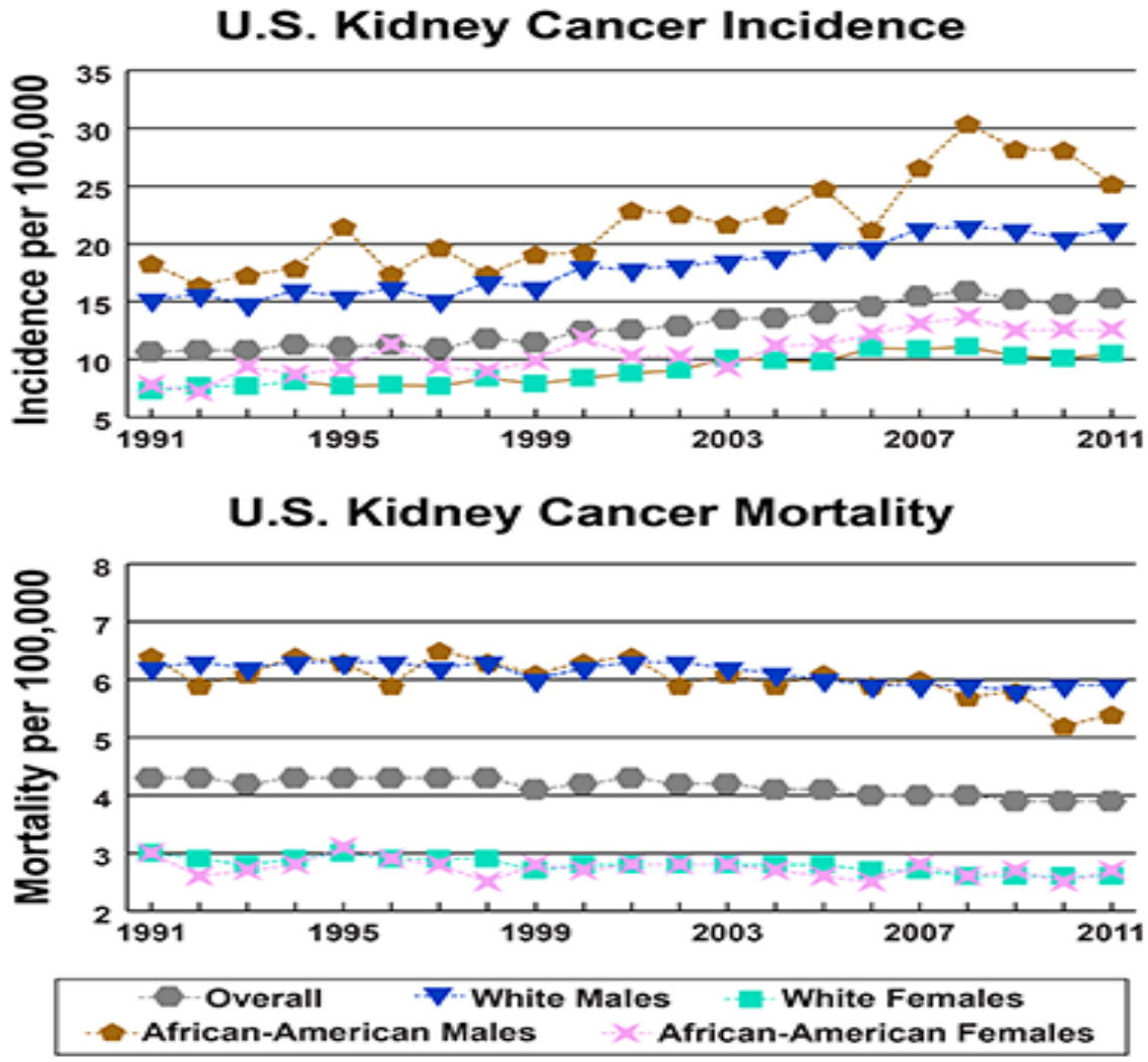

Figure 1.1. US kidney cancer incidence and mortality. Estimated age-standardized rates of incidence for both sexes (per 100,000 people) between 1990-2011. Rates are generally higher in males with the higher mortality rates. Reproduced with permission from Surveillance, Epidemiology, and End Results (SEER) Program and the National Center for Health Statistics.

1.1.1. Histological Types of RCCs

since 1990s, significant efforts from researchers and clinicians have been devoted to promoting the understanding of how molecular genetics drive RCC pathogenesis. The advancement of research in the histopathological and molecular characterization of RCC disease over the past few years have resulted into major revisions in its subtype classification [11,12,21,22]. RCC is a heterogeneous malignancy and involves many different histological subtypes [23], each of which is distinguished from the other subtypes by the (i) location of the renal tubular epithelium from which it originates, (ii) the genetic mutations involved in its occurrence, and (iii) the particular clinical options and outcome of the disease [24,25] as shown in Table 1.1. As shown in Figure 1.2 , Primary RCC subtypes with ≥5% incidence are clear cell RCC (ccRCC) , papillary RCC (pRCC), and Chromophobe RCC (chRCC) [26]. Along with ccRCC, other recognized histological sub-classifications are Type 1 (5%) and Type 2 (10%) papillary RCC, chromophobe tumors (4-5%) and collecting duct/medullary cell tumors (<1%) as shown in Figure 1.2 [21,27]. The other subtypes are very rare (each with total incidence ≤1%) [22]. Also, other known familial syndromes that might lead to renal tumors have been identified alongside RCC that arise sporadically. These hereditary subtypes of RCC have a meager rate (approximately 5%) of occurrence and that involve: (i) Von Hippel-Lindau (VHL) disease; (ii) hereditary papillary renal cell carcinoma (HPRC); (iii) hereditary leiomyomatosis renal cancer (HLRC); and (iv) Birt-Hogg-Dube (BHD) syndrome [28]. Each genetic subtype has characteristic molecular changes, which are often indicated development of specific histopathological features [29]. Molecular genetic understanding of hereditary cases contributes a significant insight into the molecular mechanisms causing cancer initiation and progression. This knowledge particularly would improve the

understanding of sporadic RCC and can possibly be converted into the more promising therapeutic approach for RCC.

1.1.2. Clear Cell Renal Cell Carcinoma

Clear cell RCC is the most common class, and the majority of deaths from kidney cancer are from this type, and ccRCC will be the focus of this Dissertation [30]. Indeed, considering the predominance of ccRCC histological manifestations in metastatic disease (83–88%) [31,32], tumors with non-clear cell histology have been named as non-clear renal cell carcinoma 'nccRCC' (Table 1.1) [33–35]. Likewise, recent cancer genome reports have explained an apparent complexity of intra-tumor [36–38] and inter-tumor [27,39] heterogeneity in ccRCC, which could contribute to the heterogeneous clinical outcomes observed [21,28,40]. Approximately 75% of all clear cell RCC is correlated with the inactivating VHL gene mutation. Papillary RCC often correlated with the activation of the Met proto-oncogene and chromosome trisomy while the other histological types do not have well-defined genetic mutation. Table 1.1 and Figure 1.2 provide a summary of tumor suppressor genes and oncogenes that might be the leading cause for development of familial and sporadic RCC [23,41–44]. Recently, five new frequently mutated genes associated with the clear cell RCC were identified. These genes encode four other proteins; KDM6A/UTX, SETD2, KDM5C/JARID1C and MLL229 which are essential for the methylation and demethylation process of histone residues and consequently control gene transcription.

Table 1.1. Classification of renal cell carcinoma (RCC) and their associated molecular alterations in hereditary syndromes associated with renal cell carcinoma. Adapted with permission from [8].

Syndrome (phenotype OMIM reference)	Gene (position)	Protein	Incidence of developing a kidney tumor (%)	Median age at diagnosis (years)	Other phenotypic features
Clear cell renal cell carcinoma*					

von Hippel–Lindau disease (193300)	*VHL* (3p25–26)	pVHL	25–45	40	Hemangioblastoma Pancreatic neuroendocrine tumors Pheochromocytoma Renal Cysts Pancreatic Cysts Ovary cystadenoma Epididymal cystadenoma
BAP1 mutant disease (also known as tumor predisposition disease; 614327)	*BAP1* (3p21)	BRCA-associated protein	No data	No data	Breast cancer Uveal melanoma Mesothelioma Other cutaneous melanocytic tumors
SDH-associated kidney cancer (185470, 602413, 602690 and 115310)	*SDHB* (1p36), *SDHC* (1q23) and *SDHD* (11q23)	Succinate dehydrogenase subunits B, C and D	5–15	30	Paraganglioma Carotid body tumors Pheochromocytoma Gastrointestinal stromal tumor
Papillary renal cell carcinoma					
Hereditary leiomyomatosis and renal cell cancer (150800) ‡	*FH* (1q43)	Fumarate hydratase	2–21	46	Uterine leiomyosarcomas Breast cancer Bladder cancer Cutaneous leiomyomas Uterine leiomyomas
Hereditary papillary kidney cancer (605074) §	*MET* (7q31)	Hepatocyte growth factor receptor	No data	<60	No additional features
Multiple tumor types					
Birt–Hogg–Dubé syndrome (135150)‖	*FLCN* (17p11.2)	Folliculin	34	50	Fibrofolliculomas and trichodiscomas Pulmonary cysts Pneumothorax

Tuberous sclerosis complex (191100 and 191092) ¶	*TSC1* (9q34) and *TSC2* (16p13)	Hamartin and tuberin	2–4	30	Subependymal giant cell astrocytomas Angiomyolipomas Renal Cysts Facial angiofibroma Ungual and periungual fibromas Hypomelanotic macule Forehead plaque Cardiac rhabdomyomas Connective tissue naevus
Cowden syndrome (also known as multiple hamartoma syndrome; 158350) #	*PTEN* (10q23)	Phosphatase and tensin homologue	34	40	Breast cancer Endometrial cancer Thyroid cancer Prostate cancer Macrocephaly Intestinal hamartomatous polyps Benign skin tumors (multiple trichilemmomas, papillomatous papules, and acral keratoses) Dysplastic gangliocytoma of the cerebellum
Hyperparathyroidism jaw tumor syndrome (145001) **	*HRPT2* (1q31)	Parafibromin	No data	No data	Parathyroid carcinomas Uterine carcinomas Renal cysts and hamartomas Hyperparathyroidism Parathyroid gland tumors Jaw fibromas

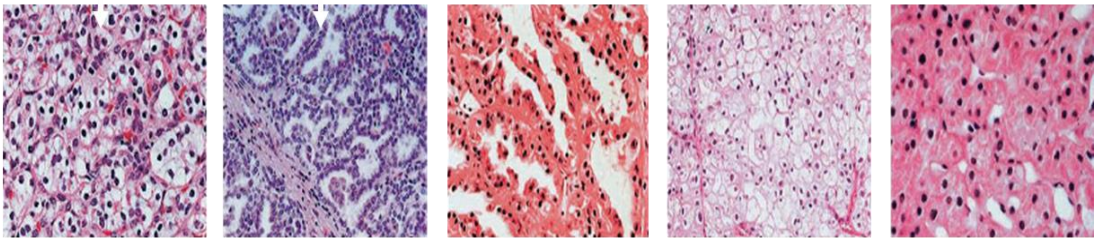

Type	Clear cell	Papillary type 1	Papillary type 2	Chromophobe	Oncocytoma
Incidence (%)	*75%*	*5%*	*10%*	*5%*	*5%*
Associated mutations	*VHL*	*c-Met*	*FH*	*BHD*	*BHD*

Figure 1.2. Distinct subtypes and distribution of common histological subtypes of renal cell carcinoma (RCCs). Different types of RCC have different histology and clinical courses and caused by a different gene profiles. Tumors are accompanied with a significantly poorer prognosis. BHD=Birt-Hogg-Dubé; FH=fumarate hydratase; VHL=von Hippel-Lindau. Approximately 75% of RCCs are clear cell RCC. Papillary RCCs make up ~15% of all kidney Cancers and are divided into two types based on staining features: type 1 (basophilic) and type 2 (eosinophilic). Chromophobe RCCs make up ~5% of kidney tumors. Additional minor subtypes include medullary RCC, clear cell papillary RCC, acquired cystic disease-associated RCC, tubulocystic RCC, mucinous tubular and spindle RCC, succinate dehydrogenase-deficient RCC, hereditary leiomyomatosis, RCC-associated RCC, and Oncocytoma. Tumors not fitting into any of these categories are designated as unclassified RCC. Adapted from [25].

1.1.3. Clear Cell-RCC and Von Hippel-Lindau (VHL) Gene Mutation

The most common form of RCC (more than 95%) is clear cell RCC (ccRCC). The mutation and inactivation of tumor suppressor VHL gene is frequently presented in this malignancy. The VHL gene is positioned on chromosome 3p25-26 and composed of three exons [35,38,45]. It yields 2 transcripts that translate to three proteins (pVHL). The common product (VHL30) is made up of 213 amino acids with a molecular weight of approximately 24 to 30 kDa [46]. A second isoform of pVHL (VHL19) contains 160 amino acids and is approximately 19 kDa [47–50]. The two isoforms show tumor suppressor activity. Exon 2 is not existed in the second mRNA transcript due to another splicing and has been recognized to encode a defective protein with no tumor suppressor activity [51]. Studies had shown that pVHL locates between the nucleus and cytoplasm [52–55] and

VHL30 is located mainly in the cytoplasm; however, VHL19 is located mainly inside the nucleus, revealing that the activities of both isoforms might overlap but are not similar [48,55].

1.1.3.1. Functions of VHL

The function of VHL and the ability to regulate and control protein expression at the post-transcriptional level has been studied extensively. VHL works as substrate recognition component of an E3 ubiquitin ligase complex and it forms a stable complex and functions as a binding and substrate recognition component [56,57] for the ubiquitination of targeted proteins. As a result, covalent binding of polyubiquitin residues onto the specific site of substrate protein promotes proteasomal degradation of the target protein [58]. For example, ligase-E3 complex ubiquitylates HIF1α and HIF2α for proteasome-mediated degradation [59–61]. As shown in Figure 1.3, both HIF-1α and HIF-1β subunits which are the heterodimeric HIF-1 are a sequence-specific DNA-binding transcription factor [62,63]. The modulation of the expression of HIF-1α regulates the transcription function of HIF-1 as the subunit HIF-1β is expressed genetically in cells [64]. The HIF subunits respond to changes in oxygen in the cellular environment and are unstable in normoxic microenvironments. Under normoxic conditions, the highly conserved proline residues inside the oxygen-dependent degradation (ODD) domain of HIF-1α subunit are hydroxylated [65–68]. The asparagine sites at the COOH-terminal transactivation domain (CAD) of HIF-1α are further hydroxylated by an enzyme called asparaginyl hydroxylase, Factor Inhibiting HIF1 (FIH-1) [69]. Hydroxylation of HIF-1α by FIH-1 inhibits the association of HIFs with the transcriptional coactivator CREB-binding protein (CBP)/p300; therefore, suppressing transcription activation. Alternately, HIF-1 binds to the β domain of pVHL, goes through polyubiquitination and subsequent degradation by the proteasome [70–72]. Under hypoxic conditions, the pVHL-HIF interaction is disordered due to the lack of oxygen-dependent hydroxylation of particular proline

and asparagine residues on HIF-1α; as a result, leading to active stabilization and translocation of HIF-1 to the nucleus. The HIF-1 complex binds to hypoxia response elements (HREs) in the target gene promoter origins and activates transcription as shown in Figure 1.3.

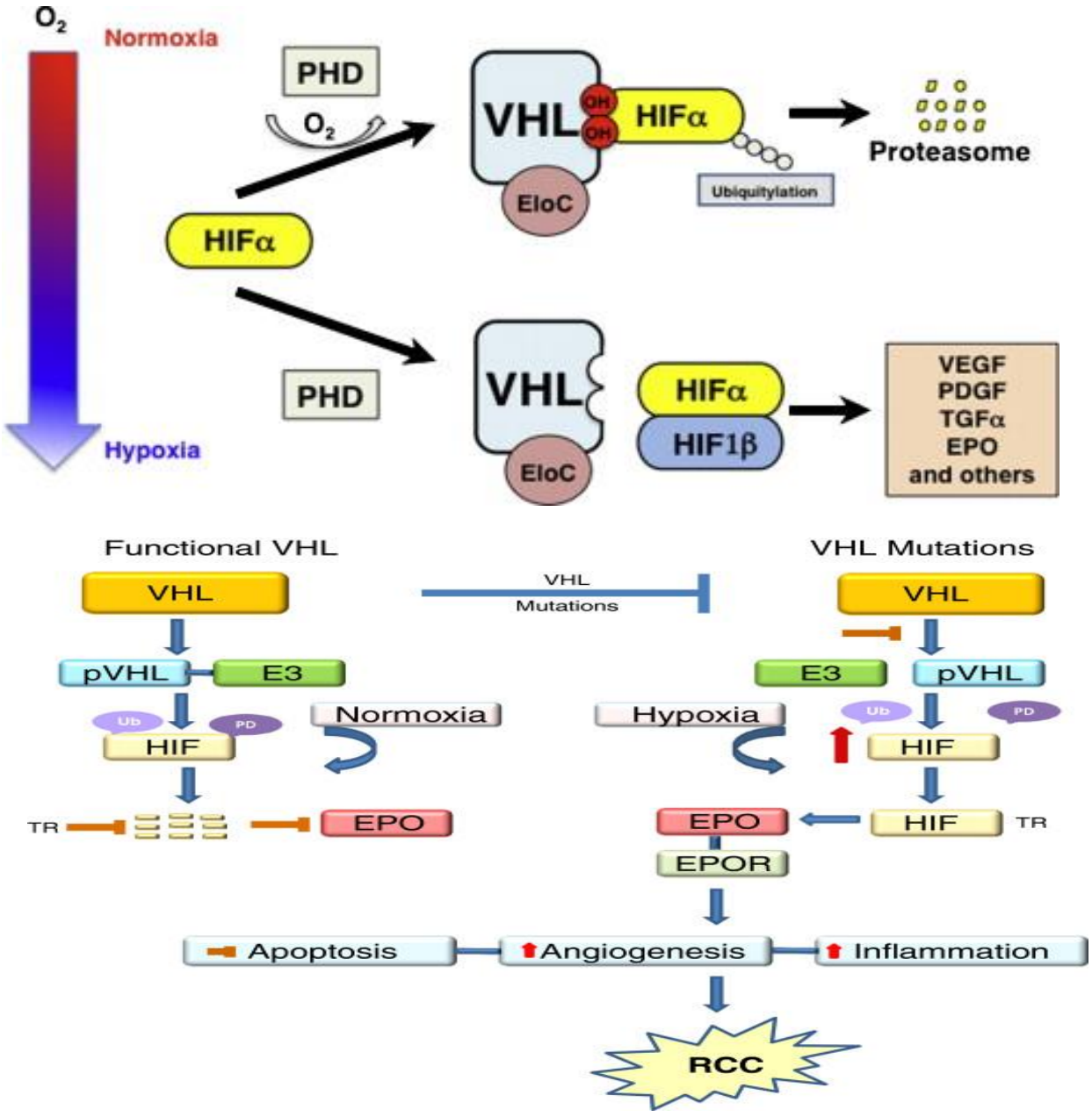

Figure 1.3. **Schematic role of pVHL in Hypoxia-inducible factors (HIF) pathway**. pVHL is the crucial part of an ubiquitin ligase protein complex that involves elongin C (EloC) and other partners. Under normoxic conditions HIFα is hydroxylated on two proline residues by prolyl hydroxylase 2 (PHD2), then conjugates to pHVL that targets it for ubiquitylation and proteasomal degradation. Under hypoxic

condition, HIF 1α is stabilized, binds to HIF1β and lead to expression of several downstream genes including VEGF, PDGFβ, TGFα and EPO. pVHL/HIF oxygen sensing pathway. HIFs are transcription factors that are affected by the changes in available oxygen in the cellular microenvironment. In conditions of physiologic oxygen availability and normal VHL gene function, pVHL is the substrate recognition component of an ubiquitin ligase complex that targets HIFs for proteolysis. In conditions of cellular hypoxia, the pVHL-HIF interaction is disrupted due to the loss of oxygen-dependent hydroxylation of specific proline residues on HIF, thus leading to active stabilization and translocation of HIF to the nucleus. When the VHL gene is defective, this interaction is dysfunctional even in the presence of adequate oxygen. As such, HIF is not subjected to proteolysis and this leads to constitutive activation of the hypoxia response pathway and transcriptional activation of genes involved in tumor proliferation. Adapted with permission from [73].

1.1.3.2. VHL Inactivation

VHL has the mutations in α- and β- domain which is responsible for abrogation of protein binding and degradation because of malfunction in assembly of the VHL ubiquitin complex. In RCC, all familial VHL-related, and around 75% of occasional cases, harbor the biallelic VHL functional inactivation through lack of heterozygosity, promoter methylation or intragenic deletion [74–76]. Because of the malfunction of VHL gene, the interaction between VHL-HIF-1 becomes defective despite the presence of adequate oxygen. Intrinsically, HIF-1 is not required for proteolysis, and this induces consequent activation of the hypoxia responsive pathway and genes transcriptional activation associated with tumor proliferation. Genes linked to short-term hypoxic condition involve inducible nitric oxide synthase (iNOS) to amplify vasodilation, glycolytic enzymes to elevate glycolysis, glucose transporter-1 (GLUT-1) to have more glucose uptake, pyruvate dehydrogenase kinase (PDK1) to block mitochondrial respiration, and cyclin-dependent kinase inhibitors p21 and p27 to minimize cell proliferation. When cells lack functional VHL gene, chronic cellular adaption is attained via the help of hypoxic condition by promoting angiogenesis. These pro-angiogenic genes are majorly controlled by HIF and involve vascular endothelial growth factor (VEGF) and its receptors (VEGFR), platelet-derived growth factor (PDGF), and basic fibroblast growth factor (bFGF).

The tumor suppressor function of VHL regulates the activity of hypoxia-inducible factor (HIF). As a result, lack of VHL gene will lead to the abnormal accumulation of HIF proteins even insufficiently oxygenated tissue microenvironment, which consequently results in uncontrolled activation of HIF target genes that control angiogenesis, glycolysis and apoptosis (Figure. 1.3). Subsequently, human ccRCC tumors are rich in lipids and glycogens, and are greatly vascular [77,78] which makes anticancer agents that primarily block VEGF and its receptor VEGFR therapeutically active for metastatic ccRCC [33,34,79]. VHL loss alone however is inadequate to produce ccRCC, as demonstrated by the long latency (>30 years) in patients who harbor VHL mutations to develop ccRCC [80] and by the fact that lack of VHL in mice does not cause ccRCC [81]. These outcomes indicate that additional genetic and epigenetic events are apparently required for ccRCC to occur [82]. To recognize these events, large-scale RCC genomic research has thus far indicated multiple new prevalent mutations in ccRCC. Complete molecular characterization of more than 400 clear cell RCC tumors identified more than 19 genes with extensive mutations, some of which changed cell metabolism and correlated with poor survival, suggesting new opportunities for therapeutic targets [83].

1.1.4. Therapy Models of RCCs

RCC is tough to treat as the cells are largely resistant to many current therapies. Surgery continues to be the best treatment choice [8], although 20-30% of patients progress to develop metastatic disease. In case of early diagnosis, there is a high chance of the cancer going into remission but if the cancer does not respond to first-line therapies there are very limited secondary options [8,32,35,84,85]. The most important treatment for many years has been cytokine therapy with interferon alpha (IFN-αa) and interleukin-2 (IL-2). There has been a host of new FDA approved chemotherapeutic agents now approved for treatment of metastatic RCC including tyrosine kinase

inhibitors, mTOR inhibitors, and monoclonal antibodies [86]. Currently, FDA approved treatments for metastatic RCC include (i) tyrosine kinase inhibitors (TKIs) such as sorafenib, sunitinib, and cabozantinib; (ii) mammalian target of rapamycin (mTOR) inhibitors such as temsirolimus and everolimus; and (iii) immunotherapeutic agents as PD-1/PD-L1 inhibitors.

1.1.4.1.Surgery

In some early stages of RCC, surgery by radical nephrectomy remains the best treatment choice for localized RCC, provided tumors can be excised with an appropriate surgical margin. Under this stage, the prognosis is excellent and hence, it is considered as the "gold standard" among treatment models. The surgery involves early ligation of the renal vessels, removing the kidney outside the Gerota's fascia, with or without removing of the adrenal gland depending on tumor sites and invasiveness score [87,88]. Data and reports indicated that 5-year survival rate of 75% or more after radical nephrectomy for stage I tumors are achieved [89,90]. Even though, about third of the RCC cases that were treated with radical nephrectomy eventually experience a local recurrence or distant metastasis [91], with the incidence based on tumor stage and grade [92,93]. If the kidney cancer is contained within the kidney, the cancer can be surgically removed with robotic partial nephrectomy. This surgery cuts out the cancer, and saves 50-75% of the remaining kidney, which can function sufficiently to keep the patient off hemodialysis. As reported earlier, about third of cases exhibit visceral metastasis at diagnosis time [94]. The overall clinical prognosis differs from less than 1 year for approximately half of the cases to more than 5 years for 10% of the patients [95].

1.1.4.2.Chemotherapy and Radiotherapy

Treatment options for metastatic RCC are insufficient because it is unresponsive to usual chemotherapeutic agents and radiotherapies; therefore, it remains one of the most difficult tumors

to treat [96,97]. Over 30% of people who are diagnosed with renal cancers will have cancer spread outside the kidney to the lymph nodes or distant metastases. With new FDA approved chemotherapeutic agents now approved for treatment of metastatic RCC, the survival has still been low. Unfortunately, renal cancers cells are usually resistant to chemotherapy; therefore, chemo drugs are not a standard treatment option for RCC. Some chemo drugs, such as vinblastine, floxuridine, 5-fluorouracil (5-FU), capecitabine, and gemcitabine have been utilized and shown to benefit a small population of patients. Importantly, chemo is often only used for kidney cancer after targeted drugs and/or immunotherapy have already been tried and failed. In the last few years, cytokine-based immunotherapy using interleukin (IL)-2 or interferon (IFN)-α have been the only therapy that have shown efficacy for metastatic RCC cases. However, it is still unsatisfactory option as only a low percentage of patients (10-15%) respond to this treatment type but often with severe side effects [98–101].

1.1.4.3. Molecular targeted therapy for RCC

VHL inactivation leads to higher intracellular level of hypoxia-inducible factors 1α and 2α (HIF1α and HIF2α). The increased level of HIF-1α in RCC effectively regulates the tumorigenesis by secreting vascular endothelial growth factor (VEGF) and hepatocyte growth factor (HGF), modifying the cellular metabolism, inhibiting apoptosis pathway, acclimatizing to acidic pH, and up-regulating metastasis associated proteins. All these factors promote RCC to develop resistance against radiotherapy and conventional chemotherapy [2,32,85,102]. Several receptor tyrosine kinase inhibitors (RTKIs), mammalian target of rapamycin inhibitors (mTOR) and serine-threonine kinase (STK) inhibitors are clinically approved for treatment of RCC [2,32], although the benefit of overall progression-free survival continues to be very poor (5-year survival rate of <10%).Thus, there is an urgent need for targeted combination therapies with novel mechanisms [85]. RCC is

generally difficult to treat since the cancer cells are largely resistant to currently available therapies. When RCC fails to respond to first-line therapies there are very limited secondary options. For example, everolimus (inhibitor of mTOR) is the first drug that was recently developed as a secondary treatment option for resistant RCC. It is very clear that newer and more effective treatment strategies for RCC are needed. In patients with an advanced form of RCC, targeted therapies including the ones using Everolimus resulted in improved clinical outcomes. However, patients ultimately develop resistance to this targeted therapy as well [103].

It is known that the pVHL/HIF molecular pathway is a crucial factor in the pathogenesis of cc-RCC [104–106]. As previously also reported, biallelic VHL mutation or inactivation by methylation occurs in majority of cases (~75%) of sporadic clear cell RCC [74,75]. Importantly, multiple strategies are being investigated to target the various aspects of this hypoxic sensing pathway and its associated molecules and growth factors. One strategy which has proven to be highly effective is the activity of agents that specifically target angiogenesis. RCC is manifested with highly vascular nature in both the primary and metastatic origins of the disease. This is because of the continuous overexpression of pro-angiogenic factors, VEGF [107] and PDGF, which are the most important factor in RCC tumor angiogenesis. The molecular association between VHL, VEGF, and hypoxia signaling pathway in the biology of cc-RCC has revealed the angiogenesis pathway as an important therapeutic approach. Moreover, the introduction of agents that target angiogenesis has advanced the treatment strategies and effectively improvise the management of patients with metastatic RCC. Significant advantages to patients include management of the cancer, improvement in the quality of life and increase the overall duration of survival [101,108–110].

Now, there are more than six molecular targeted therapeutic agents that have been approved by the US Food and Drug Administration (FDA) for treatment of metastatic RCC. They are (i) tyrosine kinase inhibitors (TKIs); sunitinib, sorafenib, pazopanib, and cabozantinib which inhibit the tyrosine kinase activation domain of vascular endothelial growth factor receptor (VEGFR) and platelet-derived growth factor receptor (PDGFR), (ii) mammalian target of rapamycin (mTOR) inhibitors temsirolimus and everolimus, and (iii) a monoclonal VEGF antibody, bevacizumab in combination with IFN-α (Figure 1.4 and 1.5). A summary of the clinical efficacies of these approved therapeutic agents is listed in Table 1.3.

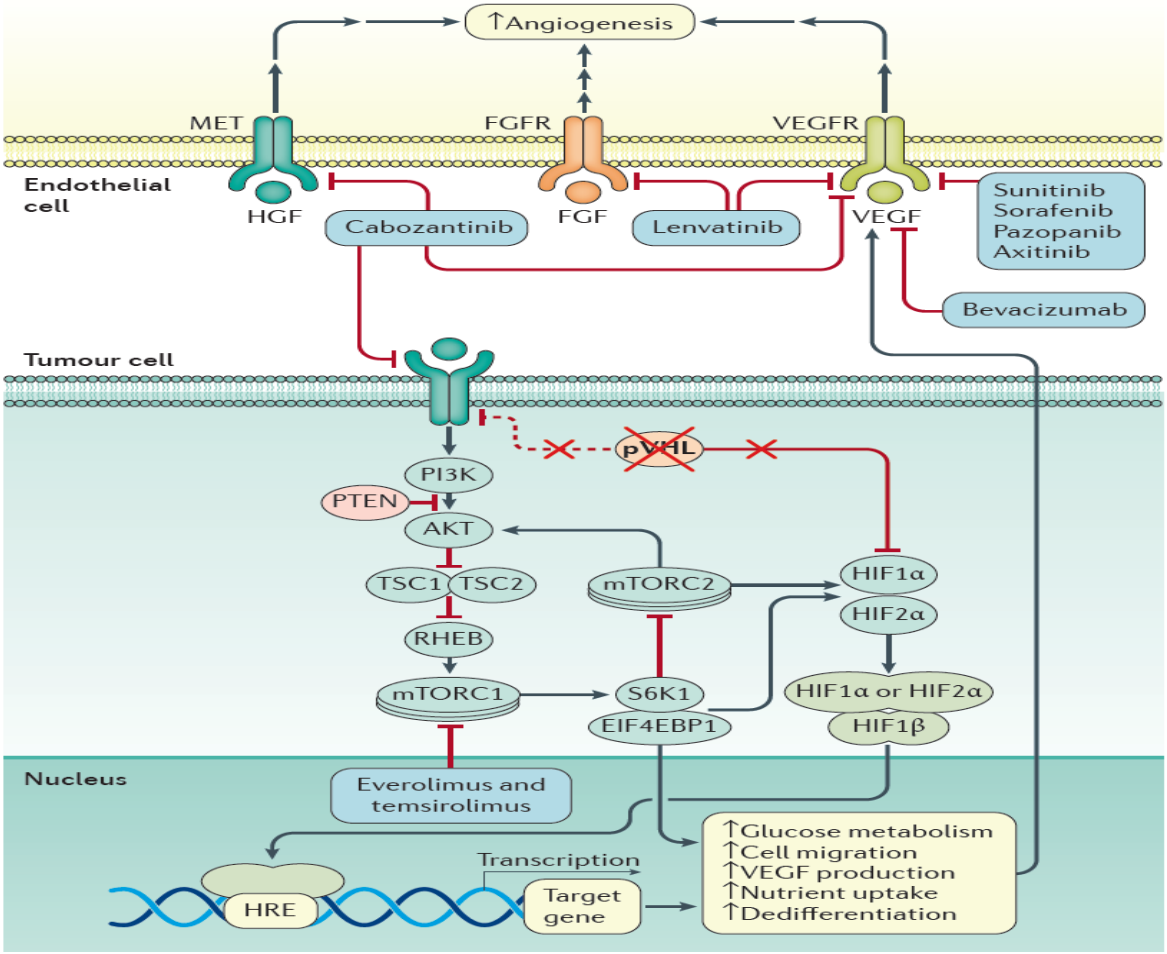

Figure 1.4. VHL inactivation in clear cell RCC and its implication in targeted therapy. Loss of VHL (which encodes pVHL) is the most frequent genetic feature of ccRCC. Its loss relieves the cell of negative regulation of the hypoxia-inducible factors (HIFs), which results in increased HIF target gene expression

and ensuing changes in cellular metabolism and signaling that enhance cell survival. For example, increased vascular endothelial growth factor (VEGF) expression increases angiogenesis in concert with increased growth factor signaling in endothelial cells in the tumor microenvironment (including fibroblast growth factor (FGF) and hepatocyte growth factor (HGF)). Consequently, these changes provide the targets for therapeutic agents to impede tumor growth, as shown. The dashed inhibitory line indicates indirect inhibition shown in limited reports. EIF4EBP1, eukaryotic translation initiation factor 4E-binding protein 1; FGFR, FGF receptor; HRE, HIF response element; MET, hepatocyte growth factor receptor; mTORC, mechanistic target of rapamycin complex; PI3K, phosphoinositide 3-kinase; PTEN, phosphatase and tensin homologue; RHEB, GTP-binding protein Rheb; S6K1, ribosomal protein S6 kinase; TSC, tuberous sclerosis complex; VEGFR, VEGF receptor. Adapted with permission from [8]

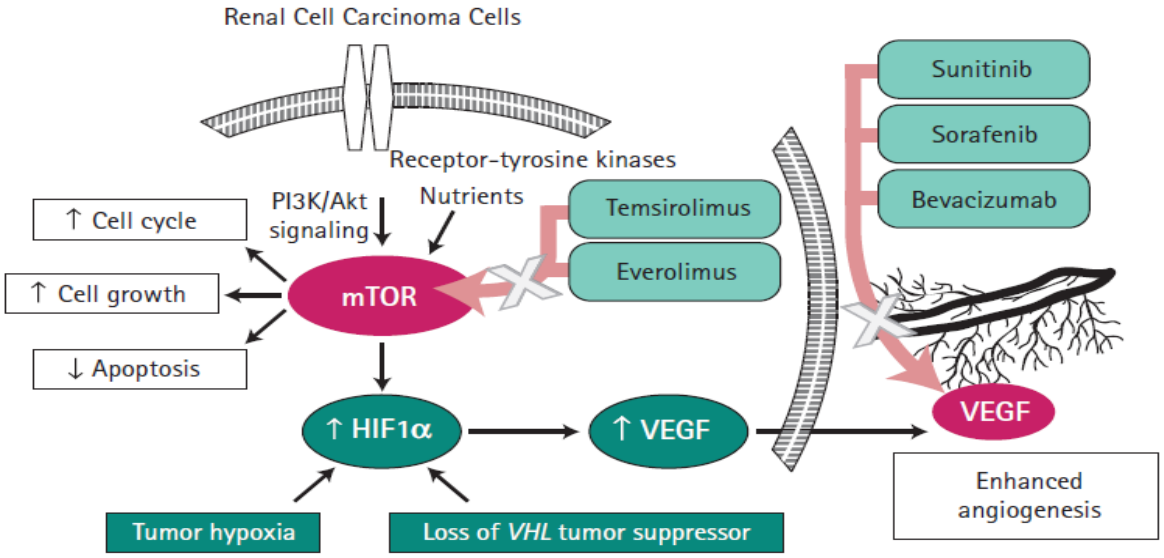

Figure 1.5. Selected current targeted therapies in metastatic RCC. Modified from [111].

1.1.4.4.Anti-Angiogenesis therapy

Antiangiogenic drugs that block the vascular endothelial growth factor receptor (VEGFR) pathway are now standard first-line treatment in metastatic RCC. They are also used sequentially to prolong clinical benefit in patients with recurrent disease [8,112,113]. However, resistance to therapy ultimately emerges in most patients, and further understanding of the underlying biology and potential therapeutic targets are urgently needed for clinical translation [8]. Everolimus is one such drug that was recently developed as a secondary treatment option for resistant RCCs [85,96,114].

However, resistance to newer drugs (including Everolimus) continues to emerge. Therefore, newer drug molecules with a different mechanism of action and novel targeted drug delivery approaches are needed to address the safety and efficacy of newer therapies. In addition, the introduction of several anticancer small molecule drugs (e.g., sunitinib, pazopanib, axitinib, temsirolimus, and everolimus) has rapidly changed the treatment of metastatic RCC [8,96,113]. Although the impact on RCC progression is encouraging, a substantial proportion of patients do not respond sufficiently, and resistance to therapy almost inevitably occurs [102]. Possibly combination treatments aimed at different, non-related pathways may be advantageous [85,115,116]. Due to their increase in vascular nature and high level of vascular permeability factor or vascular endothelial growth factor (VEGF) expression, ccRCC patients show promising success with anti-VEGF cancer therapy. Unfortunately, most of cancer patients ultimately develop a refractory response to anti-VEGFR treatment over time.

1.1.4.5.Immunotherapy for RCC

On November of 2015, the FDA approved Nivolumab (Opdivo®) for the treating of patients with advanced metastatic RCC and who already have received a specific prior anti-angiogenic cancer treatment. The FDA approval was based in part on an open-label, randomized clinical trial including 821 cases with advanced metastatic RCC. The trial included those whose disease status had deteriorated after or while on therapeutic plan with an anti-angiogenic medications. A certain percentage of cases received Nivolumab, while the rest took everolimus (Afinitor®). The Nivolumab group had an overall survival rate of more than 25 months compared to 19.6 months in Everolimus group. Furthermore, complete or partial tumor growth suppression lasting an average of 23 months was seen in 21.5% RCC patients of the Nivolumab treatment arm, compared to 13.7 months in 3.9% of the Everolimus treatment arm [117].

Table 1.2. (A) A summary of approved targeted therapies for metastatic RCC. Modified from Hutson et al., 2011. Adapted with permission. (B) Clinical trials leading to newly approved drugs for advanced renal cell carcinoma.

Agent	Year of Approval	Molecular Targets	Phase III Setting	Approval Basis
Interferon-alfa monotherapy	Not approved for RCC[a]			
High-dose interleukin-2 (Proleukin)	1992			
Sorafenib (Nexavar)	2005	VEGFR-2 RAF	Second-line vs placebo	PFS
Sunitinib (Sutent)	2006 2007	VEGFR-1,2,3	Second-line (cytokine-refratory) First-line vs interfeon-alfa	OFF PFS
Temsirolimus (Torisel)	2007	mTOR	FIrst-line	OS
Everolimus (Afinitor)	2009	mTOR	Second-line	PFS[4]
Bevacizumab (Avastin) (+ interferon-alfa 2a)	2009	VEGF	First-line	PFS
Pazopanib (Votrient)	2009	VEGFR	First-line	PFS

Name of the study	Type of study	Setting	n	Primary endpoint	Treatment arms	Median OS	Median PFS	ORR	Most common grade 3–4 AEs
METEOR trial	Phase III randomised open-label	Second-line or later-line after ≥1 VEGFR inhibitor	658	PFS	Cabozantinib (n=330)	21.4 months	7.4 months	21%	Hypertension (15%), diarrhoea (13%), fatigue (11%), PPES (8%)
					Everolimus (n=328)	16.5 months (HR 0.66, p=0.00026)	3.8 months (HR 0.58, p <0.001)	5% (p<0.001)	Anaemia (16%), fatigue (7%), hyperglycaemia (5%)
	Phase II randomised open-label	Second-line or later-line after ≥1 VEGFR inhibitor	153	PFS	Lenvatinib plus everolimus (n=51)	25.5 months	14.6 months	43%	Diarrhoea (20%), fatigue (14%), hypertension (14%), vomiting (8%), anaemia (8%)
					Lenvatinib (n=52)	19.1 months (HR 0.75, p=0.32)*	7.4 months (HR 0.66, p=0.12)*	27% (p=0.10)*	Proteinuria (19%), hypertension (17%), diarrhoea (12%), fatigue (8%)
					Everolimus (n=50)	15.4 months (HR 0.51, p=0.024)*	5.5 months (HR 0.40, p=0.0005)*	6% (p<0.0001)*	Anaemia (12%), dyspnoea (8%), hyperglycaemia (8%), hypertriglyceridaemia (8%)
CheckMate 025 trial	Phase III randomised open-label	Second-line or third-line after ≥1 VEGFR inhibitor	821	OS	Nivolumab (n=406)	25.0 months	4.6 months	25%	Fatigue (2%), anaemia (2%), diarrhoea (1%)
					Everolimus (n=397)	19.6 months (HR 0.73, p=0.002)	4.4 months (HR 0.88, p=0.11)	5% (p<0.001)	Anaemia (8%), hypertriglyceridaemia (5%), hyperglycaemia (4%)

*As compared with combination arm (lenvatinib plus everolimus).
AE, adverse events; ORR, objective response rate; OS, overall survival; PFS, progression-free survival; PPES, palmar-plantar erythrodysesthesia syndrome; VEGFR, vascular endothelial growth factor receptor.

1.1.5. Disadvantages and Limitations of Current Targeted Therapy

Despite the treatment advantages of agents targeting anti-angiogenic pathways, mostly 60% of the cases are non-responsive to these medications. Anti-angiogenic targeted agents are estimated to have less toxicity than conventional chemo and radiotherapy approach due to the higher dependence of cancerous cells on this pathway as compared to healthy cells. Also, they might cause significant side effects that need to minimize the dose; therefore, restricting its clinical utility and efficacy [118,119]. For instance, up to third of cancer patients on sorafenib needed dose reduction and of these, 50% stopped treatment because of the side effects. Another disadvantage of anti-angiogenic targeted therapy is that many active oncogenic pathways is mostly involved in oncogenesis. The utilization of a single treatment class will invariably stimulate tumor cell adaption by releasing higher amount of the many targeted growth factors. [120]. In view of the existing limitations of the current molecular single targeted therapy, sequential treatment with various targeted medications is advanced to be the standard strategy for the treatment. The efficacy of combination treatment strategy thus urgently need a better understanding of the biology of the cancer disease development, and mechanisms of action of the anticancer agents for effective utilization in combination.

1.1.6. Combinations and Sequential Treatment for RCC

Anticancer agents that are synergistic or additive would ensure higher inhibition of abnormal molecular target and their related signaling pathways. Moreover, combination therapy can bypass or hinder the development of resistance. In addition to finding molecular targets for RCC and anticancer agents that can work on these targets, another important need is to find a molecular biomarker that can predict therapeutic outcomes in RCC. Currently, classical clinical and pathologic indices provide reasonable evaluations of cancer patient response and disease

development [10] but are inadequate for patients' disease management given the heterogeneous nature of RCC. In essence, there is a crucial need for potential molecular biomarker which can be used to detect disease remission after therapeutic intervention and improve the accuracy of current prognostic indices. Also, the biomarkers will complement classical pathological and clinical indices utilized in monitoring tumor progression and the disease status. Therefore, the need for a suitable therapeutic target and an ideal molecular biomarker to predict responses of treatment in RCC remain critical and unmet need. Importantly, a patient-derived RCC xenograft or PDX model can be utilized for preclinical drug evaluation to find molecular targeted biomarkers capable of estimating therapeutic efficacy response to the new agents [121]. This approach will save time for finding new strategy and further pave the way into clinical translation.

1.2. Carbonic Anhydrase IX Targeting in Renal Cell Carcinoma

Carbonic anhydrase IX (CA IX) is a membrane-bound protein overexpressed on the surface of many cancer cells in a hypoxic environment [122]. Carbonic anhydrase enzymes tightly control the acid-base balance in the kidney [122]. CA IX is involved in tumor cell survival and metastasis, and increased expression correlates with poor clinical outcome. As shown in Figure 1.6 the over-expression of CA IX has been demonstrated in 93-97% of ccRCC with limited expression in normal tissues/organs [123]. Numerous studies have confirmed the CA IX distribution in normal tissues and malignancies [124–129]. For renal cancer, CA IX is almost homogeneously expressed in the ccRCC subtype [84,111,124–129]. Given the favorable tissue distribution, the potential of CA IX targeting of RCC for diagnosis or therapy has been studied extensively [130,131]. Due to the unique molecular basis of ccRCC, CA IX is regarded as an excellent target for diagnosis and possibly for therapy [111,126–128,132]. Clinical trials have unambiguously demonstrated that CA IX can be targeted in RCC tissues without damage to normal tissues[133,134] However, there are no approved therapies

against CA IX [135]. Monoclonal antibodies have been used to target CA IX, but their large molecular weight limits penetration throughout a poorly vascularized tumor and their slow blood clearance minimize their utilization as tumor imaging agents or radiotherapeutics because of high background and toxicity [134],[132]. Finally, the new therapeutic options have led to investigations that examine whether small molecule CA IX-inhibitors can be used in serum assays or as an imaging target to study whether CA IX monitoring can be useful to predict responses [127–129]. The future will show whether the conjugation of CA IX as a targeting moiety can be helpful in the treatment and clinical management of metastatic RCC.

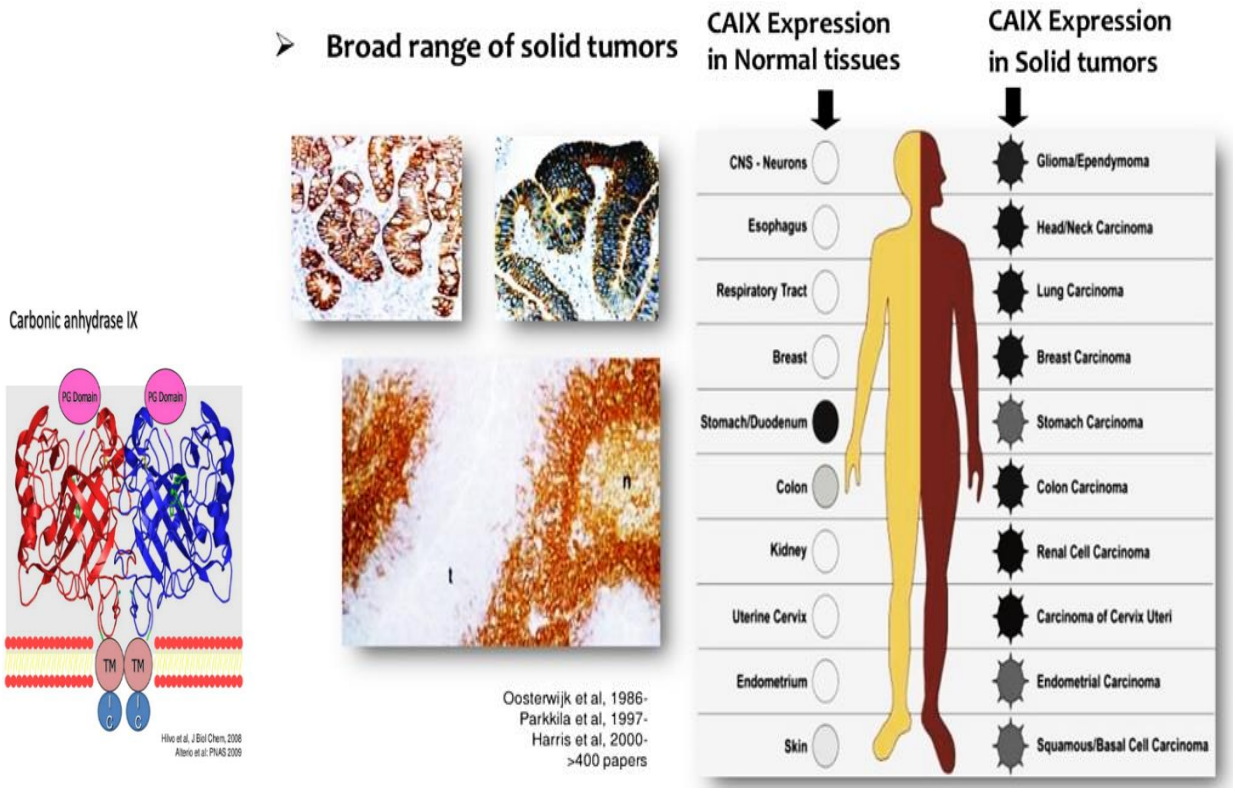

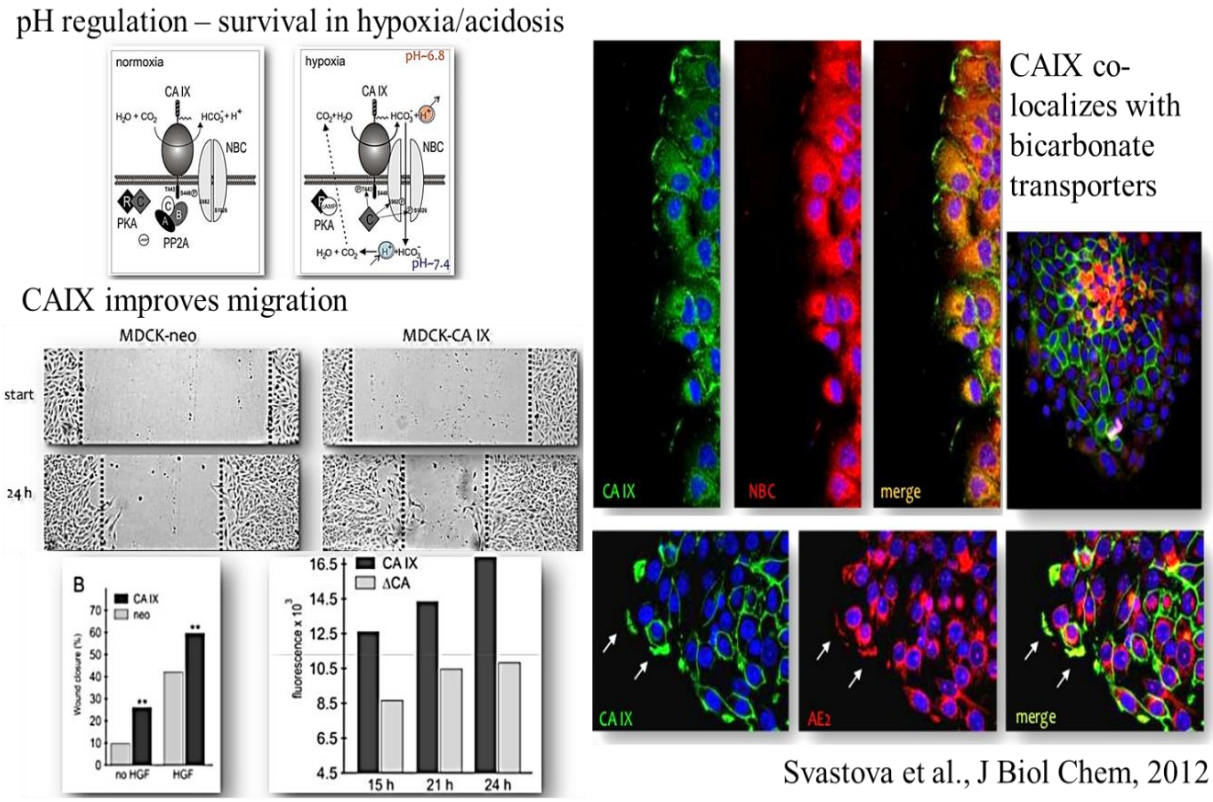

Figure 1.6. CA IX Expression and its role in cancer. Carbonic anhydrase IX (CA IX) which is a zinc containing metalloproteinase is efficiently catalyzes the reversible hydration of carbon dioxide. It is up-regulated in several cancer types. It has an important role in tumor progression, acidification and metastasis. Figures modified and adapted from many references as shown above [136].

1.3. CARP-1 Functional Mimetics as a promising molecule to target Everolimus Resistant Renal Cell Carcinoma Therapy

CARP-1 (Cell cycle and apoptosis regulator 1, aka CCAR1) is a peri-nuclear phospho-protein and a regulator of cell growth and apoptosis signaling CARP-1 (Cell cycle and apoptosis regulator 1, CCAR1) is a peri-nuclear phospho-protein and a regulator of cell growth and apoptosis signaling [137–140]. CARP-1 not only works as a transcriptional co-activator of steroid family of nuclear receptors and a regulator of adipogenesis through the glucocorticoid receptor (GR), it also regulates Adriamycin (ADR)-dependent apoptosis in part through co-activation of p53 [141,142]. CARP-1 expression is often elevated in cells experiencing stress due to growth factor withdrawal

or chemotherapy-induced cell cycle arrest and apoptosis [137,138,141]. Knockdown of CARP-1 resulted in resistance to apoptosis by ADR or EGFR tyrosine kinase inhibitors demonstrating the requirement of CARP-1 in cell growth inhibitory and apoptosis signaling by these agents [137,138,141]. CARP-1 as shown in Figure 1.7 also works as a co-activator of the APC/C E3 ligase [139]. APC/C is a multi-subunit ubiquitin E3 ligase protein that plays a distinct role in cell cycle transitions, and misregulation of APC/C substrates such as securin, polo-like kinase (Plk) has been demonstrated to correlate with tumor progression [143,144]. A chemical biology-based high-throughput screening of a chemical library resulted in the identification of some novel, small molecule inhibitors (SMIs) of CARP-1 binding with APC/C subunit APC2. These compounds, termed CARP-1 functional mimetic (CFMs), inhibit cell growth by inducing apoptosis in various cancer types as the NCI 60-panel screening indicated including non-small cell lung cancers (NSCLC), triple negative breast cancers (TNBC) and RCC [145]. Recently, a promising library of a novel class of anticancer compounds termed CARP-1 functional mimetics (CFMs) that inhibit cell growth by various mechanisms such as inducing apoptosis has been developed for resistant RCC. In the case of renal cell carcinoma (RCC), antiangiogenic drugs that block the vascular endothelial growth factor receptor (VEGFR) pathway are now standard first-line treatment in metastatic RCC. They are also used sequentially to prolong clinical benefit in patients with recurrent disease [30]. However, resistance to therapy ultimately emerges in most patients, and further understanding of the underlying biology and potential therapeutic targets are urgently needed for clinical translation [102]. Everolimus is one such drug that was recently developed as a secondary treatment option for resistant RCCs [96,114]. However, resistance to Everolimus continues to emerge. Therefore, newer drug molecules with a different mechanism of action and novel targeted drug delivery approaches need to be developed to address the safety and efficacy of newer therapies. Also, the molecular

complications of cancer manifestations and therapy-associated adverse effects often hinder the effectiveness of many therapies and warrant discovery of effective alternative therapy for certain molecular targets while minimizing the off-target effects. Therefore, the objective of most research worldwide is to develop novel, safe and effective anti-cancer therapies and that is the focus of this dissertation. One of these targets for drug discovery is CARP-1 that is an inhibitor of cell growth and survival, as well as an inducer of apoptosis signaling.

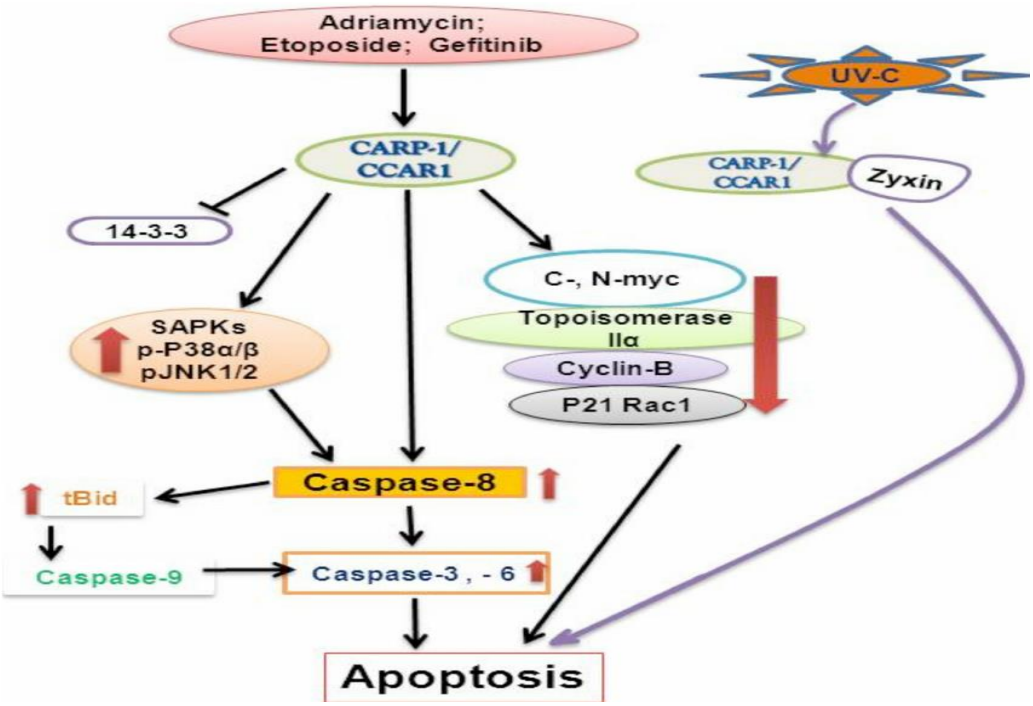

Figure 1.7. A Schematic representation of CARP-1/CCAR1 Apoptosis Signaling. Adapted from [140].

1.3.1. Combination therapy advantage of CARP-1 Functional Mimetics with TKIs

The introduction of several anticancer small molecule drugs (e.g., sunitinib, pazopanib, axitinib, temsirolimus, and everolimus) has rapidly changed the treatment of metastatic RCCs [112,113,146,147]. Although the impact on disease progression is encouraging, a substantial proportion of patients do not respond adequately, and therapy resistance almost inevitably occurs [103]. Possibly

combination treatment aimed at different, non-related pathways may be advantageous [112,113,146]. Due to their increase in vascular nature and high level of vascular permeability factor or vascular endothelial growth factor (VEGF) expression, ccRCC patients show promising success with anti-VEGF cancer therapy. Unfortunately, most of cancer patients ultimately develop a refractory response to anti-VEGF treatment over time. In this regard, novel therapeutic strategies for nonresponsive, highly aggressive tumor types to tackle the current clinical challenges are needed. Concurrently, we would like to perceive the molecular mechanism of these untreatable tumor types by using patient samples and utilizing different approaches. We speculate that the proposed experimental plan will be supportive to design new treatment options for lasting and sensitizing anti-angiogenic effects and better clinical management with the help of novel anticancer agents as CFMs. Also, we will work on different models of RCC, with a poor prognosis and because of their modest or non-response to systemic therapy. We will pursue different combination regimens, including drugs that work on the mTOR inhibition (everolimus), inhibit VEGFR (cabozantinib or sorafenib), because elevation in VEGF and CA IX levels are expected to happen in response to the hypoxic tumor environment. Escape from sorafenib and cabozantinib blockade of the VEGFR and mTOR inhibition of everolimus may also occur if levels of VEGF exceed a threshold that can circumvent the blockade. Toxicity was shown to be variable, and that will be taken into consideration. Even though in some combinations, both agents seem to be tolerable when utilized in full doses (Temsirolimus or everolimus with bevacizumab). In many instances the combination has shown not to be safe or feasible as a singular agent because combinations have required dose reductions (sorafenib with bevacizumab, Temsirolimus with sorafenib) or are not safe to be administered together (Temsirolimus with sunitinib, bevacizumab with sunitinib) [85,116,147–149].

1.4. Can Nanotechnology help improve drug delivery for RCC?

When cancer metastasizes outside of the kidney, it becomes even more complicated to treat and control. One challenge to overcome is delivery of agents targeted to metastatic cancer. Nanotechnology can combine the drug delivery system with anticancer drugs to target cancer and augment the cellular kill with higher concentrations to deliver drugs to cancer will need to be tested. One challenge to overcome is the delivery of these medications to metastatic cancer which has spread outside the kidney. Nanotechnology is the engineering of novel small molecules to direct treatment. To let cancer agents interact with cells and molecules, these drugs and carriers should have uniform particle size. One property is the high surface area to volume ratio, meaning one can encapsulate drugs to the nanoparticle in high concentrations. Therefore, the concentration of the delivery of the drug to cancer can be increased many folds [150].

One such solution is the use of nano-sized micelles as delivery vehicles for cancer therapeutics. Amphiphilic polymers self-assemble under aqueous conditions to form water-soluble micelles with a hydrophobic core. Hydrophobic drugs can then be chemically or physically incorporated into the micelle core for parenteral administration. This micelle drug delivery strategy has been applied to a variety of medical conditions, from hepatic fibrosis to knee osteoarthritis [151,152]. However, the micelle technique renders itself particularly relevant for the treatment of different types of solid tumor because of selective accumulation at the target site resulting from an enhanced permeability and retention (EPR) effect [153–156]. EPR is a phenomenon by which macromolecules, notably nanoparticles (NPs) and micelles, are delivered to, and accumulate at the tumor site in higher concentrations than are observed in healthy tissue because of anatomical and pathophysiological abnormalities or the leaky tumor vasculature of the tumor tissues [153–155]. However, angiogenesis is not always uniform throughout a tumor, leading to disproportional drug distribution by EPR; additionally, in some cases, tumors can exist with little or no evidence of EPR

[153,155]. Passive targeting by the EPR effect is a promising means of overcoming the specificity challenge of modern chemotherapeutic agents in many cases. Furthermore, newer active targeting strategies have been developed and can add to the selectivity of the EPR effect to overcome above noted limitations.

Moreover, there is a critical need to develop safe and effective delivery vehicles that can carry the payload to the specific target tissue and cell. Different types of nanoparticles recently emerged as an excellent delivery system. The CFM compounds have poor aqueous solubility and consequently poor bioavailability for their use and development as potential anti-cancer agents[157–160]. To address this issue, nanolipid formulations (NLFs) of CFM-4 and CFM-4.16 compounds were generated using chemically conjugated SMA-TPGS block polymer, then addition of DMSO contained the drug to the aqueous phase of polymer, followed by stirring, separation of unencapsulated drugs using Tangential Flow Filtration [161,162]. The NLFs caused in a significant enhancement in overall bioavailabilities of CFM-4 and CFM-4.16 when compared with respective free compound. Nanoparticles that encapsulate CFMs also protect them from premature clearance and degradation.

1.4.1. Rationale Novel Designed Theranostics Nano-platforms Utilizing Multiple Linkers with Click chemistry

In the proposed studies we will utilize a nanotechnology-based approach to address the poor aqueous solubility of a potent CFM compound (CFM-4.16) that has restricted its clinical development as a therapeutic agent. Our preliminary data thus far revealed that we have been successful in overcoming the solubility concerns of CFM-4.16 by encapsulating it in water-soluble vitamin E TPGS based nano-formulation that enabled high drug loading (up to 30% w/w of drug equivalent) and afforded its intravenous administration for animal testing. Since there is a critical

need to develop safe and effective delivery vehicles that can carry the payload to the specific target tissue and cell, different types of nanoparticles have been developed to deliver a variety of therapeutic agents. They have recently emerged as an excellent delivery system. Nanoparticles need to encapsulate CFMs and protect them from premature clearance and degradation. Ideally, they need to be loaded and functionalized with targeting ligands such as CA IX, which may potentially improve the delivery, specificity, and efficacy.

2. CHAPTER 2. RESEARCH OBJECTIVES

2.1.Introduction

Cancer remains the second cause of mortality worldwide. Throughout the last decade, cancer incidence has constantly and sharply increased all over the world. The molecular complications of cancer manifestations and therapy-associated adverse effects often hinder effectiveness of many therapies and warrant discovery of alternative effective therapy for certain molecular targets while minimizing the off-target effects. Therefore, the objective of most research worldwide is to develop novel, safer and more effective anti-cancer therapies. One of these targets for drug discovery works based on cell growth and survival inhibiting functions of an apoptosis regulatory protein, termed CARP-1. CARP-1 (Cell cycle and apoptosis regulator 1, aka CCAR1) is a peri-nuclear phospho-protein and a regulator of cell growth and apoptosis signaling [137–140] CARP-1 not only functions as a transcriptional co-activator of steroid family of nuclear receptors and a regulator of adipogenesis through the glucocorticoid receptor (GR), it also regulates Adriamycin (ADR)-dependent apoptosis in part through co-activation of p53 [141,142]. CARP-1 expression is often elevated in cells experiencing stress due to growth factor withdrawal or chemotherapy-induced cell cycle arrest and apoptosis [137,138,141]. Knockdown of CARP-1 resulted in resistance to apoptosis by ADR or EGFR tyrosine kinase inhibitors, demonstrating requirement of CARP-1 in cell growth inhibitory and apoptosis signaling by these agents [137,138,141].

2.2.Significance

Renal cell carcinoma (RCC) is one of the most common and lethal of all kidney cancers. RCC is tough to treat as the cells are largely resistant to many current therapies. In patients with an advanced form of RCC, targeted therapies including the ones using the new drug, Everolimus resulted in improved clinical outcomes. However, patients ultimately develop resistance to

targeted therapies as well. Thus, newer therapies including better ways of delivery system such as by targeting CA IX and using novel approaches are urgently needed to effectively fight this malignant disease. Our current project for uses a nanotechnology-based approach as well as clinically relevant RCC tumor model and directed address the current challenges of treating resistant RCCs. This project will be an important step forward in the development of novel drug delivery technologies and therapies for treating clinically relevant RCC. Besides that, identifying TKIs such as sorafenib or cabozantinib that can work synergistically in combination with CFMs using targeted nano-formulation will have a huge impact on kidney cancer treatment options. Our robust and positive preliminary studies provide a rational approach to investigate our hypothesis that CFMs and kinase inhibitors loaded in CA IX-PLNPs/OMs alone or combination will offer better prospects for inhibiting resistant RCCs. In the research strategy as outlined before, we will design experiments to maximize the success in overcoming naive and everolimus resistant RCC in animal models.

2.3. Specific Aims

In the light of the preceding literature review, it is apparent that CARP-1 (CCAR-1) is a potential molecular target whose functional mimetic analogs may lead to the suppression of tumor growth, that of resistant ccRCC. It may also be useful to integrate a combination strategy with CA IX targeted molecule as a predictive biomarker for patient survivability and treatment modalities, as suggested in preliminary studies. To validate this hypothesis, the small molecule mimetic of CARP-1 CFM-4.16, has been deployed. In this study, the initial step would be to elucidate the effect of CFM-4.16 on RCC cell growth and survival. This would provide insight into the molecular mechanisms by which CARP-1 is regulated in RCC. Once established, the next step

would be to investigate the effect of CFM-4.16 on a panel of RCC cells and to determine if it is inhibiting RCC cell lines growth.

In the specific aim 1, the CFM compounds will be investigated for (i) the molecular mechanisms of RCC cell growth inhibition, and (ii) to the extent these compounds inhibit growth of RCC cells. Collectively, these data would establish that CFMs inhibit growth of parental, wild-type RCC in part by promoting apoptosis signaling. However, CFM compounds suffer from an inherent drawback of poor aqueous solubility and its dose escalation for systemic administration and in vivo testing is highly challenging.

In Specific Aim 2, we will perform confirmatory studies to validate that the *in vitro* anticancer activity of CFM-4.16 is maintained when loaded in vitamin E-TPGS based micellar nano-formulation. Specifically, samples consisting of free CFM-4.16 and CFM-4.16 loaded in vitamin E-TPG based micellar nano-formulation (abbreviated as SMA-TPGS-CFM) will be tested *in vitro* and *in vivo* using parental, wild-type RCC cells as well as Everolimus-resistant RCC. The objective for SA2 is to test the safety of intravenous administration of SMA-TPGS-CFM micellar nano-formulation and the antitumor response in RCC mouse model. Our preliminary data thus far revealed that we have been successful in overcoming the solubility concerns of CFM-4.16 by encapsulating it in water-soluble vitamin E TPGS based nano-formulation that enabled high drug loading and affords its intravenous administration for animal testing. Studies will be performed (i) to test the *in vitro* efficacy of the CFM 4.16 loaded in vitamin E TPGS based nano-formulation in parental, wild-type RCC and Everolimus-resistant RCC cells as well as (ii) perform proof-of-concept studies to explore their antitumor response in a clinically relevant RCC mouse model. Specifically, we aim to achieve (1) an increased serum bioavailability of CFM-4.16 nano-formulation following i.v administration; (2) increased nano-formulation accumulation and

retention within the tumor (by the EPR effect) and therefore (3) an increased localized CFM-4.16 concentration in tumor tissues relative to free drug, thus producing a marked antitumor response. In this regard, it is worthwhile to note that in an earlier study a polymeric nano-lipid formulation resulted in enhanced serum bioavailability of CFM-4.16 when compared with the free CFM-4. Oral administration of CFM-4 NLF resulted in reduced weights and volume of the xenograft tumors derived from A549 NSCLC and MDA-MB-231 TNBC cells [160].

In Specific Aim 3, CA IX expression on the cell surface is associated with the induction of tumor hypoxia through regulation of HIF1α. The clinicopathological analysis has supported the fact that overexpression of CA IX in RCC is linked to poor disease prognosis and resistance to therapy. The accumulated literature and clinical trial data indicate that CA IX expression is 95-99% for both primary and metastatic RCC [129,132,133,163,164], whereas it has restricted expression in healthy tissues (including non-cancerous renal tissue). Thus, CA IX is significantly overexpressed in RCC tumor. These results signify that CA IX is an excellent target for site specific delivery of therapeutic payloads to renal tumors. As reported earlier, a small molecule, Acetazolamide (ATZ), has high affinity (Kd 8.3 nM) to CA IX [133,164] and ATZ-conjugated nanoformulations can deliver the payload into the inner core (more than the periphery) of the tumor. Along these lines, for the first time, development of an ATZ-conjugated polymeric lipid nanoformulations library for the selective delivery of a drug cocktail to the hypoxic region of therapy resistant RCC was proposed. It is well established that the hypoxic tumor (core) harbors aggressive and drug resistant stem-like cells that can persist after initial drug therapy and have the ability to invade normal tissues and metastasize to distant sites forming secondary tumors. Authenticated RCC cell lines such as WT (A498, UOK262) and Evr-res (A498, UOK262) will be utilized as RCC cells, as well as Raw 264.7 (macrophage) for macrophage phenotyping studies. The following will be established (i) a

synergistic anticancer effect of CFM-4.16 with TKIs, (ii) the role of M2-macrophages in tumor immune evasion, and (iii) the mechanism of inhibiting tumorigenic cross-talk between RCC epithelial cells and M2-macrophages using NPs. The tumor environment mimetic advance spheroid and Transwell cell culture models will be used to establish efficacy.

3. CHAPTER 3. A CARP-1 FUNCTIONAL MIMETIC AS A PROMISING THERAPEUTIC ANTICANCER AGENT FOR EV-RESISTANT RENAL CELL CARCINOMA

Results from the following studies have been published: Oncotarget Journal, Cheriyan, V. T. *, Alsaab, H. O., *, et al., (2017). A CARP-1 functional mimetic loaded vitamin E-TPGS micellar nano-formulation for inhibition of renal cell carcinoma. Oncotarget, 8(62), 104928. *Equal contribution.

3.1.Objectives:

In this chapter we investigated: (i) the molecular mechanisms of RCC cell growth inhibition by the CFM compounds, (ii) the extent to which these compounds inhibit growth of drug (Everolimus)-resistant RCC cells, and (iii) whether CFMs inhibit growth of parental as well as Everolimus-resistant RCC cells.

3.2.Introduction

RCCs comprise of different types of renal epithelial tumors that include most commonly occurring conventional (clear cell) renal cell carcinomas (ccRCCs) followed by the papillary renal cell carcinomas, Chromophobe renal carcinoma, Oncocytoma, and Collecting-duct carcinoma [165]. Most RCCs seem to occur sporadically while 1-4% of the cases have an inherited predisposition. Mutations in the Von Hippel-Lindau (VHL) tumor suppressor occur frequently in RCCs. RCC is generally very difficult to treat as the cells are largely resistant to many conventional therapies. Currently, surgery remains the best treatment option [165], although 20-30% of the patients progress to develop metastatic disease. If diagnosed early, there is a better chance of the cancer going into remission but if the cancer does not respond to first-line therapies there are very limited secondary options [30,97]. FDA approved agents for treatment of metastatic RCC include tyrosine kinase inhibitors (TKIs) such as sorafenib and sunitinib, and mammalian target of rapamycin (mTOR)

inhibitors temsirolimus and everolimus [8,112,113,147]. These targeted therapies result in improved clinical outcomes, and although everolimus is the first drug used as a secondary treatment option for resistant RCCs, patients ultimately develop resistance to targeted therapies that correlates with poor overall prognosis [96,166]. Dr. Rishi's group at Wayne State University previously discovered that CARP-1 also functions as a co-activator of the APC/C E3 ligase [139]. APC/C is a multi-subunit ubiquitin E3 ligase protein that plays a distinct role in cell cycle transitions. Misregulation of APC/C substrates such as Securin, Polo-like kinase (Plk) correlate with tumor progression [143,167]. A chemical biology-based high-throughput screening of a chemical library as shown in Figure 3.1 resulted in identification of a number of novel, small molecule inhibitors (SMIs) of CARP-1 binding with APC/C subunit APC2 [139]. These compounds, termed CARP-1 functional mimetics (CFMs)[159]. CFMs bind with CARP-1 and block its interaction with APC2, cause G2M cell cycle arrest, and inhibit cell growth by inducing apoptosis in various cancer types [139,140].

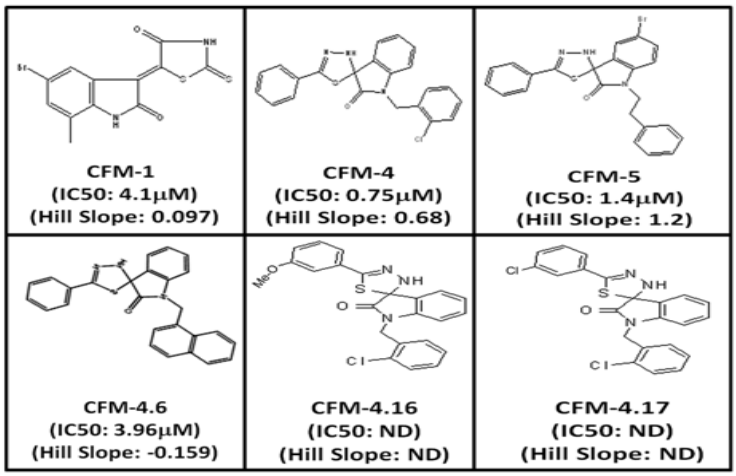

CFM	R^1	R^2	R^3	R^4
4	H	2-Cl-Ph-CH_2	H	H
4.16	3-Cl	2-Cl-Ph-CH_2	H	H
4.17	3-OCH_3	2-Cl-Ph-CH_2	H	H

Figure 3.1 CFMs (Top Row) and CFM-4 analogs (Bottom Row) that inhibit CARP-1 binding with APC-2. IC50 value for each compound was derived by conducting dose response assays. Adapted from [1].

CARP-1 (Cell cycle and apoptosis regulator 1, aka CCAR1) is a peri-nuclear phospho-protein and a regulator of cell growth and apoptosis signaling [137,138,140]. CARP-1 not only functions as a transcriptional co-activator of steroid family of nuclear receptors and a regulator of adipogenesis through the glucocorticoid receptor (GR), it also regulates Adriamycin (ADR)-dependent apoptosis in part through co-activation of p53 [140–142]. CARP-1 expression is often elevated in cells experiencing stress due to growth factor withdrawal or chemotherapy-induced cell cycle arrest and apoptosis. Knockdown of CARP-1 resulted in resistance to apoptosis by ADR or EGFR tyrosine kinase inhibitors demonstrating requirement of CARP-1 in cell growth inhibitory and apoptosis signaling by these agents [137,140].

3.3.Material and methods:

3.3.1. Chemicals and Reagents

Structure and synthesis of CFM compounds (CFM-4, -4.16, and -4.17) have been recently described and their structures are shown in Figure 3.1. A stock solution of 50mM of each CFM was prepared in dimethyl sulfoxide (DMSO) and stored at –20°C. 3-[4,5-Dimethylthiazol-2-yl]-2,5diphenyltetrazolium bromide (MTT) were obtained from Sigma-Aldrich, St Louis, MO. Everolimus was purchased from SelleckChem, Boston, MA and a 50mM stock solution was prepared in DMSO and stored at –20°C, while clinical grade Adriamycin (ADR) was obtained from Karmanos Cancer Institute pharmacy, Detroit, MI. We purchased all other analytical grade reagents from Sigma-Aldrich (St Louis, MO) and used them without further purification.

3.3.2. Cell culture conditions and cell lines

DMEM, EMEM medium and antibiotics (penicillin and streptomycin) used in this study were purchased from Invitrogen Co. (Carlsbad, CA). Fetal bovine serum (FBS) and DMSO were

obtained from Denville Scientific Inc. (Metuchen, NJ), and Fisher Scientific (Fair Lawn, NJ), respectively. The Protein Assay Kit was obtained from Bio-Rad Laboratories (Hercules, CA). The mouse monoclonal antibodies for β–actin was acquired from Sigma-Aldrich (St. Louis, MO). We purchased rabbit polyclonal antibodies for α-tubulin, Cyclin B1, Cleaved Caspase-8, PARP, phospho and total p38α/β, phospho- and total JNK1/2 SAPKs from Cell Signaling Technology (Beverly, MA). We have previously described generation and characterization of the anti-CARP-1 rabbit polyclonal antibodies [159,160,168,169].

The human RCC A498, CAKI-1, CAKI-2, and ACHN cells were from ATCC and kindly provided by Dr. Rajvir Dahiya from Department of Urology, San Francisco Veterans Affairs Medical Center and University of California San Francisco, San Francisco, CA (UCSF). The HLRCC (UOK 268 and UOK 262) cells were kindly provided by Dr. Marston Linehan Urologic Oncology Branch, Center for Cancer Research, National Cancer Institute, National Institutes of Health, and Bethesda, MD. (NCI). All the cells were routinely maintained as described before. All the cell culture media were containing 10% FBS, 100 units/ml of penicillin, and 100 μg/ml of streptomycin, and the cells were kept at 37°C and 5% CO_2. For cell growth and MTT studies, the cells were cultured in fresh media with 10% FBS prior to their treatments with various agents. The Caki-1 and Caki-2 were grown in RPMI 1640 medium, and UOK 262, UOK 268, and Huh7 were routinely cultured in DMEM medium.

3.3.3. Generation of Everolimus-resistant RCC cells

The human RCC A498, UOK262, and UOK268 cells were cultured in the chronic presence (>6 months) of Everolimus. The parental A498 cells were initially treated with 500nM Everolimus for 3-4 weeks, followed by escalation to 1.0, 2.0, 4.0 and 10.0μM doses for a period

of three to four months till the resistant subline emerged. The cells were cultured in continuous presence of each of the dose for 3-4 weeks till resistance developed and cells adapted to growth in 2μM Everolimus. In the case of UOK262 and 268 RCC cells, the parental cells were initially cultured in 10nM Everolimus for 3-4 weeks. For selection of the resistant cells, everolimus dose was escalated to 20, 50, 100, 200, 500, 1000, and 2000nM. The UOK cells were cultured in continuous presence of each of the dose for 2-3 weeks till resistance developed and cells adapted to growth in 2μM Everolimus. Subsequent, routine maintenance of the resistant cells in the presence of 2μM Everolimus was continued and multiple, resistant sublines for each of the RCC cells were isolated and characterized for their growth inhibitory (GI50) dose of Everolimus by the MTT-based viability assays as detailed below. Several resistant sublines of each cell line were then isolated and maintained in respective culture media containing 2.0 μM everolimus.

3.3.4. Generation of CARP-1 knock-down RCC cells

The human RCC UOK262 parental cells were transfected with vector plasmid pcDNA3/hygro or plasmid expressing CARP-1 anti-sense (Clone 1.6, ref 8). Multiple, stable sublines for hygromycin resistance were selected in the presence of 400μg/ml hygromycin (#10687010, Invitrogen Inc) following methods described before [159,160,168,169]. We determined the levels of CARP-1 in the parental, and vector or CARP-1 antisense plasmid-transfected RCC cells and their viabilities in the presence of CFM compounds by western blot and MTT assays, respectively, as described below.

3.3.5. Cell viability assays (MTT assay)

The cell growth inhibition was assessed by using MTT assay. The cytotoxicity of CFM-4, -4.6, -4.16, -4.17, Everolimus, and ADR in the RCC cells (A498, UOK262, and UOK268) was

assessed by MTT assay. First, we seeded 5 X 10^3 cells in the 96-well plate in triplicate, allowed the cells to grow in fresh culture media for another 24h, and treated them with respective agents for the noted dose and time. Control cells were treated with 0.1% DMSO in culture medium. After treatment, we performed an MTT assay. Briefly, 20 µl of 1mg/ml of MTT was added to each well and cells were incubated for 2-4h at 37^0C. MTT was removed, and the resulting formazan products were dissolved by adding 50µl DMSO/well followed by colorimetric analysis using a multi-label plate reader at 570 nm (Victor3; PerkinElmer, Wellesley, MA).

3.3.6. Western Blot and protein expression analysis

For protein expression analysis, we conducted western blot experiments. The RCC cells were treated with DMSO/Vehicle (Control) or indicated dose and time of the noted compound and were lysed to prepare protein extracts. Cells were harvested and lysed in RIPA buffer (50mM Tris-HCI, pH 8.0, 150mM sodium chloride, 1.0% NP-40, 0.5% sodium deoxycholate, 0.1% sodium dodecyl sulfate (SDS), and 0.1% of protease inhibitor cocktail) for 20 min at 4^0C. The lysates were then centrifuged at 14,000 rpm at 4^0C for 15 min to get rid of debris. We then determined the protein concentrations of whole cell lysates utilizing the Protein Assay Kit. 50µg from each sample of supernatant proteins were separated by SDS-10% polyacrylamide gel electrophoresis (SDS-PAGE) and transferred to polyvinylidene difluoride (PVDF) membrane (Bio-Rad, Hercules, CA) by company standard protocol. The membranes were hybridized with primary antibodies followed by incubation with appropriate secondary antibodies. The antibody-bound proteins were visualized by treatment with the chemiluminescence detection reagent (Amersham Biosciences) according to the manufacturer's instructions, followed by exposure to X-ray film (Kodak X-Omat). The same membranes were then re-probed with either the anti-β actin or anti-α tubulin antibody, which was utilized as an internal control for protein loading.

3.4.Results

3.4.1. Novel Analogs of CFM-4 Suppress Growth of Human NSCLC, TNBC, and RCC Cells

We first tested the growth-inhibitory effects of CFM-4 and 4.16 on human RCC, NSCLC, and liver cancer cell lines. CFM-4 and 4.16 inhibited the viability of all cell lines in a dose and time-dependent manner (Figure. 3.2A and B). Generally, most of cell lines were more sensitive towards all the CFM, showing at least 50% reduced proliferation in the presence of 20 μM CFM-4 and 4.16 (Figure 3.2). Doses of 1 μM and 2 μM of CFM-4 over a 24 h treatment elicited more than 40% reduced viability of HepG2 and UOK262 cell lines. Also, doses of 5 μM and 10 μM of CFM-4 showed at least 40% growth cells viability in Huh7, H1299, UOK268, and UOK 262 (Figure 3.2.A). The HepG2, A549, UOK262 cells were relatively less sensitive to CFM4 since a 10 μM dose of CFM-4 caused little more than 20% reduction in their viability (Figure 3.2.A). However, in case of CFM-4.16, there is an approximately 50% attenuation of the viability of all cells was indicated when treated with a lower dose of CFM-4.16 over a 24 h period which indicates its stronger activity against these cell lines (Figure 3.2.B).

In addition, since the RCC, NSCLC, and liver cancer cell lines were relatively more sensitive to CFM-4.16, these cells were separately treated with various doses of CFM-4 for a period of 24 h to evaluate the lowest effective dose for these agents. Despite 500 nM dose of both compounds failed to affect RCC, NSCLC, and liver cancer cells viability, a 1 μM and 5 μM dose of the CFM-4.16 agent elicited more than 60% loss in the viability of all the cell lines**.** These data suggest that the viabilities of the RCC, NSCLC, TNBC, and liver cancer cells were affected properly by the 1 μM or higher doses of free drug (CFM-4.16) and CFM-4.16 nanoformulation.

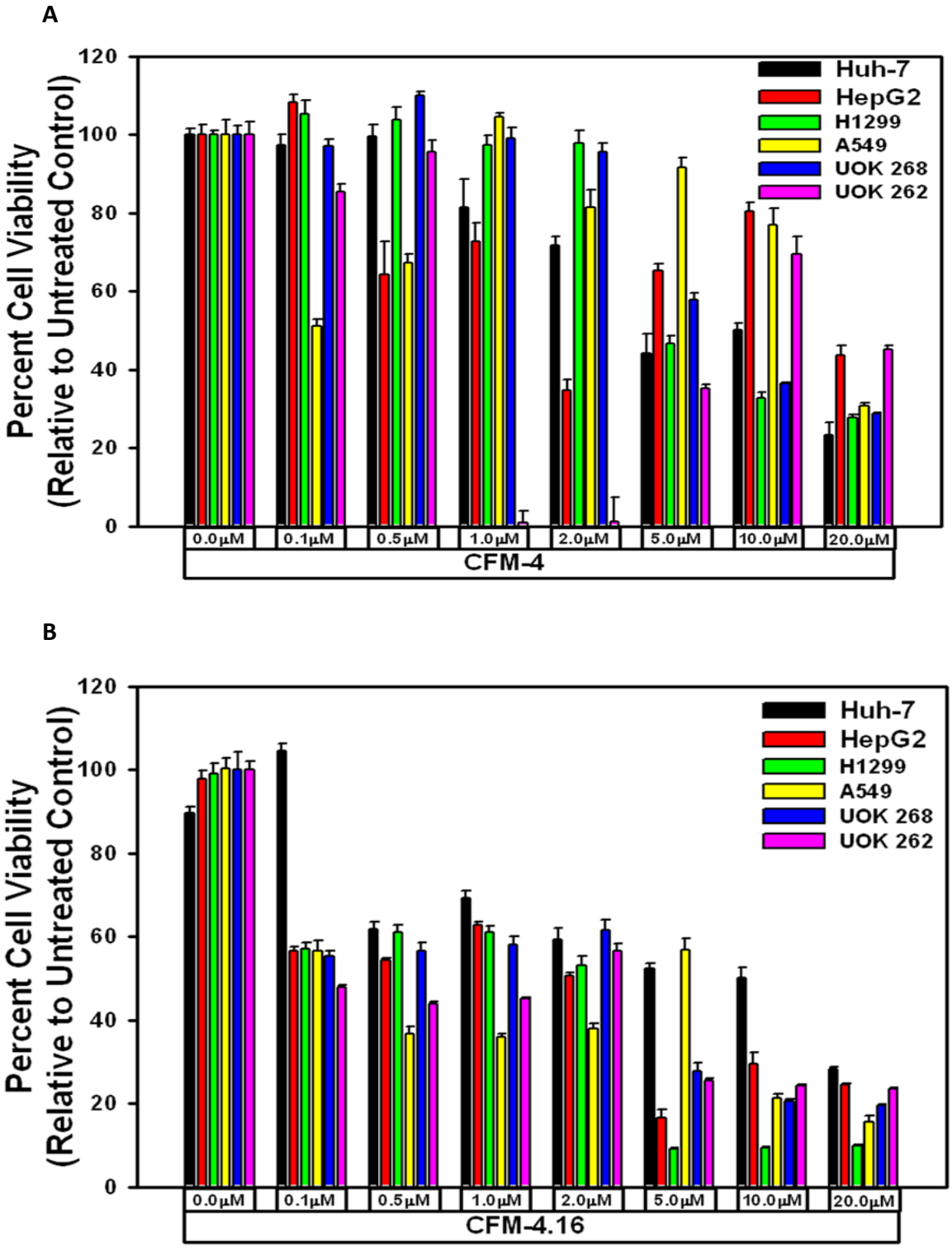

Figure 3.2. Liver cancer cells (Huh-7 and Hep G2), lung cancer cells (H1299 and A549) and renal cancer cells (UOK 268 and UOK 262) were treated with the indicated doses of (A) CFM-4 and (B) CFM-4.16 for 24 hours. The number of viable cells was then determined by MTT assay as described. Adapted from [1].

3.4.2. CFMs inhibit viabilities of RCC cells

Our prior findings had indicated anti-cancer properties of a novel class of CFM compounds [169], and our recent medicinal chemistry-based structure-activity relationship (SAR) studies reported identification of CFM analogs, in particular CFM-4.16, that was a superior inhibitor of parental and drug-resistant human and murine triple-negative breast cancer cells *in vitro* and *in vivo* [169]. Since emergence of resistance to current therapeutics remains a formidable problem in effective treatment and management of RCCs in clinic [2,96,97], we speculated whether CFM class of compounds would be effective inhibitors of RCC cells and to the extent, these compounds would be suitable to inhibit the resistant RCCs. We tested this possibility by conducting studies as detailed below. First, we evaluated potencies of the parent compound CFM-4 and its analogs CFM-4.6, and CFM-4.16 in cell culture studies utilizing RCC cell lines of ccRCC (CAKI-1, A498), papillary RCC (ACHN, CAKI-2), and HLRCC (UOK 262 and UOK 268) origins [83,170] by MTT based assays. As shown in Figure 3.3, CFM-4.16 dose of 1.0 and 2.0 μM over a period of 12h caused a greater loss of viability of all the RCC cells when compared to the RCC cells treated with similar doses of CFM-4 compound. Since Everolimus is one of the currently used targeted therapy for RCCs, we tested whether Everolimus treatments also provoked loss of viabilities of the RCC cells and to the extent anti-RCC effects of Everolimus were different from the CFM-4.16 treatments. The Everolimus doses of 0.2, 0.5, 1.0, and 2.0μM caused a moderate 20-40% loss in the viabilities of RCC cells, the doses of 5.0, and 10.0μM however provoked a greater than 60-70% reduction in the viabilities of the RCC cells (Figure 3.3 C). Given that the molecular masses of Everolimus, Doxorubicin, and CFM-4.16 are 958.22, 543.5, and 440.35, respectively, a 1μM dose of Everolimus will have an approximate molar equivalence to a 2.0μM dose of either Doxorubicin or CFM-4.16. Thus, although treatments with 5.0 or 10.0μM doses of Everolimus,

CFM-4, and CFM-4.16 provoked a similar 60-80% reduction in viabilities of the RCC cells, a 2.0μM dose of CFM-4.16 induced a 40-60% loss of RCC cell viabilities (Figure 3.3 B) while a 1μM dose of Everolimus caused a moderate 20-40% reduction in RCC cell viabilities (Figure 3.3 C). These data in Figure 3.3 and Figure 7.1. in Appendix suggest that the RCC cells are likely more sensitive to inhibition by CFM-4.16 when compared with CFM-4 or Everolimus at the equivalent doses of up to 2μM of each compound. Additional dose response studies with reference to A498, CAKI-1, and ACHN RCC cells revealed that CFM-4.16 dose for inhibition of the cell growth by 50% (GI_{50}) was ~1.5-1.8μM, its dose for inducing a 50% cytotoxic effects (LC_{50}) was 5.5-5.7 μM.

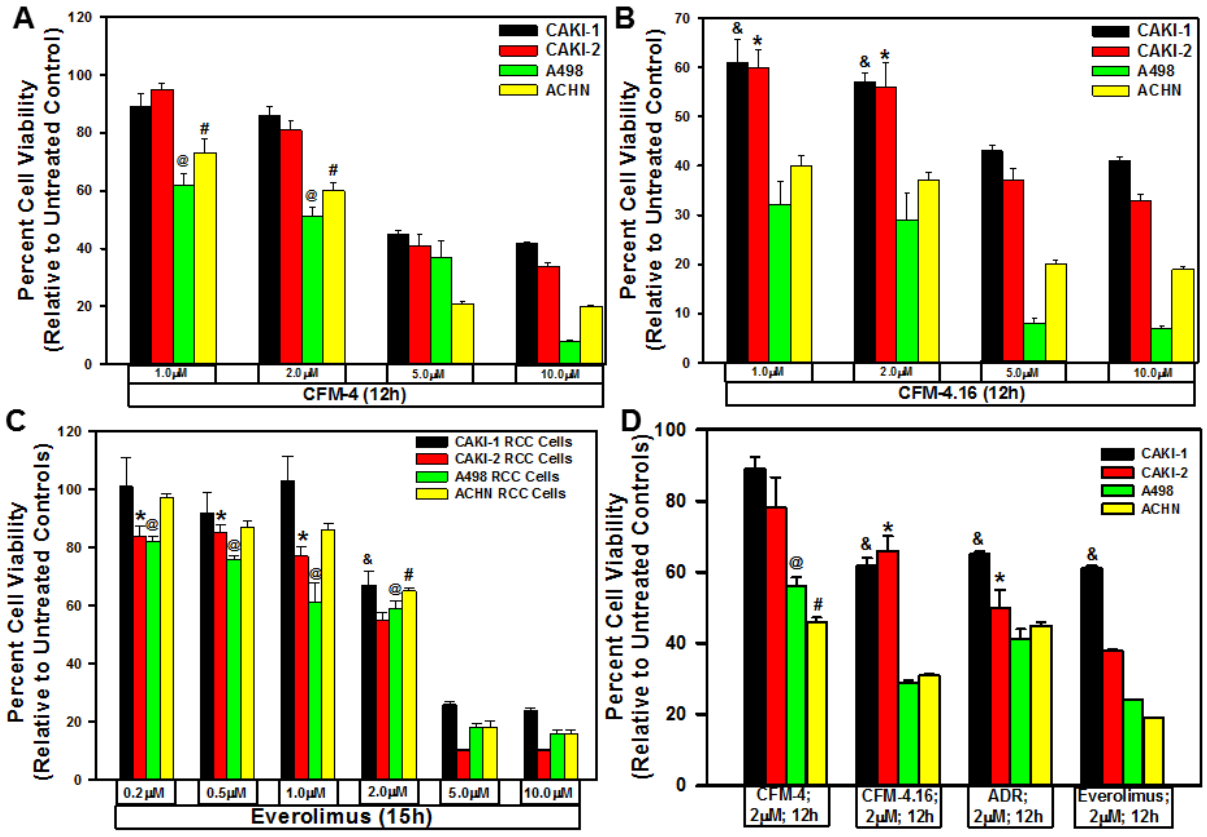

Figure 3.3. CFMs inhibit RCC cell growth. We treated noted cell lines either with DMSO (Control), with various CFMs (A, B, D-F), Everolimus (C), or ADR (D) for indicated dose and time. We determined cell viability by MTT assay. The data in the histograms represent means of three independent experiments with

4-6 replicates for each treatment; bars, S.E. A-D, @,#,&,*, E-F, α,β,γ,δ, statistically significant inhibition ($p = <0.05$) relative to DMSO-treated respective controls. Adapted from [1].

3.4.3. CFMs inhibit viabilities of the resistant RCC cells

To test whether CFM class of compounds are also effective inhibitors of the resistant RCCs, as a proof-of-concept strategy, we first generated and characterized several RCC sublines that were resistant to Everolimus. We cultured A498, UOK 262, and UOK 268 RCC cells in the chronic presence of escalating doses of Everolimus until the resistance emerged. As shown in Figure 3.4 A, the GI_{50} doses for Everolimus were 1.2, 0.02, and 0.02μM for the parental A498, UOK 262 and UOK 268 RCC cells, respectively. These data in Figure 3.4 A strongly suggest that all the RCC cells developed a robust level of resistance to Everolimus. We next investigated whether the CFM compounds inhibited viabilities of the Everolimus resistant RCC cells by conducting MTT based assays as in Figure 3.3. and 7.1. Appendix. As shown in Figure 3.4 B-D, a 4.0μM dose of CFM-4 caused ~50% loss of viability of the Everolimus resistant A498 cells while a moderate ~20% reduction in the viability of the Everolimus resistant UOK 262 and UOK 268 cells was noted. A 4.0μM dose of CFM-4.16 on the other hand provoked ~80% reduction in the viabilities of all the Everolimus-resistant RCC cells. These data corroborate our current findings in Figure 3.3 and our recent studies demonstrating increased effectiveness of CFM-4.16 in attenuating viabilities of the parental RCC cells as well as drug-resistant RCC (Figure 3.4) and TNBC cells [159].

A

RCC Cell Line		Everolimus (72h) GI_{50} (μM)
A498 ccRCC	Wild type	~1.2
	Everolimus-R Clones 1 - 6	≥10.0
UOK 262 HLRCC	Wild type	<0.02
	Everolimus-R Clone 1	~7.0
	Everolimus-R Clone 3	~2.0
	Everolimus-R Clone 5	~4.0
	Everolimus-R Clone 6	~1.8
UOK 268 HLRCC	Wild type	<0.02
	Everolimus-R Clone 2	≥10.0
	Everolimus-R Clone 3	≥10.0
	Everolimus-R Clone 4	≥10.0
	Everolimus-R Clone 6	~7.0

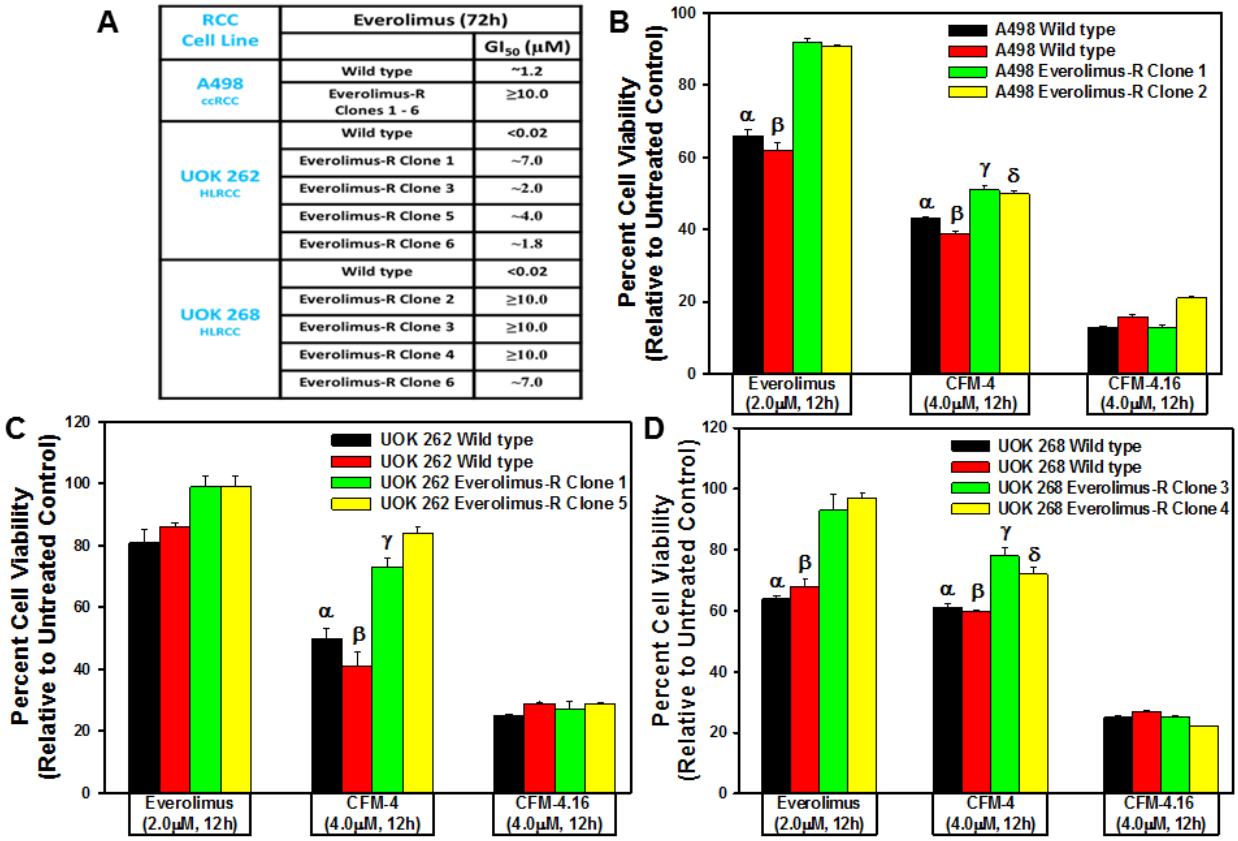

Figure 3.4. CFM-4. 16 inhibits Everolimus-resistant RCC cell growth. (A) GI50 values of parental and drug-resistant RCC cells. In the case of Everolimus-resistant cells, the respective parental and resistant sublines were treated with 0.02, 0.1, 0.2, 1.0, 2.0, 4.0, and 10.0 μM dose of Everolimus. Percent cell viabilities were determined relative to respective DMSO-treated controls. The data in the GI50 columns represent means of three independent experiments. (B-D) Indicated parental and their respective drug resistant RCC cells were either untreated (Control) or treated with noted doses of Everolimus, CFM-4, or CFM-4.16 for 12h. We determined cell viability by MTT assay. The histogram columns represent means of three independent experiments with 4-6 replicates for each treatment; bars, S.E. B-D, α, β, γ, δ, statistically significant inhibition (p = <0.05) relative to DMSO-treated respective controls. Adapted from [1].

3.4.4. CFM-4.16 Stimulates apoptosis by activating p38 MAP kinase, c-Jun N-terminal kinase (JNK) enhancing expression of CCAR-1/CARP-1

CARP-1 is a key transducer of apoptosis signaling by therapeutics such as Doxorubicin, Etoposide, and Gefitinib [137], and CARP-1 expression was necessary for transduction of apoptotic/inhibitory signaling by these therapeutics as well as by our experimental CFM class of compounds in parental and drug-resistant TNBC cells [159]. Since CFM-4.16 was more effective in

reducing viabilities of parental as well as Everolimus resistant RCC cells (Figure 3.4), we next investigated molecular mechanisms of apoptosis by CFM compounds and to the extent CARP-1 was required for inhibition of RCC cells by CFMs. Our western blot (WB) analyses revealed that equimolar (10μM) dose of CFM-4 or CFM-4.16 stimulated CARP-1 expression and activation of pro-apoptotic, stress-activated protein kinases (SAPKs) in the RCC cells in a time-dependent manner (Appendix Figure 7.2. A, B). Although activation of both the p38α/β and JNK1/2 SAPKs occurred as early as 1h of treatment with CFMs, CFM-4.16 caused a rather robust activation of these SAPKs at 6h treatment period **(**Appendix Figure 7.2. A, B). Co-incident with the SAPK activation, treatments with CFMs over a 6h period stimulated activation of PARP and caspase 8, while causing a significant decline in levels of mitotic cyclin B1 in the RCC cells. Since CFMs inhibited viabilities of Everolimus-resistant RCC cells, we then determined whether CFMs provoked apoptosis in the Everolimus-resistant RCC cells as well. As shown in Figure 7.2. C, both the compounds stimulated CARP-1 expression, activation of SAPKs, PARP cleavage, and loss of cyclin B1 in the Everolimus-resistant UOK262 RCC cells. Here again, CFM-4.16 caused a generally higher increase in CARP-1 levels, activation of SAPKs, PARP-1 cleavage in parental or Everolimus-resistant RCC cells when compared with the cells that were treated with CFM-4. CFM-4.16 treatments also provoked a greater loss of cyclin B1 in both the parental and Everolimus-resistant RCC cells when compared with their CFM-4-treated counterparts. These data suggest that CFMs inhibit RCC cell viabilities in part by promoting apoptosis.

3.4.5. CFM-4.16 Stimulates apoptosis in parental and resistant RCC cells by enhancing expression of CCAR-1/CARP-1

We next clarified whether the CFM compounds required CARP-1 to inhibit variabilities of the RCC cells. For this purpose, we first generated and characterized multiple, independent

hygromycin-resistant stable sublines of UOK262 cells that express reduced CARP-1 as detailed in methods. The parental UOK262 cells were transfected with a plasmid encoding CARP-1 antisense or its vector counterpart, and transfected cells were cultured in chronic presence of hygromycin over a period of 6-8 weeks to obtain resistant sublines essentially following our previously described methods [159]. As shown in Appendix Figure 7.3 A**,** stable expression of CARP-1 antisense plasmid caused reduced levels of CARP-1 in two sublines when compared with the levels of CARP-1 noted in two, vector-expressing sublines or the parental UOK262 cells. We then determined whether knock-down of CARP-1 expression interfered with loss of viabilities induced by treatments with CFM compounds. Our data in Appendix Figure 7.3 B demonstrate that depletion of CARP-1 in the UOK262 cells resulted in a significant abrogation of inhibitory effects of both the CFM compounds when compared with their vector-expressing counterparts. Taken together, our findings in Appendix Figures 7.2 and 7.3 suggest that CFMs stimulate apoptosis in parental and resistant RCC cells and CARP-1 expression is required in transduction of inhibitory effects of the CFM compounds.

3.4.6. CFM-4.16 suppresses three-dimensional growth of the parental and Everolimus-resistant RCC cells

Recent studies have revealed culture of the RCC cells in a three-dimensional (3D) system as spheroids, and that the overall gene expression patterns of RCC spheroids in 3D more closely mimicked those observed in RCC tumors *in vivo* [171]. These studies further suggested suitability of 3D RCC spheroids from established cell lines as well as patient-derived, primary RCC tumors for pharmacological testing and investigating molecular mechanisms of RCC metastasis. Since CFM-4.16 inhibited growth of mammospheres derived from parental and drug-resistant human TNBC cells, we tested whether CFM-4.16 will inhibit growth of the RCC spheroids in 3D culture

conditions. As shown in Figure 3.5, the parental A498, UOK262, and UOK268 RCC cells as well as their respective, Everolimus-resistant sublines formed RCC spheres in 3D culture conditions that are detailed in methods. Consistent with our observations with the human TNBC mammospheres, CFM-4.16 caused marked disintegration of spheres of parental and Everolimus resistant human RCC cells (Figure 3.5.).

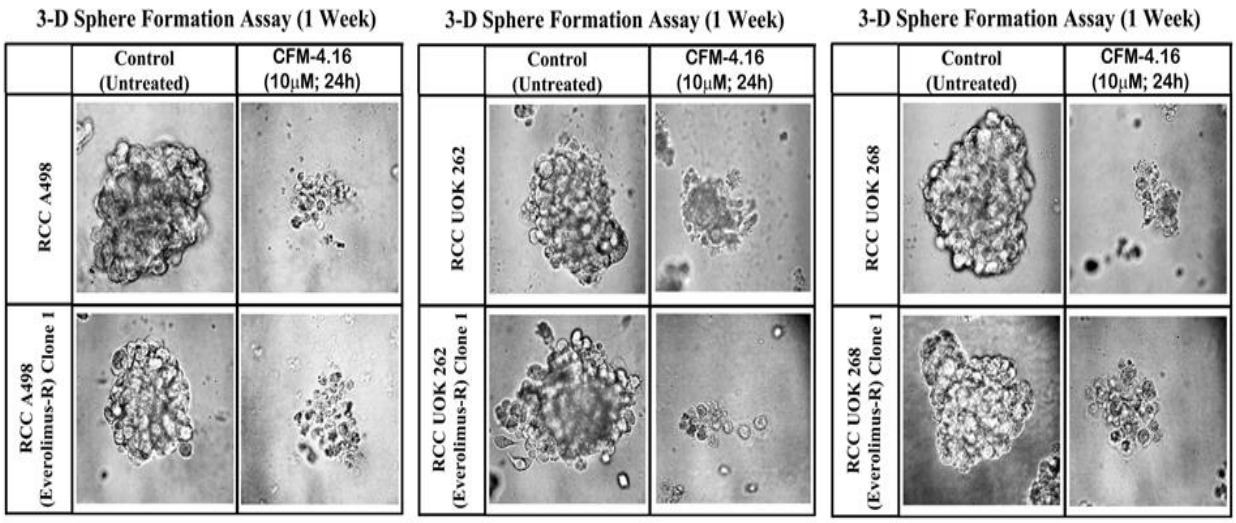

Figure 3.5. CFM-4.16 inhibits growth of RCC spheres derived from parental and Everolimus-resistant cells. Parental and Everolimus-resistant RCC cells were grown as spheres as detailed in Methods. The sphere cultures were either untreated (Control) or treated with CFM-4.16 for noted dose and time. The untreated and treated spheres were then photographed as in methods. Representative photomicrographs of untreated and CFM-4.16 treated spheres are shown. Adapted from [1].

3.5. Discussion

In this chapter, we initiated further studies to determine whether the CFM-4 and its analogs inhibit growth of RCC cells; and further explored molecular mechanism(s) of RCC cell death by these compounds. CFM-4.16 exposure resulted in a somewhat higher loss of RCC cell viability when compared with their loss of viabilities noted following treatments with CFM-4. It is therefore feasible that further rational medicinal chemistry modifications of these promising anticancer agents could yield additional novel small molecule compounds that may have greater potency and

selectivity in inhibiting RCCs. In an attempt to elucidate apoptosis signaling by chemotherapy, CARP-1 was identified as a perinuclear protein that was required for apoptosis by EGFR targeted therapeutics as well as DNA damaging agents such as Adriamycin (ADR) and etoposide [159,160]. Although CARP-1 is a coactivator of steroid-thyroid receptor superfamily, we focused our efforts to exploit apoptosis signaling of CARP-1 for development of novel anti-cancer agents. Approximately one third of RCC patients present metastases at diagnosis, and 30-70% of patients relapse within five years of surgery [31]. During the last decade, several targeted therapies have been developed and approved for treatment of metastatic RCC. These second-line targeted therapies for the metastatic RCCs include mechanistic target of rapamycin (mTOR) inhibitors such as Temsirolimus and Everolimus, and tyrosine kinase inhibitors such as Sunitinib and Sorafenib [166]. Although most of these therapies have substantially improved patient outcomes, none of these drugs are curative and resistance eventually develops. Here we utilized ccRCC cells and hereditary non-ccRCC subtypes to generate laboratory models of drug resistance by exposing them to chronic presence of Everolimus over an extended period. Several Everolimus-resistant sublines of A498 (representative of cc-RCC subtype), and UOK262 and UOK268 (representative of non-cc-RCC subtype) were obtained and characterized for their resistance to Everolimus. In this proof-of-concept investigation, we find that CFM compounds are potent inhibitors of parental as well as Everolimus-resistant RCC cells. In fact, the compound CFM-4.16 seemed to be generally more effective inhibitor of these cells when compared with the parent compound CFM-4. Nevertheless, both the compounds function in part by stimulating apoptosis. Since CFMs function in part by binding with CARP-1 and interfere with activity of the Anaphase Promoting Complex/Cyclosome (APC/C) E3 ligase, our studies also revealed a CARP-1 requirement in transduction of growth inhibitory effects of CFM-4.16 in the RCC cells. At the molecular levels, CFMs target mitotic

cyclin B1 and cause apoptosis in the parental and resistant RCC cells. This loss of cyclin B1 and stimulation of apoptosis by CFMs in RCC cells would be consistent with our prior findings demonstrating promotion of G2M cell cycle arrest, loss of mitotic cyclin B1, and apoptosis stimulation by CFMs in other cancer cell models [158–160,168]. In this regard, the novel class of CFM scaffold that stimulate G2M arrest as well as cause apoptosis hold potential for therapeutic use for targeting drug-resistant cancers especially in RCC.

3.6. Conclusion

The CFM compounds have been investigated for (i) the molecular mechanisms of RCC cell growth inhibition, and (ii) to the extent these compounds inhibit growth of drug (Everolimus)-resistant RCC cells. Conclusively, the current in vitro data is highly encouraging, and indicate that CFMs inhibit growth of parental, wild-type as well as Everolimus-resistant RCC cells in part by promoting apoptosis signaling. Clearly, there is a need for further in vivo testing of these compounds in animal tumor models of RCC. However, CFM compounds suffer from an inherent drawback of poor aqueous solubility and its dose escalation for systemic administration remains highly challenging.

4. CHAPTER 4: A CARP-1 FUNCTIONAL MIMETIC LOADED IN VITAMIN E-TPGS MICELLAR NANO-FORMULATION FOR INHIBITION OF RENAL CELL CARCINOMA UTILIZING EPR EFFECT

Some results from the following studies have been published: Oncotarget Journal, Cheriyan, V. T. *, Alsaab, H. O., *, et al., (2017). A CARP-1 functional mimetic loaded vitamin E-TPGS micellar nano-formulation for inhibition of renal cell carcinoma. Oncotarget, 8(62), 104928. *Equal contribution.

4.1.Objectives

Studies will be performed (i) to test the *in vitro* efficacy of the CFM 4.16 loaded in vitamin E TPGS based nano-formulation in parental, wild-type RCC and Everolimus-resistant RCC cells as well as (ii) perform proof-of-concept studies to explore their antitumor response in a clinically relevant RCC mouse model. Specifically, we aim to achieve (1) an increased serum bioavailability of CFM-4.16 nano-formulation following i.v administration; (2) increased nano-formulation accumulation and retention within the tumor (by the EPR effect) and therefore (3) an increased localized CFM-4.16 concentration in tumor tissues relative to free drug, thus producing a marked antitumor response.

4.2. Introduction

Recent studies reported development of various strategies to circumvent the poor aqueous solubility of many compounds in order to improve the outcomes of anticancer therapy. In this study, we will thus employ a nanotechnology advanced technique to tackle the poor aqueous solubility of a potent CFM compound (CFM-4.16) that has restricted its clinical utility as a therapeutic anticancer agent. Additionally, in order to improve the outcomes of anticancer agents, strategies to circumvent the poor aqueous solubility have been studied extensively in recent years. One of these strategies is to utilize D-alpha-tocopheryl polyethylene glycol succinate (Vitamin E TPGS) which is a water-soluble derivative of a PEGylated vitamin E (Vitamin E conjugated with

PEG). TPGS has an amphiphilic structure comprised of a hydrophobic alkyl tail and a hydrophilic polar head. The amphiphilic nature of TPGS confers it an excellent ability to encapsulate hydrophobic drugs, forming nano-micelles[172–175]. The nano-micelles with low critical micellar concentrations thereby improve the solubility, stability and bioavailability of the loaded lipophilic drug. Other groups previously have demonstrated that TPGS features such as bulky structure and large surface area makes it as an excellent solubilizer and enhancer for hydrophobic drug bioavailability. In addition, TPGS delivery system by itself could inhibit P-glycoprotein MDR and promote a synergistic anticancer effect. We also chose styrene-maleic acid (SMA) polymer with a relatively low molecular weight of 1.6 kDa for generation of SMA-TPGS block copolymer that could enhance the formation of nano-micelles. It was selected as a block copolymer with TPGS based on its favorable properties as reported earlier. The critical reason for choosing SMA for polymeric nano micelles is due to their favorable properties for in vivo delivery such as high drug loading, good water solubility, nontoxicity, and biosafety. These nano-micelles have high drug loading, good water solubility, nontoxicity, and biosafety profiles for use in vivo delivery of drug payload. In this regard, the native SMA polymer conjugated to neocarzinostatin (SMANCS) was approved for human use [176–178].

In the current study, we investigated the efficiency of drug delivery of novel CFMs analog nano-formulation and their effects on circumventing the water solubility obstacle to permit intravenous administration. Furthermore, we aimed to test the *in vitro* efficacy of the CFM 4.16 loaded in vitamin E TPGS based nano-formulation in different cancer cell lines as well as performed proof-of-concept studies to explore the mechanism of action of these newly developed small molecules inhibitors. Also, we investigated (i) the extent to which these CFM nanoformulations inhibit growth of drug (Everolimus)-resistant RCC cells, and (ii) whether the

SMA-TPGS nano-formulation of CFM-4.16 circumvents the solubility concerns of CFM compounds to permit its intravenous administration in conducting *in vivo* studies. Our data indicate that CFMs inhibit growth of parental as well as Everolimus-resistant RCC cells in part by promoting apoptosis. The TPGS-based nano-formulation of CFM-4.16 inhibits viability of RCC cells *in vitro* and their growth as xenografted tumors in immunocompromised mice.

4.3. Materials and Methods

4.3.1. Chemicals and Reagents

CFM-4.16 was synthesized by Dr. Scott Larsen (University of Michigan) and provided to Dr. Rishi (KCI) and has been recently described. All the CFMs were dissolved in DMSO at a stock solution of 10-50 mM and stored at –20°C. Everolimus was purchased from SelleckChem, Boston, MA. Styrene maleic anhydride (SMA, MWt 1600) and D-alpha-tocopheryl polyethylene glycol succinate (Vitamin E TPGS) were obtained from Sigma Aldrich, St Louis, MO). All other reagents will be purchased at analytical reagent grade from Sigma Aldrich (St Louis, MO) and used without further purification.

4.3.2. Cell Lines and Cell culture supplies

RCC cell lines Caki-1, Caki-2, ACHN, and A-498 were kindly provided by and Dr. Rajvir Dahiya, Department of Urology, San Francisco Veterans Affairs Medical Center and University of California San Francisco, San Francisco, CA. The RCC UOK262 and UOK268 cells were kindly provided by Dr. WM Linehan, Urologic Oncology Branch, Center for Cancer Research, National Cancer Institute, National Institutes of Health, Bethesda, MD. The Caki-1 and Caki-2 were grown in RPMI 1640 medium, and UOK 262, UOK 268, and Huh7 were routinely cultured in DMEM medium. All the cell culture media were also supplemented with 10% FBS, 100 units/ml

of penicillin, and 100 μg/ml of streptomycin, and the cells were maintained at 37 °C and 5% CO2. For cell growth and MTT studies, the cells were cultured in fresh media with 5% FBS prior to their treatments with various agents.

DMEM, EMEM medium and antibiotics (penicillin and streptomycin) were purchased from Invitrogen Co. (Carlsbad, CA). Fetal bovine serum (FBS) was purchased from Denville Scientific Inc. (Metuchen, NJ), and DMSO was purchased from Fisher Scientific (Fair Lawn, NJ). Enhanced Chemiluminescence Reagent kit was purchased from Amersham Biosciences (Piscataway, NJ) and the Protein Assay Kit was purchased from Bio-Rad Laboratories (Hercules, CA). The affinity purified, anti-CARP-1 polyclonal antibodies were described before [160,168]. The mouse monoclonal antibody for b–actin and 3-[4, 5-Dimethylthiazol-2-yl]-2,5diphenyltetrazolium bromide (MTT) were obtained from Sigma-Aldrich (St. Louis, MO). Rabbit polyclonal antibodies for Cyclin B1, Cleaved Caspase-8, PARP, phospho and total p38a/b, phospho and total JNK1/2 SAPKs were obtained from Cell Signaling Technology (Beverly, MA).

4.3.3. SMA-TPGS Synthesis and micellar nano-formulation fabrication and characterization

The block copolymer (SMA-TPGS) was first synthesized by adding known amounts of TPGS in $NaHCO_3$ buffer at pH 8.9 with fixed amounts of anhydrous SMA to afford the anhydride ring opening reaction of SMA with the alcohol group of TPGS. All unconjugated reagents were removed by ultrafiltration (Millipore TFF, Milford, MA) of the SMA-TPGS conjugate prior to its lyophilization. We characterized nano-micelles by proton nuclear magnetic resonance spectroscopy (^{1}H NMR) and Fourier transform infrared spectroscopy (FTIR). The structure of the synthesized SMA-TPGS copolymer was detected by ^{1}H NMR in D_2O. The -CH protons and methyl protons of SMA segment had signals at 5.2 and 1.69 ppm, respectively. The -CH2 protons

of PEO part of TPGS had the peak at 3.65 ppm. We noted the lower peaks in the aliphatic region that belong to various moieties of vitamin E tails [179,180]. The proper synthesis of the SMA-TPGS copolymer was also confirmed by the FTIR analysis and was not found to be a physical mixture of TPGS with SMA as all measurements indicated the absence of any free crystalline particles in nano-micelles preparation. Both SMA and TPGS inhibited crystallization of CFM-4.16 during nano-micelles formulation. We then fabricated the CFM loaded micelles according to our earlier published protocols [155,161,162,181–187], followed by characterization of micelles for size, charge, critical micelles concentration (CMC), and drug loading as below. For Morphology, Transmission Electron Microscopy (TEM) of the nanoparticles was assessed using JEOL JEM-1000 instrument (JEOL Ltd, Tokyo, Japan). Then, the products obtained were stored in the freezer until further use.

4.3.4. Particle size, and zeta potentials

The particle size and surface charge (zeta potential, ζ), measurements were performed using a Beckman Coulter Delsa Nano-C-DLS Particle analyzer (Miami, FL) equipped with a 658 nm He-Ne laser. For particle size, we suspended the nano-micelles in de-ionized (DI) water and detected the scattered light at 165° angle. We then obtained the peak average histograms from the intensity, volume and number from 70 scans to calculate the average diameter of the particles. The zeta potentials were evaluated by measuring the electrophoretic mobility of the charged particles under an applied electric field.

4.3.5. The Loading efficiency of SMA-TPGS-CFM nano-micelles

We evaluated the CFM-4.16 loading content percentage in SMA-TPGS nano-micelles by High-Performance Liquid Chromatography (HPLC). First, a method for analyzing drug content

was developed and validated according to ICH guidelines [188]. We measured the standard curve of CFM-4.16 in DMSO and its successive dilutions with mobile phase at 309 nm (λ_{max}). The calibration curve was linear in the range of 50–50,000 ng/ml with a correlation coefficient (R2) = 0.9999. The loading efficiency of micelles was calculated by dissolving a known amount of nano-micelles directly in DMSO and further dilution of drugs with the mobile phase followed by determination of the absorbance at 309 nm with respect to the standard curve as described previously [169].

4.3.6. Drug Encapsulation Efficiency (EE)

Free drug (non-incorporated in the SMA-TPGS) was separated by ultrafiltration centrifugation technique. Briefly, 1 mL of CFM-4.16 and SMA-TPGS-CFM 4.16 colloidal solution were placed in the upper chamber of a centrifuge tube matched with an ultrafilter and centrifuged for 15 min at 4000 rpm. The total drug content in CFM-4.16 nano-formulation was determined as follows. Aliquots of 1mL formulation dispersion were diluted appropriately by ethanol to dissolve the TPGS-SMA ingredient, and the resulting suspension was then filtrated through 0.45μm membrane filters. The filtered solution was analyzed by Waters® Alliance e2695 HPLC using Symmetry® C18 column (250mm × 4.6mm, 5μm). The mobile phase was a mixture of Acetonitrile, Methanol, 10mM KH2PO4 buffer (65:20:15 v/v) with pH adjusted to 2, and the flow rate was maintained at 1.0mL/min. All the samples were analyzed at 309nm using empower PDA software. We then calculated the encapsulation efficiency (EE) and drug loading content (DLC) by the following equations:

$$\textbf{Drug loading content (DLC)} = \frac{\textbf{weight of CFM-4.16 encapsulated in micelles}}{\textbf{Total weight of CFM-4.16 loaded in micelles}} \textbf{x100} \qquad \text{Equation (1)}$$

$$\textbf{Encapsulation Effeciency (EE)} = \frac{\textbf{Mass of CFM-4.16 encapsulated in micelles}}{\textbf{Total mass of CFM-4.16 initially loaded in micelles}} \textbf{x100} \qquad \text{Equation (2)}$$

4.3.7. Cell viability assays (MTT)

The cytotoxicity of CFM-4.16, SMA-TPGS copolymer, SMA-CFM-4.16, SMA-TPGS-CFM-4.16 in the RCC cells (A498, UOK262, and UOK268) was assessed by MTT assay. First, we seeded 5 X 10^3 cells in the 96-well plate in triplicate, allowed the cells to grow in fresh culture media for another 24h, and treated them with respective agents for the noted dose and time. Control cells were treated with 0.1% DMSO in culture medium. After treatment, we performed an MTT assay. Briefly, 20 µl of 1mg/ml of MTT was added to each well and cells were incubated for 2-4h at 37^0C. MTT was removed, and the resulting formazan products were dissolved by adding 50µl DMSO/well followed by colorimetric analysis using a multi-label plate reader at 570 nm (Victor3; PerkinElmer, Wellesley, MA).

4.3.8. Protein expression (WB) Assays

For protein expression analysis, the cells will be either untreated or treated with CFM-4.16 or SMA-TPGS-CFM-4.16 nano-formulation for various times. Cells will be lysed in cell lysis (10X) buffer containing 0.1%% of protease and phosphatase inhibitor cocktail (Sigma) for 20 min at 4ºC. The cell lysates will be centrifuged at 14,000 rpm at 4ºC for 15-20 min to remove debris. Protein concentrations of the clarified cell lysates will be determined using the Protein Assay Kits. The cell lysates (50-100µg from each sample) will be separated by SDS-PAGE and transferred to PVDF membrane (Bio-rad, Hercules, CA) by standard procedures. The membranes will be then hybridized with primary antibodies followed by incubation with appropriate secondary antibodies. The antibody-bound proteins were pictured by treatment with the chemiluminescence detection reagent based on manufacturer's instructions, followed by exposure to X-ray film (Denville Scientific Inc.). The same membranes will be re-probed with the anti-β-actin antibody, which will be used as an internal control for protein loading.

4.3.9. Three-dimensional Renal sphere assays

The RCC cells were obtained from xenograft tumors derived from parental cells (see below) or from the parental and Everolimus-resistant RCC cells from a two-dimensional culture plate with ~70-80% confluence. We performed the three-dimensional renal sphere cultures by essentially following the methods described by us before [169]. Briefly, the cells were washed twice in 1 x PBS and trypsinized following established protocols. We then pelleted the cells at 200 x g at room temperature and re-suspended them in 5ml of sphere media (DMEM/F12 supplemented with 2mM L-glutamine, 100 U/ml penicillin, 100 U/ml streptomycin, 1 x B27 supplement, 20ng/ml recombinant human epidermal growth factor (EGF; Sigma), and 10ng/ml recombinant human basic fibroblast growth factor (bFGF; R&D Systems). We seeded ~5000 viable cells per ml in an ultra-low adherent 60mm plate and incubated them at 37°C and 5% CO_2 for two weeks without disturbing the plates. After the spheres formed, we added fresh media with or without 10μM CFM-4.16 and continued incubating cells for additional 24h at 37°C and 5% CO_2. At the end of the incubation period, we photographed the spheres in the untreated and treated plates as described [45].

4.3.10. Maximum tolerated dose (MTD) analysis and experimental design

Healthy non-tumor mice will be used to establish the MTD of the CFM-4.16. The MTD of CFM-4.16 is 30 mg/kg [159], thus the tolerance study will be find. The dose-limiting toxicity (DLT) is weight loss ≥10%. The study will begin at dose 30 mg/kg for CFM-4.16 and 60 mg/kg. If there are any DLTs, the level of CFM-4.16 will be reduced to 25 mg/kg and another cohort evaluated. If there are any DLT in this cohort, then CFM4.16 will be reduced by 20%.

4.3.11. Establishment of RCC cell-derived xenografts in immunocompromised mice

The experiments involving generation of RCC cell-derived sub-cutaneous xenografts were performed according to our previously published methods and protocols approved by the Institutional Laboratory Animal Care & Use Committee (IACUC) at the Wayne State University [160,169]. Female, 5-weeks old NCR SCID mice with Lc Background were purchased from Charles River Laboratories (Horsham, PA). For subcutaneous (sc) tumor xenograft studies, we first determined maximal tolerated doses for CFM-4.16 (prepared in 10% DMSO/Cremophor + distilled, sterile water, and pH adjusted to 4.5), SMA-TPGS copolymer, SMA-TPGS-CFM-4.16, and SMA-CFM-4.16 preparations. The MTD for free CFM-4.16 (prepared in DMSO/Cremophor) have been described before, and a 30mg/kg/day iv injection was judged safe a total dose of 482mg/kg provoked a mild ataxia with some tail and leg twitching that resolved within 1-2 minutes. This dose/schedule of free CFM-4.16 produced a mild weight loss of 1.6% body weight by day 7(recovery by day 18). No other histological abnormalities were noted [160,169]. A 30mg/kg/day dose of SMA-TPGS, was injected (iv) while a 30mg/kg/day of SMA-TPGS-CFM-4.16 was administered by oral gavage in two female, NCR SCID mice for 10 days. The animals did not show any signs of toxicity, discomfort, or any histological abnormalities. These observations indicate suitable toxicity profile of SMA-TPGS copolymer and its CFM-4.16 formulation. However, the iv injections of a 30mg/kg were best tolerated when administered on alternate days. Accordingly, for the efficacy studies we chose to administer daily the block copolymer by iv route while the micellar formulation with CFM-4.16 was administered by oral gavage. The iv administration of the CFM-4.16 micellar formulation was conducted on every alternate day.

For efficacy studies, after a suitable period of acclimation, we subcutaneously implanted a suspension of 1 x 10^6 A498 RCC cells in 200µl of serum-free Hank's balanced salt solution in

flanks of each animal using a 27-gauge needle. Tumors were allowed to grow unperturbed for 10-14 days. When tumors became palpable (200 mm^3), the mice were randomly assigned to treatment or control groups of eight animals each. Mice were treated with Control, PBS only, SMA-TPGS copolymer (30mg/kg; iv), SMA-TPGS-CFM-4.16 formulation (30mg/kg/day) by oral gavage for 10 days. In the case of the group of mice treated with iv administration of SMA-TPGS-CFM-4.16 formulation (30mg/kg), only two injections were administered where the first dose was followed by the second dose on the alternate day. The tumor weight and volume were measured daily, and mice were observed for changes in weight and side effects. The endpoints for assessing antitumor activity consisted of tumor weight, tumor growth inhibition (%T/C), and tumor cell kill Log10. Tumor weight (mg) = (A X B2)/2 where A and B are the tumor length and width (in mm), respectively. Tumor growth inhibition (T/C) was the median tumor weight in the treated group (T) when the median tumor weight in the control group reached 750mg. Results were expressed as percentage. According to NCI-accepted criteria, a treatment is considered effective if T/C is < 42%. Tumor growth delay (T-C) is the difference between the median time (in days) required for the treatment group tumors (T) to reach 1000 mg and the median time (days) for the control group tumors to reach the same weight. The animals were sacrificed on day 10 and tumor tissues were collected immediately after tumor volume measurement. Tumor volumes were calculated by the modified ellipsoidal formula. Tumor volume = 1/2(length × width2). Representative tumor samples were stored at –80°C for subsequent analysis.

4.3.12. Statistical analysis

The Data will be presented as mean ± SD for the absolute values for all experiments. The cell growth inhibition after treatments will be statistically evaluated using Graph Pad Prism 6.0 software (Graph Pad Software Inc., San Diego, CA Comparisons will be made between control

and treatment groups. P<0.05 will be used to indicate statistical significance. For *in vivo* experiments, the statistical significance of differential findings between all formulations and control mice will be determined by Student's t-test. The p-values smaller than 0.05 will be considered statistically significant. The data were expressed as mean ± SEM and analyzed using a two-tailed Student t-test or one-way ANOVA followed by a post hoc test. A p value of <0.05 was considered statistically significant.

4.4. Results

4.4.1. Nanomicellar formulation Synthesis and characterization

The block copolymer (SMA-TPGS) was first synthesized and well characterized. The so-formed SMA-TPGS conjugate was purified by ultrafiltration to remove all unconjugated molecules before lyophilizing. Figure 4.1 illustrates the schematic representation of the Nanocarrier synthesis by using EDC/NHS coupling chemistry.

4.4.1.1. H-NMR and FTIR

Nanomicelles were characterized by proton nuclear magnetic resonance spectroscopy (^{1}H NMR) and Fourier transform infrared spectroscopy (FTIR). The structure of the synthesized SMA-TPG copolymer was detected by ^{1}H NMR in D2O. Figure 4.2(A) shows a typical ^{1}H NMR spectroscopy of the SMA-TPGS copolymer and monomers. The signals at 5.2 and 1.69 ppm were assigned to the -CH protons and methyl protons -CH3 of SMA segment, respectively. The peak at 3.65 ppm was assigned to the -CH2 protons of PEO part of TPGS. The lower peaks in the aliphatic region belong to various moieties of vitamin E tails [173,179,189]. In FTIR analysis, we confirmed that the SMA-TPGS copolymer was synthesized by the EDC/NHS coupling chemistry as it is shown in Figure 4.2(B). The product was not a physical mixture of TPGS with SMA and all measurements indicated the absence of any free crystalline particles in nanomicelles preparation and both SMA and TPGS could inhibit crystallization of CFM4.16 during nanomicelles formulation.

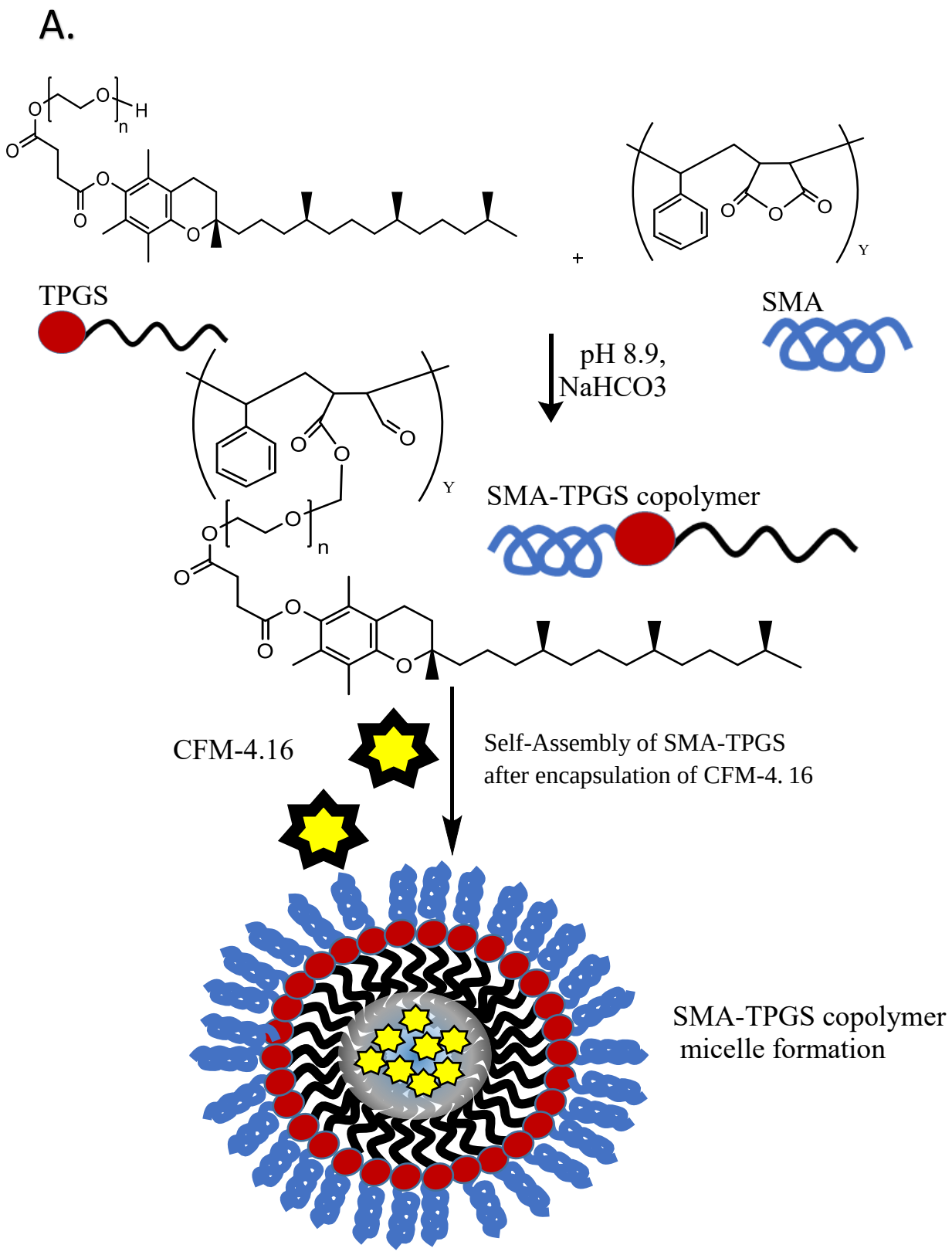
A.
TPGS
SMA
pH 8.9,
NaHCO3
SMA-TPGS copolymer
CFM-4.16
Self-Assembly of SMA-TPGS
after encapsulation of CFM-4. 16
SMA-TPGS copolymer
micelle formation

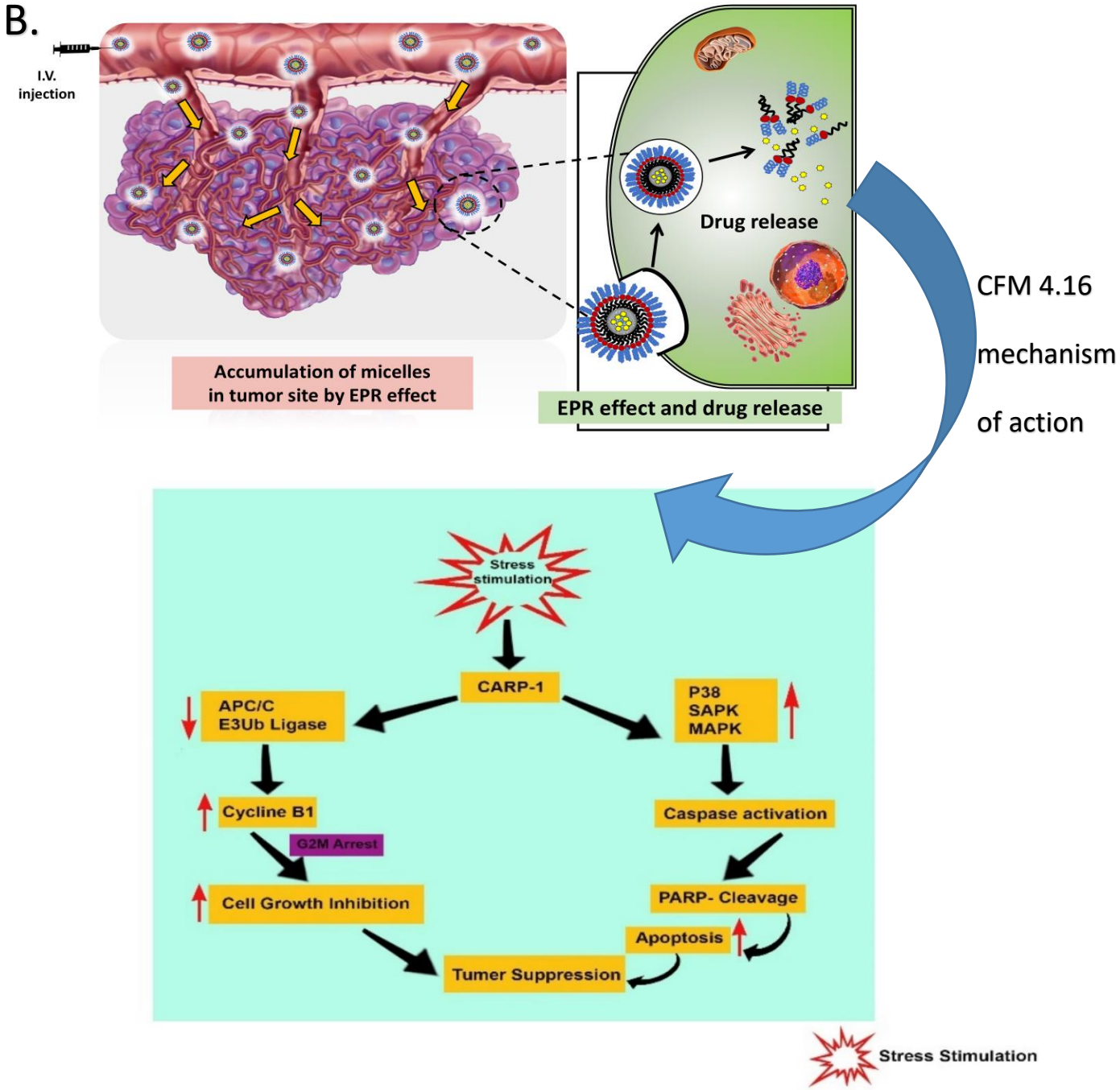

Figure 4.1. (A) The pictorial representation of SMA-TPGS copolymer synthesis with encapsulation of CFM-4.16 and (B) accumulation of nano-micelles (SMA-TPGS-CFM-4.16) and internalization at tumor site by endocytosis due to EPR effect. Then, a schematic representation for mechanism of action of CFM-4.16. It is works on inhibition of CARP-1 binding with APC/C subunit APC2. Also, it inhibits the growth of tumor cells in part by inducing CARP-1 expression, promoting PARP cleavage, activating pro-apoptotic stress-activated protein kinases (SAPK) p38 and JNK, and apoptosis.

(A)

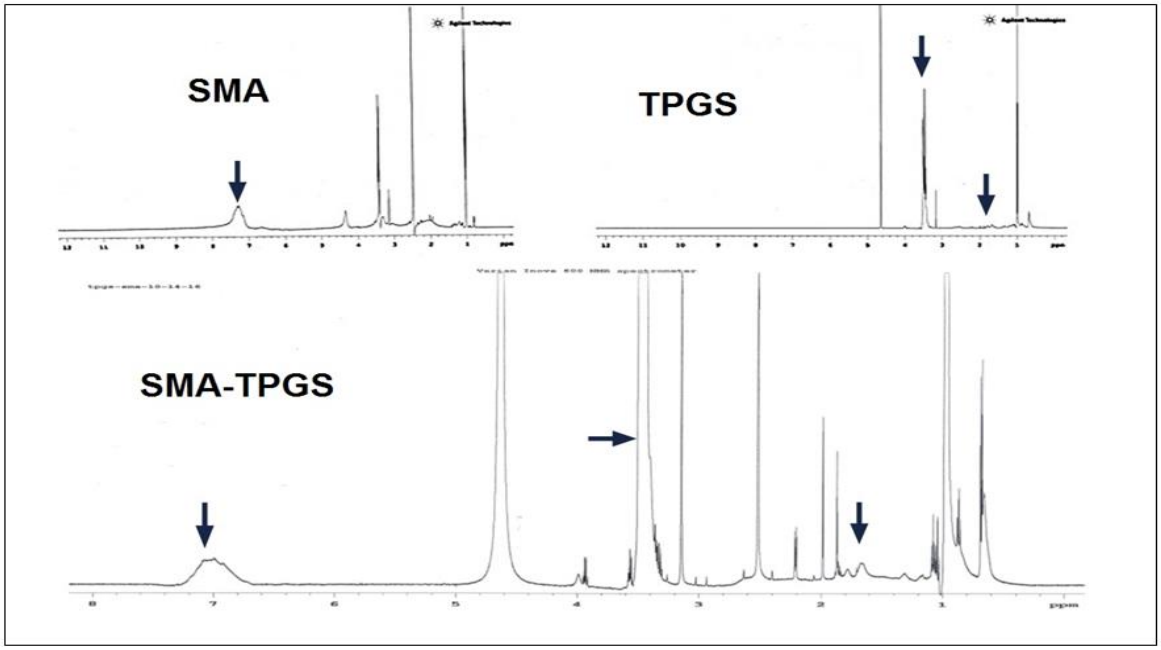

(B)

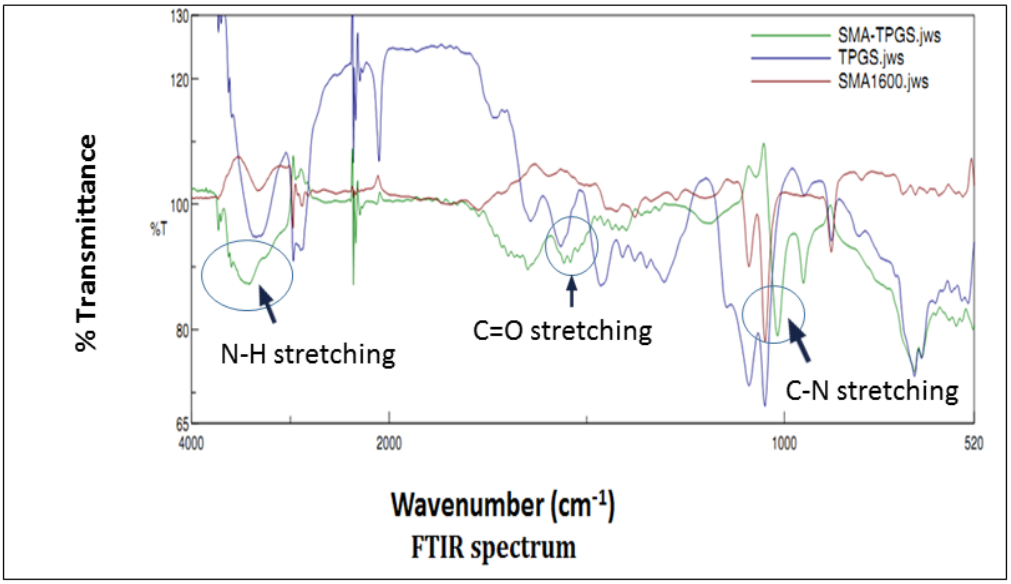

Figure 4.2. (A) [1]H NMR profile for polymers used (SMA and TPGS) and the conjugated polymer (SMA-TPGS). The structure of the synthesized SMA-TPGS copolymer was detected by [1] H NMR in D2O. The -CH protons and ring protons of SMA segment had signals at 1.69 ppm and 7.3 ppm, respectively. The-CH2 protons of PEO part of TPGS had the peak at 3.65 ppm. We noted the lower peaks in the aliphatic region that belong to various moieties of vitamin E tails. These peaks have been identified as well in the conjugated polymer as indicated by arrows. **(B)** FTIR data for polymers used (SMA and TPGS) and the conjugated polymer (SMA-TPGS). The arrows indicated

forming an amide bond between the conjugated polymer (SMA-TPGS). Peaks were identified for C-N bond, C=O stretching, and N-H stretching at around 1100, 1640-1690, and 3100-3500 cm−1, respectively. Adapted from [1].

4.4.1.2.Particle size distribution and zeta potential

Using dynamic light scattering (DLS), the average size and size distribution of the micelles was shown in Figure 4.3 and Table 1 (mean ± SD, n=3). The mean diameter, the polydispersity index, and the Zeta potential of SMA-TPGS-CFM-4.16 were 144.6nm±20nm, 0.275, and -7.86Mv, respectively. The drug-loaded nanoparticles can be prepared with or without TPGS added as a copolymer in the fabrication process. This is because the TPGS component in the copolymer has a self-emulsifying function. This is an advantage of the SMA-TPGS copolymer in nanoparticle formulation, which circumvents the side effects of the traditional formulation vehicle Cremophor EL®, which has been used for various poorly-water soluble drugs.

The particle size for all samples was found around 146 nm with narrow size distribution of less than 0.275 polydispersity. The obtained results, of particle size of CFM4-16 loaded nanomicelles was ~145 nm and surface charge were -7.86 mV Figure 4.3 (A). It can be observed from Table 4.1 that addition of TPGS in the process as emulsifier slightly increased the particle size. This is because the coating effects of TPGS on the particle surface and extra TPGS on the particle surface may cause aggregation of the formed nanoparticles. Zeta potential determines the particle stability in dispersion. High absolute value of the zeta potential defines high surface charge of the nanoparticles, which leads to strong repellent interactions among the nanoparticles in dispersion and thus high stability. The zeta potential of the TPGS emulsified, CFM-4.16-loaded SMA-TPGS nanoparticles was found to be about -7.86 mV. Similar results were found for the SMA-CFM-4.16 loaded nanoparticles.

(A)

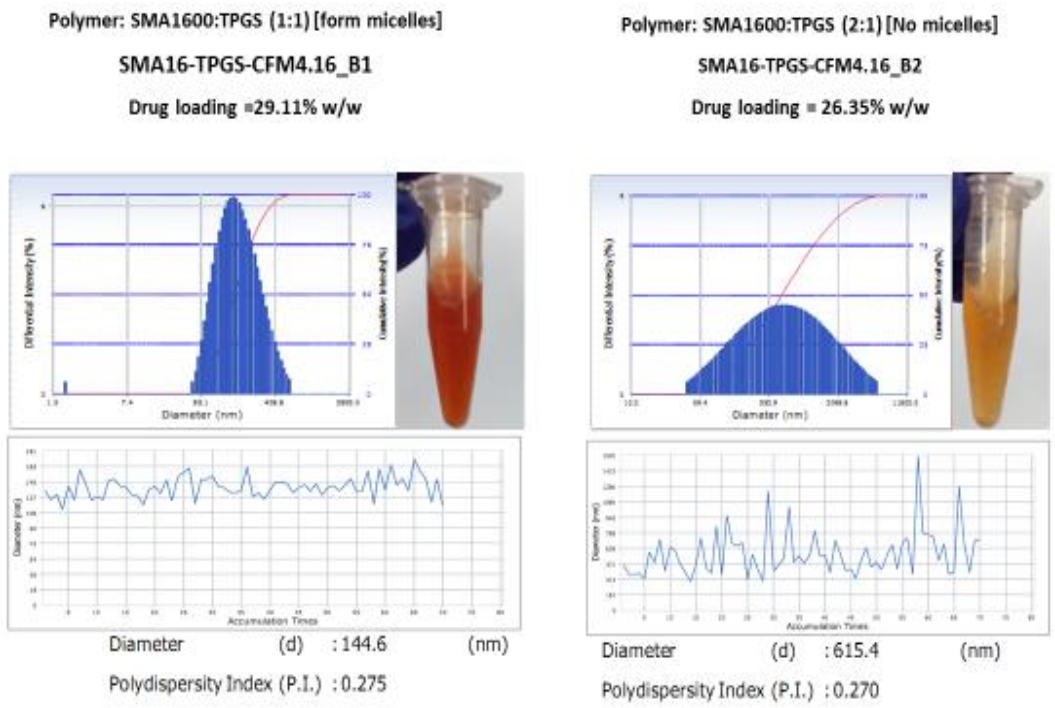

(B)

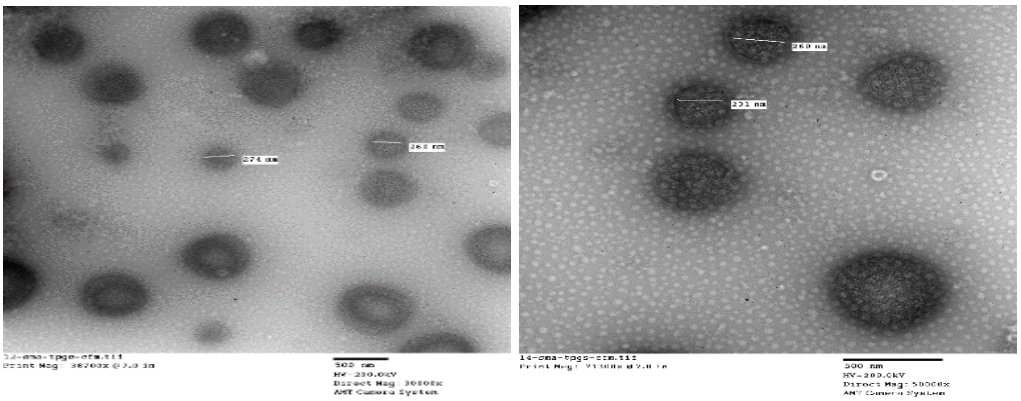

Figure 4.3. (A) Particle size and Zeta potential characterization of SMA-CFM and FA-SMA-CFM using Dynamic light scattering (DLS) technique; (B) Transmission Electron Microscopy for optimized SMA-TPGS Nano micelles.

4.4.1.3. Critical Micellar Concentration (CMC) and TEM (Morphology)

Additionally, Surface morphology of the drug-loaded SMA-TPGS nanoparticles was examined by Transmission Electron Microscopy (TEM). It showed in Figure 4.3 (B) the particle

size (160nm) little bigger than the one tested by DLS. It also showed the micelles nanoparticles were spherical or quasi-circular and homogenous with no aggregates were existed. The particles seemed to have smooth surface within the TEM resolution level. The smooth surface may contribute to a slower drug release from the nanomicelles than that from those of rough surface. No difference was noticed between CFM-4.16 loaded and unloaded nanomicelles in term of morphology. The loading of CFM-4.16 has no significant effect in nanomicellar mean diameter, polydispersity index, and Zeta potential in comparison to unloaded nanomicelles. These results indicate that the size and surface properties are optimal and safe for intravenous injection as well as ideal for tumor delivery by passive targeting (by the EPR-effect[153,155,190,191]). The micelles were also characterized for critical micelles concentration (CMC) and it was identified as 0.01 mg/ml Figure 4.3(A).

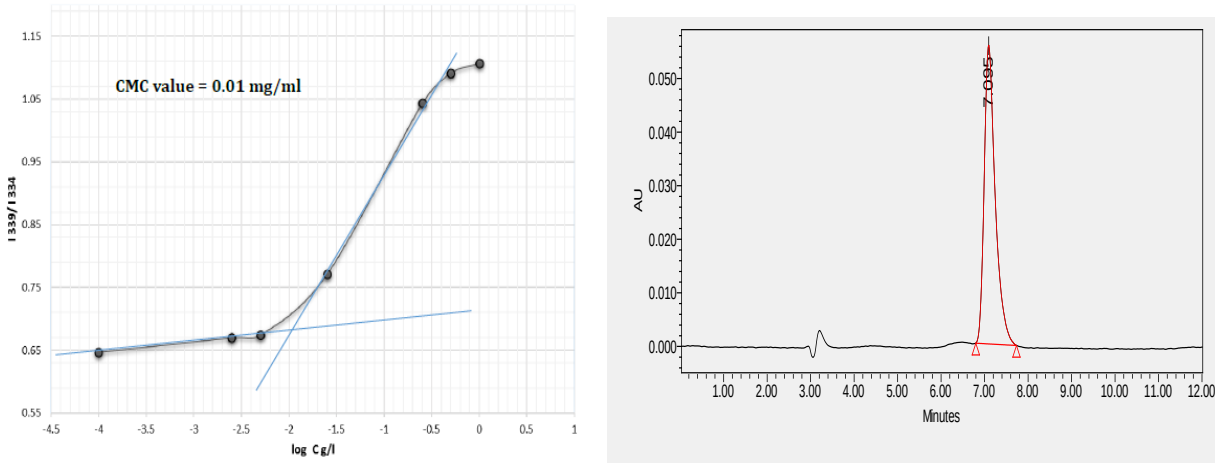

Figure 4.4. (A) Critical micellar concentration (CMC) for SMA-TPGS nanomicelles.(B) HPLC method validation and chromatogram.

4.4.1.4. Drug Loading and Encapsulation efficiency

It has been known that the polymer used in the fabrication process and the drug loading level are important factors to influence the particle size and size distribution and the drug

encapsulation efficiency in the polymeric nanoparticles [192]; as results, it will determine the drug release kinetics, cellular uptake and then the therapeutic efficacy of the drug-loaded nanoparticles [189,193,194]. Table 4.1 also shows the drug loading and TPGS effects on size and size distribution and the drug loading efficiency. It can be identified that the SMA-TPGS nanoparticles prepared with no emulsifier (TPGS) added can result in satisfactory drug EE, which was found to be 77% for 17% drug loading and with TPGS to be 85.5% for 29% drug loading found by HPLC as shown in Figure 4.4 (B). This is normal since the higher the drug loading is because there will be more space for drug encapsulation with taking the advantage of TPGS amphiphilic structure. For the less drug loading of 17% in case of SMA-CFM-4.16; however, the EE of the CFM-4.16-loaded SMA-TPGS nanoparticles can be improved by adding TPGS in the process as emulsifier. Nevertheless, the amount of TPGS to be added should be carefully figured out. The amphipathic surfactants align themselves at the oil–water interface to promote the stability of the particles by lowering the surface energy and thus resist coalescence and flocculation of the particles.

Table 4.1. Characterization of SMA-TPGS nano-micelles

Sample	**CMC (mg/ml)**	**Hydrodynamic size (nm)**	**PDI**	**Zeta potential (mV)**	**EE (%)**
SMA-TPGS-CFM-4.16	0.010	144.6±20nm	0.275±0.05	-7.86 ±4	85.5±12
SMA-CFM-4.16	0.023	123±31nm	0.163±0.07	-18±5	77±9

Abbreviations: SMA, styrene maleic acid; TPGS, d-α-tocopheryl polyethylene glycol succinate; CMC, critical micelle concentration; PDI, polydispersity index; EE, encapsulation efficiency.

4.4.1.5. Stability indication characterization

Storage conditions of 4 °C, 25 °C, and 35°C with light protection for 2 months as shown in Table 4.2 indicated that the CFM-4.16 remains encapsulated in the nano-micelles, indicating that SMA-TPGS-CFM-4.16 nanoformulations were very stable with a recovery percentage of

99.73±1.10 at 4 °C, 94.9±7.2 % at 25 °C, and 92.88 ±1.78 at 35°C. These results indicated that both conditions (4 °C and 25 °C) would be more appropriate for storing the nanoformulations.

Table 4.2. Percent drug content of nanomicellar formulations after 60 days (n=3). Values expressed as mean ± standard deviation (SD)

Formulation	**Temperature**		
	4ºC	**25ºC**	**35ºC**
SMA-TPGS-CFM4.16 (% drug content)	99.73±1.10	94.9±7.2 %	92.88 ±1.78
SMA-CFM4.16 (% drug content)	101.41± 0.53	96.42±0.42	90.81±1.32

4.4.2. Nanomicellar formulation of CFM-4.16 improve its release kinetics characteristics

The CFM compounds have poor aqueous solubility and consequent poor bioavailability for their use and development as potential anti-cancer agents. To address this issue, we previously generated and tested nano-lipid formulations (NLFs) of CFM-4 and CFM-4.16 compounds. These NLFs resulted in significant improvements in overall bioavailabilities of CFM-4 and CFM-4.16 when compared with the respective free compound [160,169]. Here we generated nano-micellar formulations of CFM-4.16 and tested their abilities to inhibit growth of parental and resistant RCC cells *in vitro* and *in vivo*. As a first step, we synthesized, purified, and characterized a block copolymer (SMA-TPGS) as detailed in methods. The proton nuclear magnetic resonance spectroscopy (^{1}H NMR) and Fourier transform infrared spectroscopy (FTIR) analysis revealed that the SMA-TPGS copolymer was a conjugate and not a physical mixture of TPGS with SMA Next, we generated and characterized SMA-CFM-4.16 and SMA-TPGS-CFM-4.16 formulations. The mean diameter, the polydispersity index, and the Zeta potential of SMA-TPGS-CFM-4.16 formulation were 144.6nm ±20nm, 0.275 ±0.05, and -7.86 ±4 mV, respectively. The mean diameter, the polydispersity index, and the Zeta potential of SMA-CFM-4.16 formulation however

were 123nm ±31nm, 0.163 ±0.07, and -18 ±5 mV, respectively. The slight increase in the particle size of the TPGS containing formulations is understandable, due to the hydrophilic PEG chains protruding out thereby increasing the hydrodynamic diameter. The critical micelles concentration (CMC) of the formulations was 0.010 and 0.023 mg/ml for SMA-TPGS-CFM-4.16 and SMA-CFM-4.16, respectively indicating high stability even on dilution of the sample. The Transmission Electron Microscopic (TEM) analyses did not indicate any morphological differences between CFM-4.16 loaded and unloaded nano-micelles (appendix). The loading of CFM-4.16 also had insignificant effect on the nano-micellar mean diameter, polydispersity index, or Zeta potential in comparison to the unloaded nano-micelles.

The type of polymer and the drug loading levels are critical factors that often influence drug release kinetics, cellular uptake and the therapeutic efficacy of the drug-loaded nanoparticles [192,195,196]. We then determined the encapsulation efficiency (EE) and drug loading content (DLC) for our formulations as detailed in methods. The EE and DLC for the SMA-CFM-4.16 was 77% and 17% respectively. The EE and DLC parameters for SMA-TPGS-CFM-4.16 preparation were 85.55 and 29%, respectively, suggesting improved loading due to the inclusion of emulsifier, TPGS. We next determined the stability of the formulations by their extended (2 months) storage at 4°C, 25°C, or 35°C with light protection. CFM-4.16 remained encapsulated in the SMA-TPGS nano-micelles with a recovery percentage of 99.73 ±1.10 at 4°C, 94.9 ±7.2 at 25°C, and 92.88 ±1.78 at 35°C. The recovery percentage of CFM-4.16 in SMA encapsulated formulation was 101.41 ±0.53 at 4°C, 96.42 ±0.42 at 25°C, and 90.81 ±1.32 at 35°C. Altogether, our results indicate that the CFM-4.16 micellar formulations have suitable drug loading and particle characteristics and can be stored at 4°C or at room temperature (25°C). Based on this information, we proceeded

to determine whether the CFM-4.16 nano-micellar formulations inhibit growth and viability of parental and drug-resistant RCC cells in vitro and in vivo as detailed below.

4.4.3. Nanomicellar formulation of CFM-4.16 inhibits growth of parental and Everolimus-resistant RCC cells *in vitro* and *in vivo* in part by stimulating apoptosis

Next, we treated the parental RCC cells and their respective, Everolimus-resistant sublines with various doses of block copolymer (SMA-TPGS), free CFM-4.16, SMA-CFM-4.16, and SMA-TPGS-CFM-4.16 for 24h. The RCC cell viabilities were determined as described in methods. As shown in Figure 4.5 A and B, the treatments of cells with various doses of block copolymer alone elicited a very modest to no loss of their viabilities when compared with their untreated counterparts. The free CFM-4.16 or its nano-micellar formulations, on the other hand, inflicted a significant loss of viabilities of the parental as well as Everolimus-resistant RCC cells when compared with their respective, untreated counterparts. Of note is the fact that the free compound or its formulations at the three respective doses of each provoked a generally similar degree of reduction in RCC cell viabilities that ranged between 40-80%. A498 parental and resistant RCC cells albeit were more sensitive to the 10μM dose of either of the micellar formulations when compared with their CFM-4.16 treated counterparts, overall a similar range of reduction in the viabilities of cells that were treated with free compound or its micellar formulations would suggest for an excellent *in vitro* activity of CFM-4.16 formulations. Consistent with our data in Chapter 3, the western blot analysis further revealed that treatments of parental or Everolimus-resistant RCC cells with 10μM dose of respective micellar formulations of CFM-4.16 also caused activation of pro-apoptotic SAPKs, P38α/β and JNK1/2, CARP-1 expression, and PARP cleavage when compared with their respective block copolymer (SMA-TPGS)-treated cells (Figure 4.5. C, D).

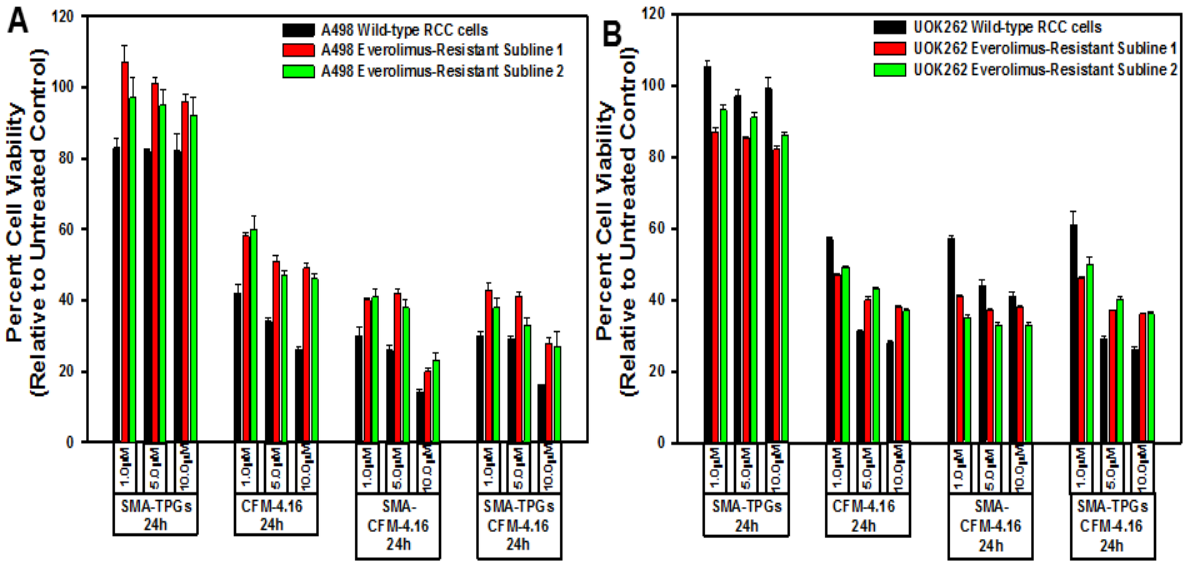
A
Percent Cell Viability
(Relative to Untreated Control)
A498 Wild-type RCC cells
A498 Everolimus-Resistant Subline 1
A498 Everolimus-Resistant Subline 2
1.0μM
5.0μM
10.0μM
SMA-TPGs 24h
CFM-4.16 24h
SMA-CFM-4.16 24h
SMA-TPGs CFM-4.16 24h
B
Percent Cell Viability
(Relative to Untreated Control)
UOK262 Wild-type RCC cells
UOK262 Everolimus-Resistant Subline 1
UOK262 Everolimus-Resistant Subline 2
SMA-TPGs 24h
CFM-4.16 24h
SMA-CFM-4.16 24h
SMA-TPGs CFM-4.16 24h

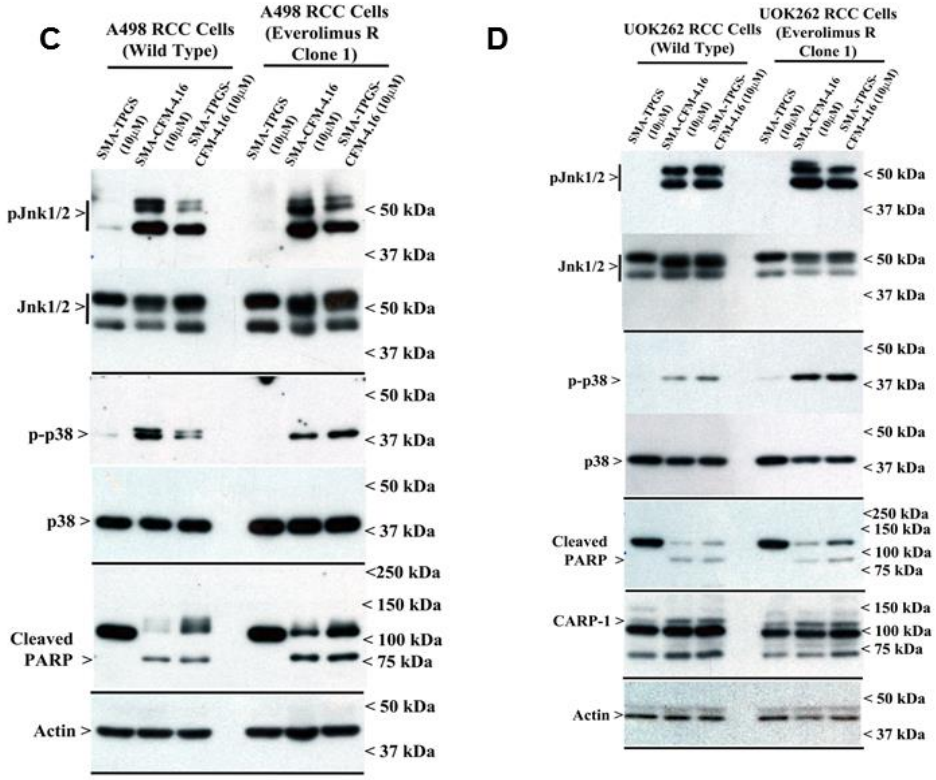
C
A498 RCC Cells (Wild Type)
A498 RCC Cells (Everolimus R Clone 1)
SMA-TPGS (10μM)
SMA-CFM-4.16 (10μM)
SMA-TPGS-CFM-4.16 (10μM)
pJnk1/2 >
Jnk1/2 >
p-p38 >
p38 >
Cleaved PARP >
Actin >
< 50 kDa
< 37 kDa
<250 kDa
< 150 kDa
< 100 kDa
< 75 kDa
D
UOK262 RCC Cells (Wild Type)
UOK262 RCC Cells (Everolimus R Clone 1)
CARP-1 >

Figure 4.5. Nano-micellar formulations of CFM-4. 16 inhibits growth and stimulates apoptosis in parental and Everolimus-resistant RCC cells. (A, B) Indicated RCC cells were either untreated (Control), treated with SMA-TPGS, CFM-4.16, SMA-CFM-4.16, or SMA-TPGS-CFM-4.16 for noted dose and time. (A, B) Cell viability was determined by MTT assay. The histogram columns represent means of three independent experiments with 4-6 replicates for each treatment; bars, S.E. (C, D) Cell lysates were analyzed by Western blotting (WB) as noted in Methods for levels of CARP-1, cleaved PARP and activation (phosphorylation) of pro-apoptotic p38, and JNK1/2 SAPKs essentially. Adapted from [1].

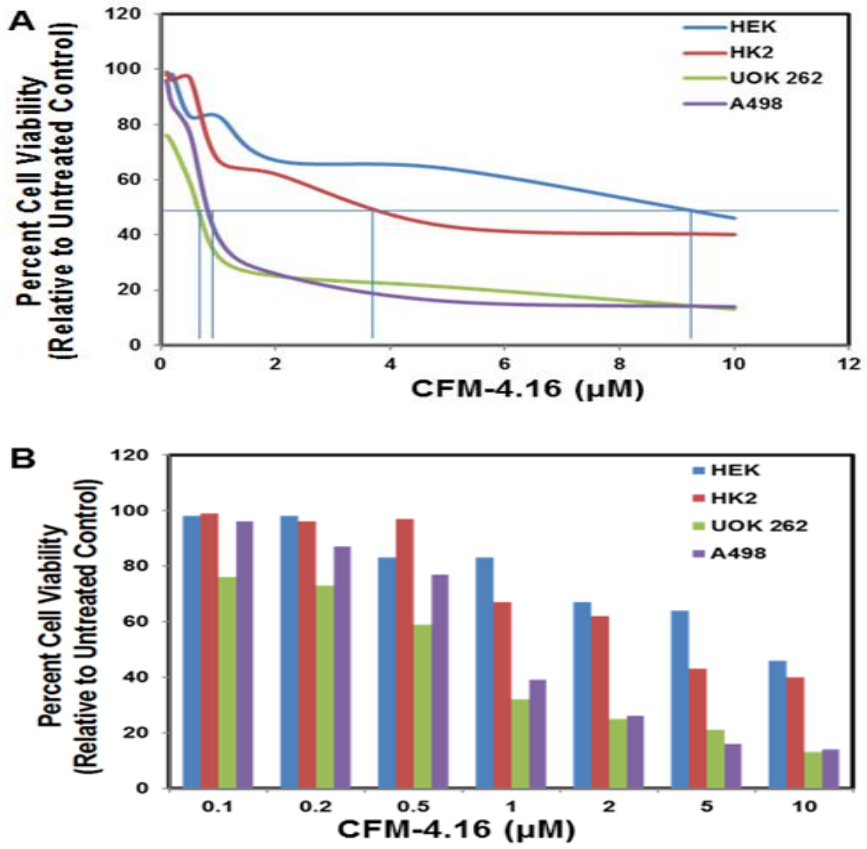

C

Cell Line	CFM-4.16, 72h, IC50 (uM)
A498 Wild type	≈0.90
UOK262 Wild type	≈0.85
HEK 293 Wild type	≈9.2
HK2 Wild type	≈3.8

Figure 4.6. RCC cells are more sensitive to inhibition by CFM-4.16 when compared with non-cancer renal epithelial cells. (A, B) Indicated cells were treated with 0.1, 0.2, 0.5, 1.0, 2.0, 5.0, and 10.0 uM dose of CFM-4.16. Percent cell viabilities were determined relative to respective DMSO-treated controls. The histogram (Lines in A or Columns in B) represent means of two independent experiments with 4-6 replicates of each dose for the respective cell type (C) IC50 values of RCC and Renal epithelial cells treated with CFM-4.16 as in panels A and B.

4.4.4. Nanomicellar formulation of CFM-4.16 inhibits growth of parental and Everolimus-resistant RCC cells *in vivo*

We next examined the *in vivo* antitumor efficacy of nano-micellar formulation of CFM-4.16 (SMA-TPGS-CFM-4.16) in a highly aggressive RCC A498 orthotropic xenograft tumor bearing SCID mice as described in methods and our published protocols [157,159]. In our previous studies, we prepared CFM-4.16 by dissolving it in 10% DMSO/Cremophor plus sterile, distilled water with a pH of 4.5. We administered a dose of 30mg/kg/day of this preparation by intravenous (tail vein) injections for a total dose of 482mg/kg in SCID mice bearing human TNBC cell-derived xenografts. With the exception of a mild, <2% loss in body weight, the preparation did not cause any histological abnormalities in the treated animals and lacked a therapeutic T/C values [159]. On this basis, we chose a 30mg/kg/day dose of CFM-4.16 (free compound as DMSO/Cremophor preparation or nano-micellar formulation) for use in current *in vivo* experiments. As shown in Figure 4.7A, intravenous (iv) administration of vehicle (Control) SMA-TPGS (total dose of 120mg/animal), DMSO/Cremophor preparation of CFM-4.16 (total dose of 240mg/animal), or administration of SMA-TPGS-CFM-4.16 (total dose of 210mg/animal) by oral gavage failed to inhibit tumor growth. However, only two i.v. injections of 30mg/kg/day of SMA-TPGS-CFM-4.16 (total dose of 60mg/animal) caused a significant reduction in tumor size when compared with the tumor sizes noted in the other treatment groups (Figure 4.7A). The HPLC analysis of the tumors from animals treated with i.v. injections of SMA-TPGS-CFM-4.16 revealed presence of CFM-

4.16 in tumors. In addition, after the completion of the animal experiment, tumors from treatment and control groups were dissected, and cryosectioned for imaging of apoptotic signs using TUNEL (Terminal deoxynucleotidyl transferase dUTP nick end labeling) and CARP-1. The immuno-histological analysis of tumors from animals treated with i.v. injections of SMA-TPGS-CFM-4.16 showed elevated levels of CARP-1 and TUNEL-positive cells when compared with the tumors derived from the animals of control group (Figure 4.7B). Thus, the data suggest that nano-micellar formulation of CFM-4.16 enhance anti-tumor efficacy of CFM-4.16 when administered i.v. but not orally, at a significantly lower total dose when compared with the free compound.

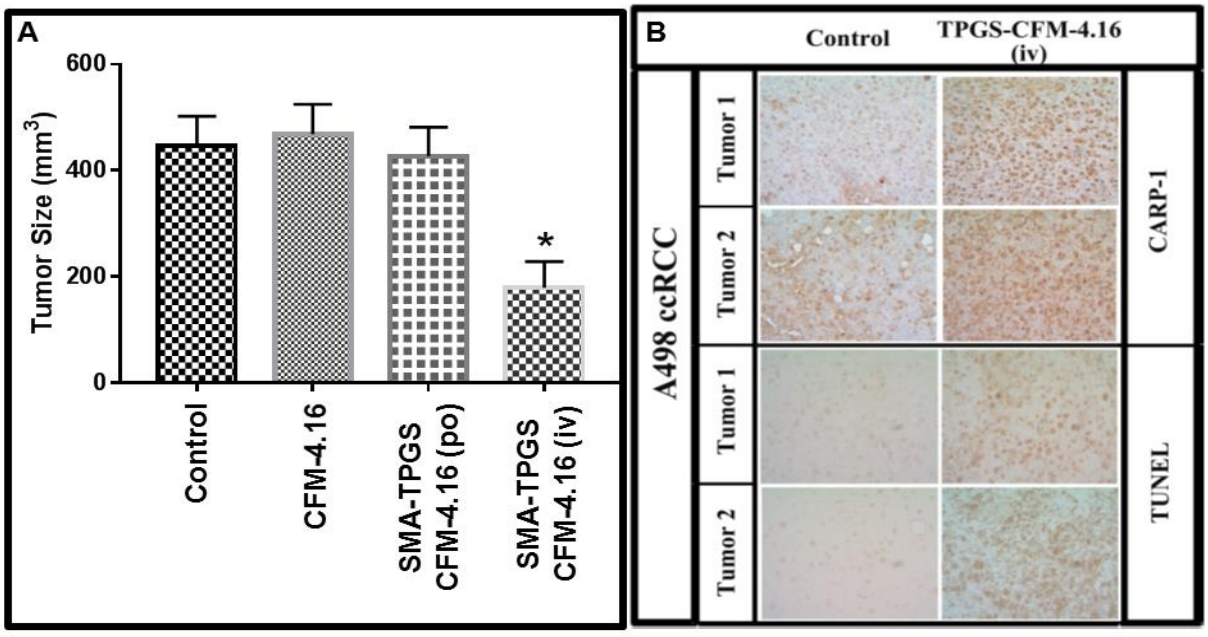

Figure 4.7. Nano-micellar formulation of CFM-4. 16 inhibits growth of RCC cell-derived xenografts. (A) Histogram showing tumor size in the vehicle-treated (indicated as Control), CFM-4.16, or SMA-TPGS-CFM-4.16 (p.o. or i.v.) treated, RCC (A498) xenograft-bearing animals. The xenograft establishment, treatment and analysis procedures were carried out essentially as detailed in Methods. The columns represent average values from a total of eight animals in respective group, bars, SE, significant where *p = 0.05 vs Control. (B) SMA-TPGS-CFM-4.16 treatments (iv) induce CARP-1 expression and apoptosis in RCC tumor xenografts. Representative tumor tissues from two animals each from the vehicle-treated (noted as Control) or SMA TPGS-CFM-4.16 treated groups were fixed in formalin, paraffin embedded, processed, and subjected to immuno-staining as detailed in Methods. Photomicrographs (400 x magnification) are shown for

apoptosis (by TUNEL assay), and levels CARP-1 protein as noted in methods. Elevated apoptosis is indicated by increased brown staining or dark-brown spots in SMA-TPGS-CFM-4.16 panels stained with anti-CARP-1 antibodies or TUNEL, respectively. Adapted from [1].

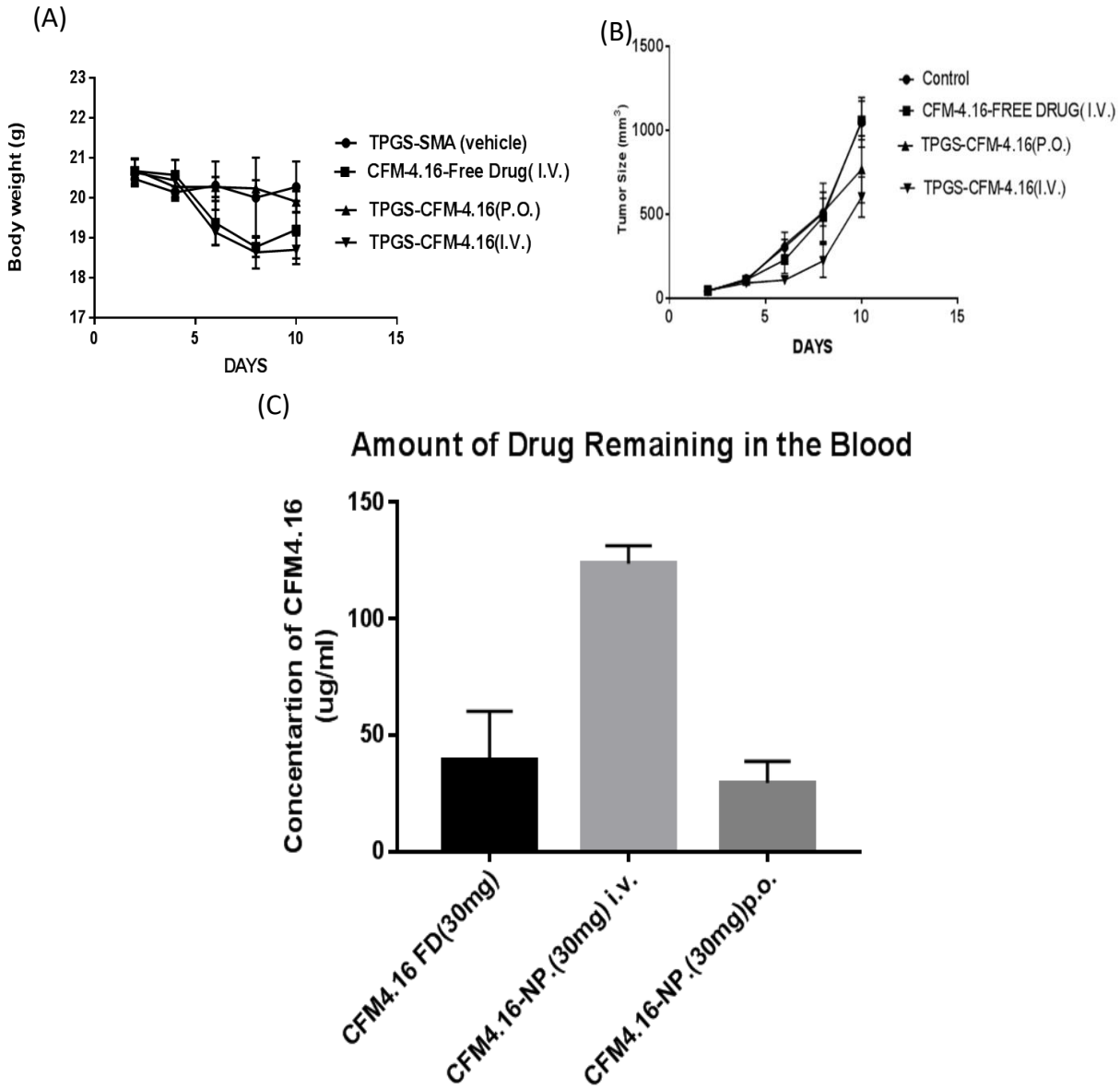

Figure 4.8. (A) Body weight changes of mice during treatment course. The lines represent average body weight from a total of eight animals in respective group that were measured on the indicated days; bars, SE. (B) Tumor size of mice during treatment. The line represents average values from a total of eight animals in respective group, bars, SE. (C) Amount of CFM4.16 remaining in the blood after the last injection of drug. The histogram columns represent means of CFM-4.16 concentrations from three animals from the indicated treatment group; bars, S.E.

4.5. Discussion

CFM-4 and its analog CFM-4.16 have poor aqueous solubility of <1mg/ml. This attribute contributes to poor dissolution with consequent poor absorption and bioavailability. Recent advances in nano-formulation-based technology have allowed optimization of poorly soluble compounds for preclinical as well as clinical testing and use. In our prior proof-of-concept studies, nano-lipid formulations of CFM-4 and CFM-4.16 compounds were prepared by combining high-melting solid lipid carriers and vitamin E TPGS co-surfactant. These formulations were demonstrated to not only enhance solubility and oral bioavailability of the CFMs, but also were effective in suppressing NSCLC and TNBC cell-derived tumor growth in pre-clinical animal models when administered orally [159,160]. Here we prepared a polymeric micelle based nano-drug delivery system of CFM-4.16 to improve its dissolution and bioavailability. A nanomicellar formulation of SMA-TPGS and CFM-4.16 resulted in improved dissolution and consequent enhanced absorption, which was also evident by the improved pharmacokinetic profile as previously reported [159,160]. Vitamin E-TPGS is FDA approved co-surfactant that acted as stabilizer and permeation enhancer while SMA contributed to good micellar property [172,197,198]. Thus, chemical conjugation of SMA and TPGS, namely SMA-TPGS creates more hydrophobic space, which provides higher CFM-4.16 encapsulation efficacy. Due to the crystalline nature of matrix lipids in solid particles, the space for the drug loading is often limited. Size and surface coating also play an important role in determining the mechanism and efficiency of nanoparticle. The particle size of ~145 nm and surface charge is -7.86 mV of the CFM-4.16 loaded nanomicelles are optimal and safe for systemic (intravenous or oral) drug administration as well as competent for tumor delivery by passive targeting EPR-effect [178,190,199].

Our preliminary studies here indicate that both free and SMA-TPGS formulation of CFM-4.16 inhibit growth of RCC cells *in vitro,* in part by stimulating apoptosis. Consistent with our prior findings, CFM-4 or CFM-4.16 caused loss of cyclin B1, and upregulation of CARP-1, activation of p38 and JNK1/2 SAPKs, and cleavage of PARP in the RCC cells. Intravenous administration of the nano-micellar formulation of CFM-4.16 inhibited growth of RCC cell-derived tumor xenografts *in vivo* in part by stimulating CARP-1 levels and apoptosis. Taken together, our current data provide us with a further rationale to develop CFM compounds and their formulations for targeting parental and resistant RCCs.

4.6. Conclusions

CARP-1 functional mimetics (CFMs) are novel small molecule inhibitors of RCC. In addition, CFMs induce apoptosis by activating SAPKs and elevating CARP-1. In this study, we employed a nanotechnology to tackle the poor aqueous solubility of a potent CFM compound (CFM-4.16) which restricts its *in vivo* therapeutic efficacy. This SMA-TPGS-CFM-4.16 formulation maintained its nanoparticulate nature, homogenous polydispersity and high drug encapsulation efficacy. Since free CFM-4.16 or SMA-TPGS-CFM-4.16 elicited similar effects on cell viability, and levels of apoptosis would indicate that the anti-cancer effects of CFM-4.16 are retained in nanoformulation. Moreover, the physicochemical analyses indicate an optimum release of CFM-4.16 from nanoformulation. Together the physicochemical characteristics and biological activity of SMA-TPGS-CFM-4.16 seem promising for their use in future pre-clinical *in vivo* studies for the RCC tumor models.

5. CHAPTER 5. TUMOR HYPOXIA DIRECTED MULTIMODAL NANOTHERAPY FOR OVERCOMING DRUG RESISTANCE IN RENAL CELL CARCINOMA AND REPROGRAMMING MACROPHAGES

Results from the following studies have been submitted to Biomaterials Journal: CA-IX as a selective approach for targeting RCC and overcoming resistance with combining drugs approach

5.1. Objectives

Studies conducted includes: (i) Development of an ATZ-conjugated polymeric lipid nanoformulations library for the selective delivery of a drug cocktail to the hypoxic region of therapy resistant RCC. (ii) Also, to alleviate the RCC drug resistance, we have used Sorafenib (Sor) in combination with tumor hypoxia directed nanoparticle (NP) loaded with a new class of apoptosis inducer, CFM 4.16 (C4.16), namely CA IX-C4.16. (iii) Authenticated RCC cell lines such as WT (A498, UOK262) and Evr-res (A498, UOK262) will be utilized as RCC cells, as well as Raw 264.7 (macrophage) for macrophage phenotyping studies. The following will be investigated (1) a synergistic anticancer effect of CFM-4.16 with TKIs, (2) the role of M2-macrophages in tumor immune evasion, and (3) the mechanism of inhibiting tumorigenic cross-talk between RCC epithelial cells and M2-macrophages using NPs. The tumor environment mimetic advance spheroid and Transwell cell culture models will be used to establish efficacy.

5.2. Introduction

Renal Cell Carcinoma (RCC) contributes to >90% of the most common form of kidney cancer and remains one of the ten leading causes of cancer deaths. It has been estimated that each year around 60,000 new patients are diagnosed with, and about 13,500 succumb to RCC [8]. Thus, RCC represents one of the most lethal malignant urological tumor [200]. The common form of RCC (more than 95%) is clear cell renal cell carcinoma (ccRCC) [83]. The

mutation and inactivation of tumor suppressor Von Hippel-Lindau (VHL) gene is frequently observed in this malignancy that leads to a higher intracellular level of hypoxia-inducible factors 1α and 2α (HIF1α and HIF2α). The increased level of HIF-1α in RCC effectively regulates the tumorigenesis by upmodulating the function of AKT and VEGFR kinases that play an essential role in cellular metabolism, apoptosis inhibition, and hypoxia induction [201]. All these factors promote RCC to develop resistance to radiotherapy and conventional chemotherapy [202,203]. Several receptor tyrosine kinase inhibitors (TKIs), mammalian target of rapamycin inhibitors (mTOR) and serine-threonine kinase (STK) inhibitors are clinically approved for the treatment of RCC [166], although the benefit of overall progression-free survival remains poor (5-year survival rate of <10%). Thus, there is an urgent unmet need for targeted combination therapies with novel cell killing mechanisms [102,204]. Although, TKIs and mTOR inhibitors have increased therapeutic possibilities for treating RCC, a substantial proportion of patients do not respond adequately, and therapy resistance almost inevitably occurs. Recently, new strategies have also emerged that include immunotherapy such as PD-1 inhibitor (Nivolumab) [117] and the combination of chemo-immune therapy [103]. These developments suggest that combination treatments aimed at different, non-related pathways could be advantageous [112,113,146]. In addition, due to the increase in vascular nature and high level of vascular permeability factor, ccRCC patients have benefited from anti-VEGFR cancer therapy. Over a period of time, the majority of the RCC patients ultimately develop a refractory response to anti-VEGFR treatment that is due to poor vascularization at the tumor core associated with tumor hypoxia [205]. In this regard, delivery of the therapeutic payload to the tumor hypoxic (core) is a rational approach for improving the current therapy. Additionally, development

of novel synergistic therapeutic strategies, such as the resurrection of apoptosis, inhibition of AKT, and suppression of tumorigenic macrophages are desirable to tackle the current clinical challenges of drug-resistant and highly aggressive RCC [157]. We have developed Evr-res RCC cell model to evaluate the reversal of drug resistance using nano-combination therapy. We pursued different combination regimens, including drugs Evr (mTOR inhibitor) and Sorafenib or Cabozantinib (both VEGFR and MET inhibitors).

The hypoxic tumor environment, highly prevalent in poorly vascularized and necrotic tumor core is well known to stimulate expression of VEGF and CA IX. CA IX is a membrane-bound protein that is overexpressed on the surface of many cancer cells in a hypoxic environment [122]. CA IX tightly controls the acid-base balance in the kidney [122], whereas during malignancy CA IX is involved in tumor cell survival and metastasis, and its increased expression correlates with poor clinical outcome. More than 7-clinical trials are underway to target CA IX in RCC and other solid tumors [NCT00059735, NCT00884520] that fortifies CA IX as an excellent biomarker for selective hypoxia mediated payload delivery. Numerous studies have investigated CA IX distribution in normal tissues and malignancies [124–129]. Over-expression of CA IX has been documented in 93-97% of ccRCCs with rather low to limited expression in normal tissues/organs making it a selective biomarker for RCC [123]. Indeed, CA IX is almost homogeneously over-expressed in the ccRCC subtype [84,111,124–129]. Given the favorable tissue distribution, the potential of CA IX targeting of RCC for diagnosis or therapy has also been studied [130,131]. Due to the unique molecular attribute of RCC, CA IX is regarded as an excellent target for diagnosis and possibly for targeted therapy [111,126–128,132]. Clinical trials have unambiguously demonstrated that CA IX can be targeted to RCC tissues with minimal damage to normal tissues, further

highlighting suitable toxicity profiles of CA IX targeting [133,134]. However, there are no currently approved therapies against CA IX [164]. Monoclonal antibodies have been used to target CA IX, but their large molecular weight limits penetration through the poorly vascularized tumor and their slow blood clearance minimize their utilization as tumor imaging agents or radiotherapeutics because of high background and toxicity [134]. Finally, some recent studies have investigated whether small molecule CA IX-inhibitors can be used in serum assays or as an imaging target to monitor therapy responses [127–129]. Importantly, there is a critical need to develop safe and effective delivery vehicles that can carry the payload to the desired target tissue and cells [157,185,206–209].

Toward this end, we developed a simple and efficient multistage nanoplatform for systemically targeted polypharmacy payload delivery to induce the combination of chemotherapeutic and immunotherapeutic effect in RCC. The oligomer we developed comprised of Vitamin-E- α-D-Tocopherol (TPGS) and styrene maleic anhydride (SMA) ligated with Acetazolamide (ATZ), namely CA IX-SMA-TPGS. The CA IX-SMA-TPGS oligomer was further encapsulated with C4.16 to obtain highly potent therapeutic payload containing nanoparticle CA IX-C4.16, respectively. The CA IX-C4.16 NPs have homogenous nanoparticle nature with narrow polydispersity index that is suitable for *in vivo* delivery. For ease of chemical synthesis of oligomers, we utilized copper free '*click*' chemistry. We have discovered and demonstrated CCAR1/CARP-1 protein as an inducer of apoptosis in RCC and other types of cancer. Upregulation of CARP-1 activates "apoptosis hallmarks", such as caspase mediated PARP cleavage, downregulation of PI3K/AKT signaling and loss of cyclin B1 in RCC[157]. Our collaborator recently identified the potent activators of CARP-1, a library of small molecule CARP-1 functional mimetic

(CFM) compounds. CFM-4.16 (namely C4.16), is highly efficient in RCC cell killing as noted from NCI-60 screen [157]. Our data revealed that C4.16 is a superior inhibitor of both WT and Evr-resistant RCC cells with 4-5-fold improvement in IC50 value as compared to FDA approved Evr or Sor. In 2007, Sorafenib (Sor), a potent multi-kinase inhibitor of tumor-cell proliferation and angiogenesis, was clinically approved for oral treatment of advanced RCC with the median progression-free survival of 5.5 months [210]. Along with this encouraging clinical outcome, there are a few reports on durable responses of Sor or the other VEGFR pathway blockers. However, the majority of patients develop resistance to Sor within a median of 5–9 months [211]. Thus, more efficient and divergent combination therapy for inhibiting multiple tumorigenic pathways in RCC is required. Toward this, we found the combination of Sor and CA IX-C4.16 showed remarkable synergy in killing WT and Evr-res RCC cells. This combination treatment caused a complete wipeout of activated AKT (P-AKT) level, upregulated apoptosis hallmarks, such as caspase 3/7 and annexin V. The CA IX-C4.16+Sor is promising in upmodulating tumoricidal function of M-1 macrophage, while downmodulating tumorigenic M-2 macrophage-associated biomarkers, such as CD206, arginase-1. Further, NIR imaging of CA IX-SMA-TPGS-S0456 confirmed the selective tumor accumulation of the vehicle with ~6-fold higher tumor/liver as compared to control. The high intensity of NIR-dye in tumor core indicates selectivity of CA IX-SMA-TPGS-S0456 in tumor hypoxia targeting. Finally, the significant tumor growth inhibition by CA IX-C4.16+Sor in Evr-res A498 model underscores the rationale of using Sor in combination nanotherapy as a promising platform in reversing drug resistance with untraceable liver and kidney toxicity (Scheme 1).

5.3. Materials and methods

5.3.1. Cell culture, reagents, and chemicals

Structure and synthesis of the C4.16 compound have been previously described [157,159]. A stock solution of 50mM of C4.16 was solubilized in dimethyl sulfoxide (DMSO) and stored at –20°C for further use. Sor was obtained from LC Laboratories, Woburn, MA, and a 10mM stock solution was prepared in DMSO and stored at –20°C. Everolimus (Evr) was obtained from selleckchem, Boston, MA, and a 10mM stock solution were prepared in DMSO and stored at –20°C. Acetazolamide (ATZ), '*click*' chemistry reagents, Styrene maleic anhydride (SMA, MW 1600), D-alpha-tocopheryl polyethylene glycol succinate (Vitamin E-TPGS), and 3-[4, 5-Dimethylthiazol-2-yl]-2, 5 diphenyltetrazolium bromide (MTT) were purchased from Sigma-Aldrich (St Louis, MO). NIR dye, S0456 was obtained from FEW Chemicals GmbH, Germany. We obtained all other analytical grade reagents from Fisher Scientific (Hampton, NH) and Sigma-Aldrich (St Louis, MO) and used them without further purification. DMEM, RPMI medium and antibiotics (penicillin and streptomycin) utilized in this work were purchased from Invitrogen Co. (Carlsbad, CA). Fetal bovine serum (FBS) and DMSO were purchased from Fisher Scientific (Fair Lawn, NJ). The Protein Assay Kit was obtained from Bio-Rad Laboratories (Hercules, CA). The rabbit monoclonal antibodies for β–actin was acquired from Sigma-Aldrich (St. Louis, MO). We purchased rabbit monoclonal antibodies to phospho- and total AKT, and Carbonic Anhydrase-IX (CA IX) from Cell Signaling Technology (Beverly, MA).

5.3.2. Cell lines development and culturing condition

The human RCC A498 cells were from ATCC and kindly provided by Dr. Rajvir Dahiya (UCSF). All the cells were regularly maintained following procedures published

before [212,213]. The cells were cultured in Dulbecco's modified Eagle's medium (DMEM) with GlutaMAX that was supplemented with 10% FBS, 100 units/ml of penicillin, and 100 μg/ml of streptomycin, and the cells were cultured at 37°C and 5% CO2. For cell viability and MTT studies, the cells were cultured in fresh media supplemented with 10% FBS before their treatments with various agents [214,215]**.** Resistant RCC cell-lines, including Evr-res A498, have been already established and validated in our previous work [157]. For inducing hypoxia, cells were treated with 200 μM Cobalt Chloride ($CoCl_2$) in standard growth media for 72 h before experiment [216,217]. RCC 3D-spheroid cell lines were grown in low density with 2% FBS containing culture media and before treatment they were induced with the hypoxic condition.

5.3.3. General procedure for synthesis of compound SMA-TPGS and ATZ-SMA-TPGS by Copper-free 'click' chemistry

As illustrated in Figure 1 (Scheme 1), we first synthesized acetazolamide-amine (ATZ-NH2) from acetazolamide (ATZ) by acid hydrolysis as previously described [218]. Subsequently, ATZ-NH2 was being reacted with DBCO-NHS-ester to finally arrive at ATZ-DBCO (compound a) which is CA IX (hypoxia) targeting ligand. Secondly, in scheme 2, we synthesized SMA-TPGS oligomer (SMA-TPGS) by adding known amounts of TPGS in NaHCo3 buffer at pH 8.9 with fixed amounts of anhydrous SMA to permit its anhydride ring opening reaction with the alcohol group of TPGS. Then, we conjugated the oligomer with azido functional compound (NH2-PEG8-N3) by acid-amine coupling (EDC/NHS) reaction to finally get (compound b). Finally, the Cupper free click chemistry reaction will occur by reacting (compound a) with (compound b) to form triazole ring. All unconjugated reagents were removed prior lyophilization.

5.3.4. Preparation and Characterization of C-4.16-loaded NPs

After '*click*' reaction, we obtained CA IX-SMA-TPGS (CA IX-targeted oligomer), and in parallel, we generated SMA-TPGS (non-targeted oligomer). Both, (SMA-TPGS and CA IX-SMA-TPGS-C4.16) NPs were developed using our previously reported methods with slight modification [157]. In brief, 100 mg of conjugated polymer was dissolved in 100 ml of deionized (DI) water under stirring. Then C4.16 (30 mg) was dissolved in 1 ml of DMSO and mixed with the polymer solution. Subsequently, 40 mg of EDC was added dropwise into solution and pH was kept at 5.0 to stir for 30 min. Then, the pH was raised to 11 and kept for other 30 min. Finally, pH was adjusted to 7.8 – 8.0 and the free drug C4.16 were removed by dialysis for 4-5 h in a bag with a cut-off of MW 2 kDa. Then, the products obtained were lyophilized to obtain the final powder and stored in the freezer until further use. Subsequently, the particle size and surface charge (zeta potential) measurements were performed using a Beckman Coulter Delsa Nano-C-DLS Particle analyzer (Miami, FL) equipped with a 658 nm He-Ne laser. For particle size, we suspended the NPs in DI water and detected the scattered light at 165° angle. We then obtained the peak average histograms of intensity, volume and number from 70 scans to calculate the average diameter of the particles. The zeta potentials were evaluated by measuring the electrophoretic mobility of the charged particles under an applied electric field. For Morphology, Transmission Electron Microscopy (TEM) of the NP was evaluated using JEOL-JEM-1000 instrument (JEOL Ltd, Tokyo, Japan). We also characterized oligomer by proton nuclear magnetic resonance spectroscopy (^{1}H NMR) and Fourier transform infrared spectroscopy (FTIR). The structure of the synthesized SMA-TPGS and CA IX-SMA-TPGS copolymer was detected by ^{1}H NMR in D_2O as previously described [157209]. The proper synthesis of the SMA-TPGS and CA IX-SMA-TPGS oligomer was also confirmed by the MALDI/MS and was found not to be a physical mixture of TPGS with SMA as all measurements indicated the absence of any free crystalline particles before NPs preparation.

5.3.5. The Drug Loading (DLC) and Encapsulation efficiency (EE) of C4.16 loaded-nanoparticles

We evaluated the C4.16 loading content percentage and the encapsulation efficiency (EE %) in NPs by High-Performance Liquid Chromatography (HPLC, Waters, Milford, MA). Samples of the C4.16 NPs preparations were taken, and the unentrapped C4.16 was quantified using our previously published HPLC method [157]. The loading efficiency of micelles was calculated by dissolving a known quantity of NPs directly in DMSO and further dilution of drugs with the mobile phase followed by determination of the absorbance at 309 nm (λ_{max}) with respect to the standard curve. Free drug (unentrapped C4.16 in the SMA-TPGS or CA IX-SMA-TPGS) was separated by ultrafiltration centrifugation technique. Briefly, 1 mL of CA IX-SMA-TPGS-C4.16 (targeted CA IX-C4.16 NPs) and SMA-TPGS-C4.16 (non-targeted) colloidal solutions were placed in the upper chamber of a centrifuge tube matched with an ultrafilter and centrifuged for 15 min at 4000 rpm. The total drug content in C4.16 NPs was determined as follows. Aliquots of 1mL formulation dispersion were diluted accordingly by ethanol to dissolve the ingredient, and the resulting suspension was then filtrated through 0.45μm membrane filters. The filtered solution was analyzed by Waters® Alliance e2695 HPLC using Symmetry® C18 column (250mm × 4.6mm, 5μm). The mobile phase was a mixture of Acetonitrile, Methanol, 10mM KH_2PO_4 buffer (65:20:15 v/v) with pH adjusted to 2, and the flow rate was maintained at 1.0mL/min. All the samples were analyzed using empower PDA software. We then calculated the encapsulation efficiency (EE) and drug loading content (DLC) by the following equations:

$$\text{Drug loading content (DLC)} = \frac{\text{The weight of C}-4.16 \text{ encapsulated in micelles}}{\text{Total weight of C}-4.16 \text{ loaded in micelles}} \text{ x}100 \qquad \text{Equation (1)}$$

$$\text{Encapsulation Effeciency (EE)} = \frac{\text{Mass of C}-4.16 \text{ encapsulated in micelles}}{\text{Total mass of C}-4.16 \text{ initially loaded in micelles}} \text{ x}100 \qquad \text{Equation (2)}$$

5.3.6. Expression of CA IX by A498 RCC cells and A498 RCC tumor models

The expression of CA IX on the surface of A498 and Evr-A498 cells was investigated under a normoxic or hypoxic condition by exposing cells to normoxia (no treatment) or hypoxia (cobalt chloride, $CoCl_2$ treatment) for 72 h, followed by CA IX detection using immunofluorescence analysis or western blot. Proteins from tumor tissues were extracted using RIPA buffer with the Halt Protease and Phosphatase Inhibitor Cocktail. A498 cells or tumors were fixed with 4% cold paraformaldehyde for 15 min after incubation for 24 h under normoxic or hypoxic condition. Cells were washed three times with DPBS and blocked with 10% bovine serum albumin for 1 h at room temperature, then incubated with primary rabbit monoclonal anti-CA IX antibody (20 μg/mL) overnight at 4 °C. Cells were subsequently washed three times followed by incubation with FITC-conjugated rabbit anti-mouse secondary antibody for 1 h at room temperature. A498 cells under the normoxic or hypoxic condition, only treated with FITC-conjugated goat anti-mouse secondary antibody served as controls to avoid interference of cell auto-fluorescence. Cells were observed using a Confocal Laser Scanning Microscope (CLSM). For tumor tissues, mice were implanted with A498 cells using the technique previously reported [157]. Briefly, A498 cell suspensions were prepared in PBS and mice were injected with 1×10^6 cells subcutaneously by syringes with 29-gauge needles. On day 14 after tumor cell implantation, mice were sacrificed, and RCC tumor tissue was collected for histology performed by Biobank core facility.

5.3.7. Hypoxic core penetration of CA IX-SMA-TPGS oligomer in hypoxic A498 3D tumor spheroid

Cancer cell specific uptake of CA IX-SMA-TPGS oligomer was performed in tumor spheroids by immunofluorescence. Cells were cultured with ~70-80% confluence. We cultured Evr-res A498 cells to form 3D spheroid structure based on previously published methods [157,159]. Briefly, the cells were washed twice in 1 x PBS, trypsinized and pelleted the cells with 200 x g centrifugation at room temperature. It was re-suspended in 5ml of sphere media (DMEM/F12 supplemented with 2mM L-glutamine, 100 U/ml penicillin, 100 U/ml streptomycin, 1 x B27 supplement, 20ng/ml recombinant human epidermal growth factor (EGF; Sigma), and 10ng/ml recombinant human basic fibroblast growth factor (bFGF; R&D Systems). Cells were seeded approximately 5000 cells per ml on an ultra-low adherent 60mm plate and incubated at normal cell culturing conditions for two weeks without disturbing the plates. Seventy-two h prior to treatment, media was replaced with the hypoxic condition. Once the sphere was formed, spheres were treated with 1µM Rhodamine B conjugated CA IX-SMA-TPGS oligomer (CA IX-Rhoda-B) for 4 h or kept untreated at 37°C and 5% CO_2. At the end of the incubation period, the spheroids were washed with cold DPBS and scanned beginning from the top of the equatorial plane to obtain the Z-stack images by CLSM for the spheres of untreated and treated plates as described as reported before [196].

5.3.8. In vitro cytotoxicity assay

MTT assay was used to evaluate the anti-cancer effects of targeted CA IX-C4.16 NP and free anticancer drugs (C4.16, Evr, and Sor) in CA IX-positive (A498 RCC cells). First, the cells were seeded in a 96-well plate at a density of $5x10^3$ cells per well and allowed to grow in fresh

culture media overnight. Cells were subjected to parallel treatments under hypoxic and normoxic conditions as described above. After 20 h, the medium was removed, and the cells were washed twice with PBS. Cells were then treated with various concentrations of respective agents for the noted dose and time. Control cells were treated with 0.1% DMSO in the culture medium[219–221]. After treatment, cell viabilities were measured by the MTT assay. Briefly, 20 µl of 1mg/ml of MTT was added to each well and cells were incubated for 2-4 h at 37^0C. MTT was removed, and the resulting formazan products were dissolved by adding 50µl DMSO/well followed by colorimetric analysis at 595nm using a multi-label plate reader (Victor3; PerkinElmer, Wellesley, MA).

5.3.9. Apoptosis analysis by flow cytometry and Caspase 3/7 Glo assay

We determined apoptosis induction in A498 RCC cells that were treated with free C.4.16 or CA IX-C4.16 NP by flow cytometry with Annexin V/7-AAD dual staining. The percentage of Annexin V^-/7-AAD $^-$ (R5), Annexin V^+/7-AAD $^-$ (R6) and Annexin V^-/7-AAD $^+$ (R4) and Annexin V^-/7-AAD $^+$ (R3) cells were obtained to determine the number of live, as well as early and late apoptotic, and necrotic cells. To evaluate caspase-3/7 activities, cells were cultured and treated with DMEM medium (Free oligomer or control), C4.16, Sor, or C4.16+Sor for 24 h and were tested by Caspase-Glo 3/7 Assay (Promega) according to the manufacturer's recommendations.

5.3.10. Western Blot analysis

The RCC cells were treated with DMSO/Vehicle (Control) or indicated dose and time of the noted compound. Cells were harvested and lysed in RIPA buffer (50mM Tris-HCI, pH 8.0, 150mM sodium chloride, 1.0% NP-40, 0.5% sodium deoxycholate, 0.1% sodium dodecyl sulphate (SDS), and 0.1% of protease inhibitor cocktail) for 20 min at 4^0C. The lysates were then centrifuged at 14,000 rpm at 4^0C for 15 min to get rid of debris. We then determined the protein

concentrations of whole cell lysates using the Bradford Protein Assay Kit. Supernatant proteins, 50μg from each sample, were separated by SDS-10% polyacrylamide gel electrophoresis (SDS-PAGE) and transferred to polyvinylidene difluoride (PVDF) membrane (Bio-Rad, Hercules, CA) by standard procedures. The membranes were hybridized with primary antibodies followed by incubation with appropriate secondary antibodies. The antibody-bound proteins were visualized by treatment with the chemiluminescence detection reagent (Amersham Biosciences) according to the manufacturer's instructions, followed by exposure to X-ray film (Kodak X-Omat). The same membranes were then re-probed with the anti-β actin antibody, which was used as an internal control for protein loading.

5.3.11. Reprogramming macrophages with (CA IX-C4.16+Sor)

Transwell inserts 0.4 μM Corning, Falcon®, catalog number: 353493 and Corning® 6 well cell culture plates were used. Figure 6 A shows a diagram representing a brief outline of the steps of the protocol and a timeline indicating the order of events that were all carried out under sterile conditions following protocol published by Smith *et al*. Briefly, Raw264.7 cells were placed into the Transwell inserts. Raw-264.7 cells were first polarized to M1-macrophage using IFN-γ and LPS, and to M2-macrophage using IL-4 recombinant protein. Then, A498 RCC cell lines were cocultured with activated macrophages followed by treatment of Sor, C4.16, and CA IX-C4.16+Sor for 24 h. Caspase 3/7 assay was performed in Evr-res A498 cells treated with Sor, C4.16, and CA IX-C4.16+Sor while co-culturing with Raw-264.7 macrophage to demonstrate whether combination treatment can reeducate macrophage to induce apoptosis mediated A498 cell death.

5.3.12. A-498 Three-dimensional RCC tumor spheroids uptake

CA IX expression of tumor spheroids was checked by immunofluorescence. The RCC cells were obtained from xenograft tumors derived from WT cells and Everolimus-resistant RCC cells from a two-dimensional culture plate with ~70-80% confluence. We performed the three-dimensional renal sphere cultures by mostly following the methods described before [14,36]. Briefly, the cells were washed twice in 1 x PBS and trypsinized following established protocols. We then pelleted the cells at 200 x g at room temperature and re-suspended them in 5ml of sphere media (DMEM/F12 supplemented with 2mM L-glutamine, 100 U/ml penicillin, 100 U/ml streptomycin, 1 x B27 supplement, 20ng/ml recombinant human epidermal growth factor (EGF; Sigma), and 10ng/ml recombinant human basic fibroblast growth factor (bFGF; R&D Systems). We seeded approximately 5000 cells per ml in an ultra-low adherent 60mm plate and incubated them at normal cell culturing conditions for two weeks without disturbing the plates. After the spheres formed, we added fresh media with or without 1µM Rhodamine B conjugated CA IX targeted-OMs and continued incubating cells for additional 4h at 37°C and 5% CO2. At the end of the incubation period, the spheroids were washed with cold DPBS and scanned began from the top to the equatorial plane to obtain the Z-stack images by CLSM for the spheres in the untreated and treated plates as described as reported before by another group [42].

5.3.13. Antitumor therapy study in highly aggressive Evr-res A498 tumor in nu/nu xenograft model

The generation of RCC cell-derived subcutaneous tumor was done according to our previously published protocols approved by the Institutional Laboratory Animal Care & Use Committee (IACUC) at the Wayne State University [157,159]. Female, 5-6 weeks old nu/nu mice were obtained from Jackson Laboratory, Bar Harbor, ME. For therapy studies, after an appropriate period of acclimation, a suspension of 1 x 10^6 Evr-res A498 cells in 150µl PBS was subcutaneously

implanted in flanks of each animal using a 27-gauge needle. Tumors were allowed to grow for 10 days. When tumors became palpable (200 mm^3), the mice were randomly assigned for treatment or control groups of five animals each. Mice were treated with Vehicle (Control), CA IX-C4.16 NP (24mg/kg/day), Sor (10mg/kg/day) via intravenous (i.v) administration. Sor was formulated with 10% Kolliphor EL in PBS with DMSO concentration is <5%. In case of CA IX-C4.16 and Sor combination, only two doses were administered where the first dose was on day 1 was followed by the second dose on the third day. The tumor volume was measured, and mice were monitored for body weight changes. Antitumor activity was measured by using NIH formula, tumor volume (mm^3) = 1/2(length × $width^2$). The tumor volume of the last day of therapy study was represented to demonstrate the endpoint outcome of combination therapy as described before [157]. The animals were sacrificed, and tumor tissues were collected. Representative tumor samples were stored at –80°C for subsequent analysis. The histology of normal organs (Kidney and Liver) was performed by Biobank core facility.

5.3.14. NIR imaging and bio-distribution of CA IX-SMA-TPGS-S0456 oligomer

A CA IX-targeted oligomer was conjugated with Near-infrared (NIR) dye CA IX-SMA-TPGS-S0456, namely CA IX-S0456 (CA IX-oligomer) and administered via i.v route to 5-6 weeks old nu/nu mice, and the bio-distribution of NIR dye was monitored after 24 h of the single dose with 10 nmole NIR dye per mouse. Fluorescence images were collected in Bruker Carestream Xtreme in vivo imaging system at excitation (750 nm) and emission (830 nm) wavelength. The bio-distribution and tumor-targeting properties of CA IX-S0456 was evaluated after euthanizing the mice after 24 h post i.v injection. The instrument has dual fluorescence and X-ray imaging modalities with light source: 400 W Xenon illuminator. Both fluorescence and X-ray images of the mouse were merged to demonstrate the localization of NIR dye. We obtained PDx tumor mice

from Jackson laboratory, and tumor slice was passaged to mice using trocar and imaging was performed as similar with nu/nu mice.

5.3.15. Statistical analysis

The statistical analysis was done using Prism 7.0 software (Graph Pad Software Inc., San Diego, CA). The data were expressed as mean ± SEM and analyzed using a two-tailed Student t-test or one-way ANOVA followed by a post hoc test unless specified otherwise. A p value of <0.05 was considered statistically significant.

5.4. Results and discussion

5.4.1. General procedure for synthesis of compound SMA-TPGS and ATZ-SMA-TPGS by Copper-free 'click' chemistry

The current work aims to synthesize and formulate nanosystems targeting hypoxia in tumors. CA IX enzyme on the surface of kidney cancer cells was targeted by ATZ-containing oligomers using a modular copper-free *'click'* chemistry-based approach. As illustrated in Scheme 1 of Figure 5.1, we first synthesized acetazolamide-amine (ATZ-NH_2) from acetazolamide (ATZ) by acid hydrolysis as previously described [218]. Subsequently, ATZ-NH_2 was reacted with DBCO-NHS-ester to arrive at ATZ-DBCO (compound a) which functions as a CA IX targeting ligand. Second, in Scheme 2 of Figure 5.1, we synthesized SMA-TPGS oligomer (SMA-TPGS-Cys) by adding known amounts of TPGS and Cysteine in dichloromethane at pH 8 with fixed amounts of anhydrous SMA to permit its anhydride ring opening reaction with the alcohol group of TPGS and amine group of cystine. Then, we conjugated the SMA-TPGS-Cys with azido (N_3) group of (NH_2-PEG_8-N_3) compound by acid-amine coupling (EDC/NHS) reaction to finally get (compound b). Finally, the Copper-free '*click*' reaction was carried out by reacting compound 'a' with compound

'b' to form triazole ring, compound 'c'. All unconjugated reactants were removed by dialysis prior to lyophilization. The compound 'c' was reacted with Rhodamine B NCS to obtain "CA IX-Rhoda" for in vitro 3D spheroid uptake study [222] and reacted with S0456 to get "CA IX-S0456" for in vivo tumor imaging [163]. S0456 is a near-infrared (NIR) fluorescent dye used in phase III clinical trials for image guided tumor surgery [223]. The final compounds were characterized by MALDI-MS, ^{1}H-NMR (Supplementary, S1 A-C) to assure chemical identity. ^{1}H-NMR results confirmed the triazole ring formation in CA IX-SMA-TPGS (Supplementary, S1 A, C) as the characteristic peaks were found for the -NH group of-triazole ring around δ7.9 ppm, O-CH_2 of triazole ring around 5.2, and CH_2-N_3 peak around 4.2 respectively. The molecules were analyzed by MALDI-MS spectroscopy to confirm the chemical conjugation. This work expands upon our previous success in the design, synthesis, and development of SMA-TPGS-C4.16 and SMA-C4.16 nanomicellar formulation [157].

1. Chemical synthesis of CA IX targeting oligomer

Scheme 1:

Scheme 2:

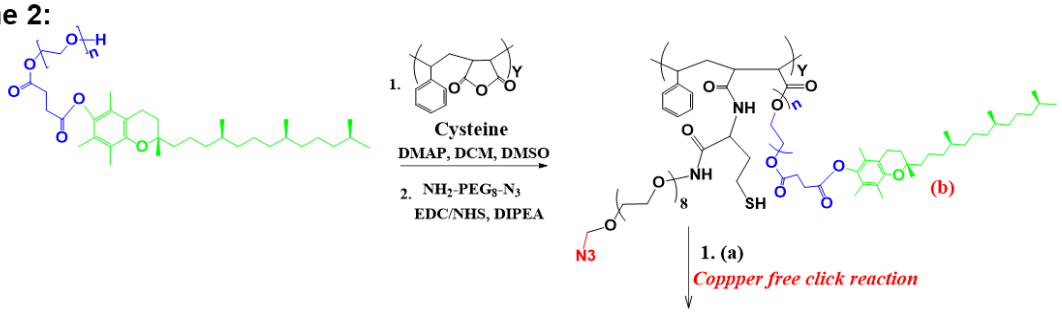

Scheme 3:

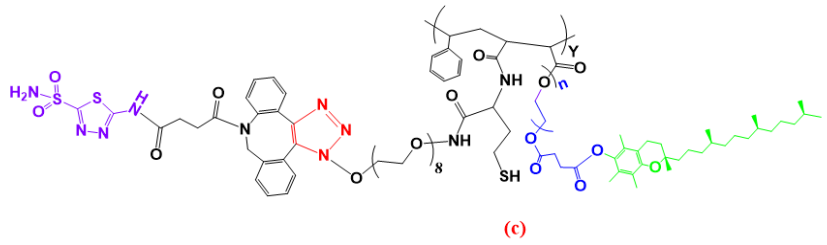

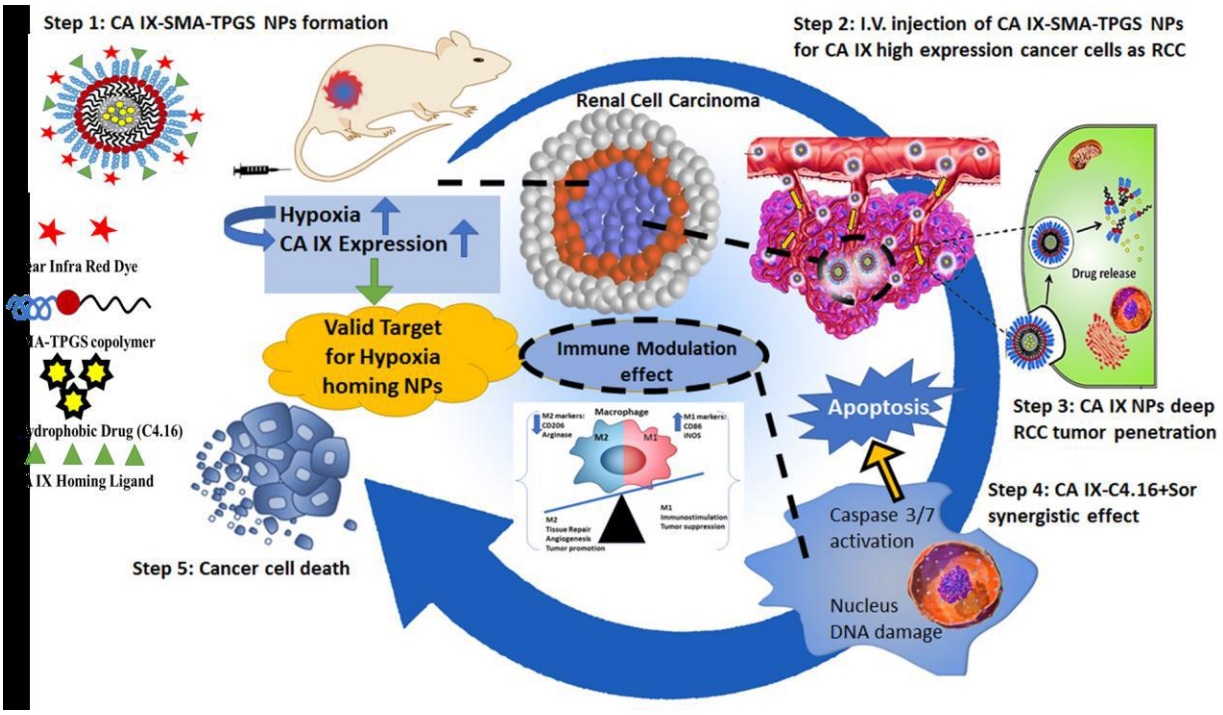

Figure 5.1. Scheme 1 and 2 indicate the general procedure for acetazolamide-oligomer fragment synthesis. Scheme 3 indicates the preparation of OMs with C-4.16 and mechanism of CA IX receptor mediated internalization of OMs in RCC. Summary of tumor hypoxia directed nanotherapy in combination with Sorafenib for achieving multiple benefits against cancer, such as reversing drug resistance, inducing apoptosis and reprogramming macrophages.

5.4.2. Preparation and characterization of CA IX targeting NP

The oligomers (SMA-TPGS and CA IX-SMA-TPGS) conjugate was purified by ultrafiltration (Millipore TFF, Milford, MA) and then lyophilized. The NPs were prepared with different methods, such as solvent evaporation, and oil-in-water emulsion method to formulate spherical micelles with SMA-TPGS and CA IX-SMA-TPGS. Both, CA IX targeted NP and non-targeted NP were loaded with water-insoluble C4.16 to produce CA IX-C4.16 NPs and SMA-TPGS-C4.16. The NPs were characterized for size, charge and drug loading and these parameters are presented in Table 1. The particle size of non-targeted C4.16 loaded NPs were ~105.2 nm with a Polydispersity index (PDI=0.165) (Figure 5.2A). Morphology of the NP was also assessed using

Transmission Electron Microscopy (TEM) instrument (Figure 5.2 B) and the particle size resembled with DLS data and a favorable negative surface charge of NPs was noted (Figure 5.2C). After incorporation of targeting ligand (ATZ) to NPs, the particle size slightly increased compared to that of the non-targeted NPs suggesting the presence of ATZ on the surface of NPs. These results indicate that both the size and surface properties are optimal and safe for intravenous injection as well as ideal for tumor delivery. The Figure 5.2 C show histograms of comparative analyses of the particle size and zeta potential of the NPs. Figure 5.2 D indicates the results of MALDI-MS analysis of CA IX-SMA-TPGS and SMA-TPGS. The increment of molecular weight in CA IX-SMA-TPGS (m/z 3126) compared to SMA-TPGS (m/z 2399) and their corresponding fragmented peaks indicates the successful conjugation of ATZ to the SMA-TPGS polymers. Also, The C4.16 loading content and encapsulation efficiency in both NPs were evaluated by High-Performance Liquid Chromatography (HPLC). First, a method for analyzing drug content was developed and validated according to ICH guidelines [188]. The loading efficiency of micelles was then calculated by dissolving known quantity of NPs directly in DMSO followed by determination of the absorbance at 309 nm with respect to the standard curve performed by HPLC method. The encapsulation efficiency was 85 % and 75.5 % for SMA-TPGS NPs and CA IX-C-4.16 NPs, respectively.

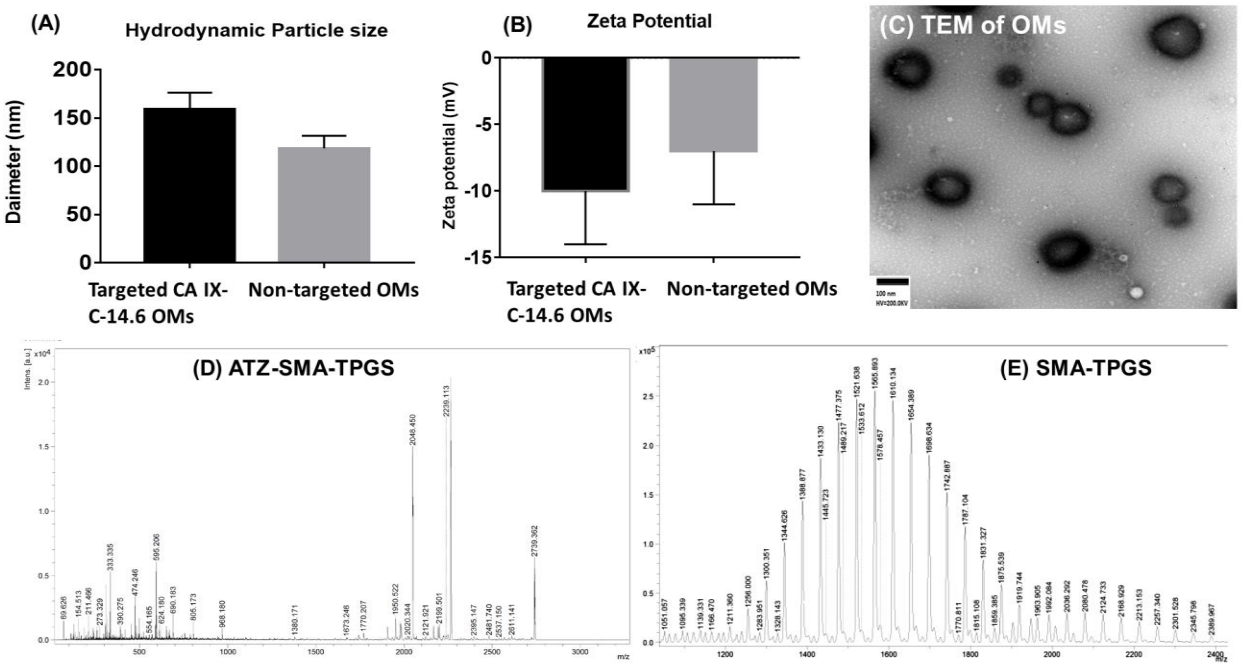

Figure 5.2. Oligomicelles formulation and characterization. **(A)** Hydrodynamic size of targeted CA IX-C4.16 OMs and non-targeted SMA-TPGS-C-4.16 OMs and (**B)** Zeta potential by Dynamic Light Scattering (DLS) are shown. **(C)** The morphology of representative OMs is characterized by TEM as shown. Scale bar = 100 nm. **(D and E)** MALDI-MS analysis of ATZ-SMA-TPGS and SMA-TPGS are shown. The increment of m/z value in ATZ-SMA-TPGS (m/z 2239.1) compared to SMA-TPGS(m/z1565.6) oligomers indicates the successful conjugation of ATZ to the SMA-TPGS polymers.

Table 5.1. Characterization of Oligomicelles.

Sample	**CMC (mg/ml)**	**Hydrodynamic size (nm)**	**PDI**	**Zeta potential (mV)**	**EE (%)**
ATZ-SMA-TPGS-C-4.16 (Targeted)	0.021	159.5±20nm	0.094±0.05	-10.21 ±4	75.5±12
SMA-TPGS-C-4.16 (non-targeted)	0.010	105.2±31nm	0.165±0.07	-7.86 ±4	85±9.8

Abbreviations: C-4.16, CARP-1 Functional Mimetics; SMA, styrene maleic acid; TPGS, d-α-tocopheryl polyethylene glycol succinate; ATZ, Acetazolamide; CMC, critical micelle concentration; PDI, polydispersity index; EE, encapsulation efficiency.

5.4.4. Rationale for choosing CA IX protein for RCC therapy

In this study, we have shown that CA IX was overexpressed in A498 and Evr-res A498 RCC cells and tumor. In Figure 5.3A, immunohistochemistry of CA IX-positive A498 RCC tumor xenografts collected from tumor tissue section is shown. The intense bright green fluorescence indicates the presence of CA IX. In Figure 5.3B, Western blot data show levels of CA IX protein in A498 and Evr-res A498 RCC cells that were cultured under normoxic (no cobalt chloride treatment) or hypoxic conditions (treated with cobalt chloride for 72 hrs.). Together with immunohistological localization of CA IX in RCC tumor, the up-regulation of CA IX expression in hypoxic WT and Evr-res A498 RCC cells in comparison to their respective, normoxic counterparts provides a rational strategy for delivering the payload into the hypoxic core of RCC tumor. Moreover, CA IX has been shown to be specifically overexpressed in 93 to 97% of both ccRCC and some papillary RCCs, with limited expression in normal tissues [224]. CA IX is also an important biomarker for RCC, and it plays a pivotal role in tumor progression, acidification, metastasis, and the intra-tumoral hypoxic condition. CA IX expression on the cell surface is associated with induction of tumor hypoxia through regulation of HIF1α. The clinicopathological analysis have supported the fact that overexpression of CA IX in RCC is linked to poor disease prognosis and resistance to chemo and immunotherapy. Many clinical trials are evaluating CA IX linked inhibitors or antibodies for monotherapy or diagnostic imaging. Recently, a small molecule, acetazolamide (ATZ), with high affinity (Kd~ 8.3 nM) to CA IX [225] has been reported to deliver the payload into the inner core (more than the periphery) of a tumor [163,218]. These results signify that CA IX is an excellent target for site-specific delivery of therapeutic payloads to renal tumors [226,227]. Along these lines, we developed ATZ-conjugated NPs for selective delivery of drug cocktail to the hypoxic region including the tumor core of therapy resistant RCC. It is well established that the hypoxic tumor core harbors aggressive and drug-resistant stem-like cells can persist after initial drug

therapy, which can invade normal tissues and metastasize to distant sites forming secondary tumors. Targeting the hypoxic core using CA IX is thus a highly innovative approach needing immediate attention.

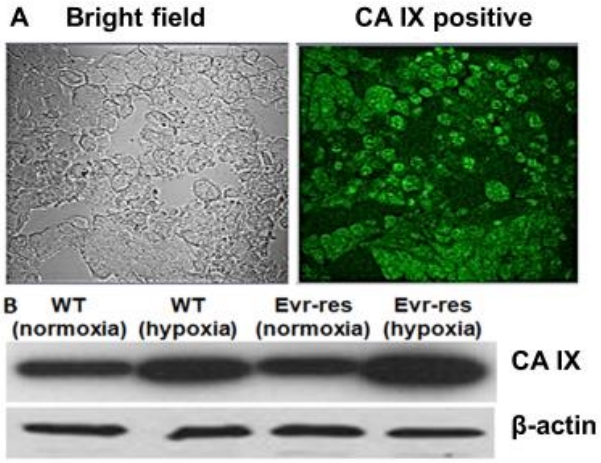

Figure 5.3. Overexpression of CA IX protein in A498 RCC cells and xenograft model. (A) Immunohistochemistry of CA IX positive A498 renal cell carcinoma tumor xenografts collected from tumor tissue section is shown. The intense bright green fluorescence indicates the rationale of choosing CA IX as an excellent RCC targeted therapy. **(B)** Western blot detection of CA IX protein in A498 and EV-A498 RCC cells lysates after normoxia (no cobalt chloride treatment) and hypoxia (treated with cobalt chloride for 72 hrs. to induce hypoxia) are shown. The fold up-regulation of CA IX expression in hypoxic WT and EV-res A498 RCC cells than normoxia provides a solid foundation for delivering the payload into oxygen deprived regions and hypoxic core of RCC tumor.

5.4.5. Selective uptake and tumor spheroid core penetration of CA IX oligomers to RCC.

The 3 D spheroid cell culture model is an in vivo mimetic study for testing NPs deep tumor core penetration ability. Thus, culturing A498 RCC cell lines with a spheroid model in hypoxic condition could be predictive of the tumor permeability of CA IX targeted NPs. In Figure 5.4 C, we found that the rhodamine-conjugated ATZ oligomer (CA IX-Rhoda) has deep tumor matrix penetration and superior uptake in hypoxic Evr-res A498 spheroid model. The cell uptake study

of CA IX targeted NPs was performed using Evr- res A498 spheroid model followed by imaging of spheroid using confocal microscopy. Interestingly, Z-stacking from 10, 40, 60, and 100 µm in confocal microscopy of CA IX targeted oligomer-treated cells indicate that rhodamine-signal is significantly higher in the core of the spheroid than the periphery (Figure 5.4. C-D). This is a strong indication that CA IX targeted oligomer can penetrate deep into the tumor spheroid and likely reached the hypoxic regions very efficiently. The highest fluorescence intensity at the center (as indicated by arrow) of 3D- plot (Figure 5.4 C) suggests that CA IX targeted oligomer efficiently reached the core of tumor spheroid. Also, in Figure 5.4 C, with the lower range of Z-stacking from 40-60 µm section (which is the core) has more fluorescence intensity than the periphery. Z-stacking of the spheroid at different sections from 10-100µm with CA IX targeted formulations also shows superior fluorescence intensity from 40-60 µm sections representing organoid core. Figure 5.4. E showed the overall merged view of CA IX-Rhod-B oligomer with bright field and compared with untreated control. Figure 5.4 F shows the overall shape of the spheroid from along the three dimensions (x, y, and z) as another way of representation to demonstrate spheroid core penetration.

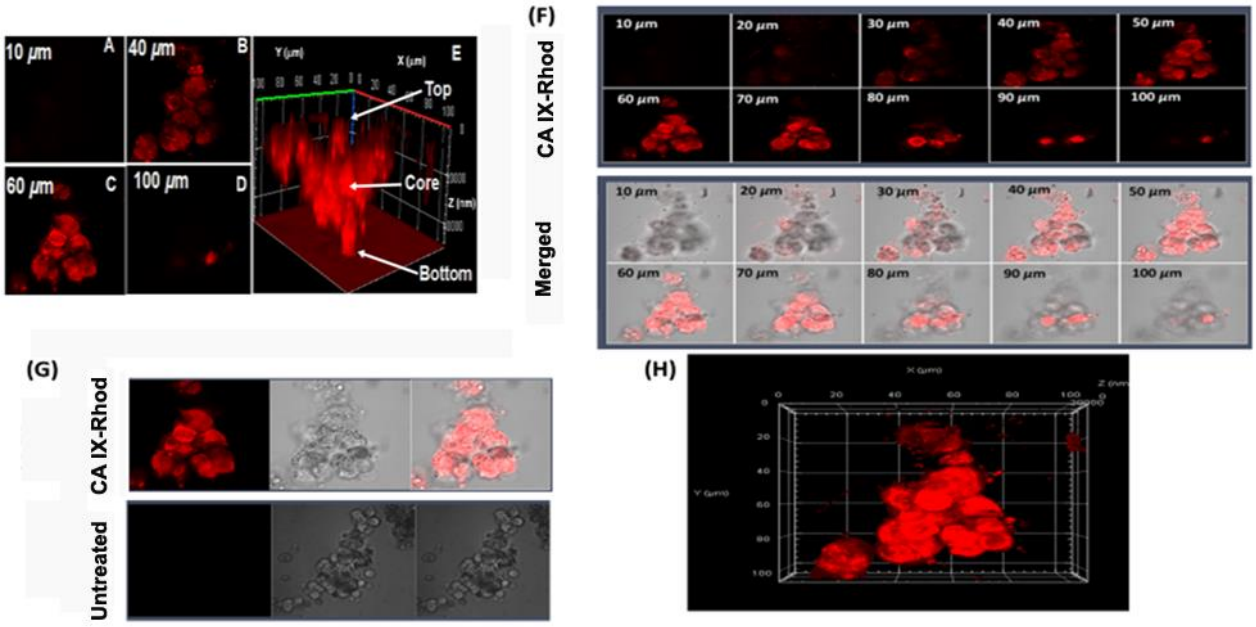

Figure 5.4. 3D spheroid uptake studies of hypoxia targeted-oligomer. Confocal microscope images of ATZ-oligomer conjugated with rhodamine B and treated with hypoxic A498 RCC cells -spheroid indicates tumor matrix penetration of CA IX targeted Oligomicelles. The untreated and treated spheres were then photographed as noted in methods section. Z-stacking of the spheroid (A-D) clearly indicates that fluorescence intensity is superior in 40-60 µm section. The highest fluorescence intensity at the center (as indicated by arrow) of 3D- plot (E) suggests that CA IX-Rhoda oligomer is highly efficient to reach deep into the core of the tumor spheroid. (F) Z-stacking of the spheroid at different sections from 10-100□m with CA IX targeted formulations also reveals similar findings as noted for the 40-60 µm that had superior fluorescence intensity. Figure (G) shows the untreated control experiments in comparison with CA IX-Rhoda oligomer and Figure (H) shows the overall shape of the spheroid from along the three dimensions (x, y, and z).

5.4.6. C4.16 anti-cancer effect and Hypoxia targeting ability of CA IX NP

RCC is very difficult to treat as the cells are mostly resistant to many current therapies. Therefore, newer treatments including better ways of drug delivery are urgently needed to fight this malignant disease efficiently. Our previous work has demonstrated generation and characterization of RCC cells that are resistant to Evr, a frontline mTOR-targeted therapy, and revealed that a class of CARP-1 functional mimetic (CFM) compounds especially C-4.16 inhibited parental (WT) and Evr-res RCCs[157]. In this study, we utilized C-4.16 and current clinical anti-RCC therapeutics Sor

and Evr. First, we determined cytotoxicity of individual drugs C4.16, Sor, and Evr in both A498 as shown in Figure 5.5. Our results from Figure 5.5. A, B indicated that C4.16 was more effective in inhibiting growth of WT and Evr-res A498 compared with Sor. Evr, however, did not inhibit growth of Evr-res A498 RCC cells as previously published [14]. We then clarified whether a combination of C4.16 and Sor were more effective when compared with individual treatment. In vitro cytotoxicity assay of C4.16 and Sor on Figure 4 A, B indicates C4.16 was more potent than FDA approved drug (Sor) and combining both drugs showed significantly lower the IC50 value. All the results indicate C4.16 and Sor inhibited viabilities of WT and Evr-res RCC cells, and C4.16 when combined with sor was more effective than C4.16 or Sor alone. However, C4.16's poor water solubility limits it's in vivo testing and clinical translation. We addressed the solubility and delivery concerns of C4.16 by utilizing a nanotechnology-based approach. Thus, encapsulation of C4.16 in NP and conjugating them with CA IX targeting oligomer was considered as a functional approach for resolving the challenges to deliver the compounds selectively to resistant RCC. The results as noted in Figure 5.5 C show that CA IX-C4.16 was more effective in inhibiting growth of A498 (WT and Evr-res) compared to Sor and Evr and supported that CA IX-C4.16 nano-formulation was more potent compared to FDA approved drugs. The table in Figure 5.5. D summarizes IC_{50} values for all drugs with the WT and Evr-res RCC cell lines. The data in Figure 5.5. C, D showed that CA IX-C4.16 was more effective in inhibiting growth of A498 (WT and Evr-res) compared to Sor and Evr and collectively indicate that CA IX-C4.16 was more potent compared to other drug options. Furthermore, to confirm the synergism, we utilized CompoSyn® software to evaluate the combination index (CI) value of C4.16 and Sor. As shown in Figure 5.5. E, C4.16 and Sor had CI value (less than 1) of 0.531 for A498 WT and 0.654 for Evr-Res, which indicated synergism between the two compounds. Figure 5.5. F also demonstrated a combination

of CA IX-C4.16 with Sor is synergistic in RCC cell killing as obtained from isobologram analysis. Thus, low dose of CA IX-C4.16 NP could potentially sensitize RCC cells for inhibition by Sor. Moreover, as shown in Appendix Figure, a combination of 500 nM dose of CA IX-C4.16 with various doses of Sor further support their synergistic inhibition of RCC cells. A 500 nM dose of CA IX-C4.16 caused greater inhibition of RCC cell growth when combined with low doses of Sor (100, 200, 500 nM).

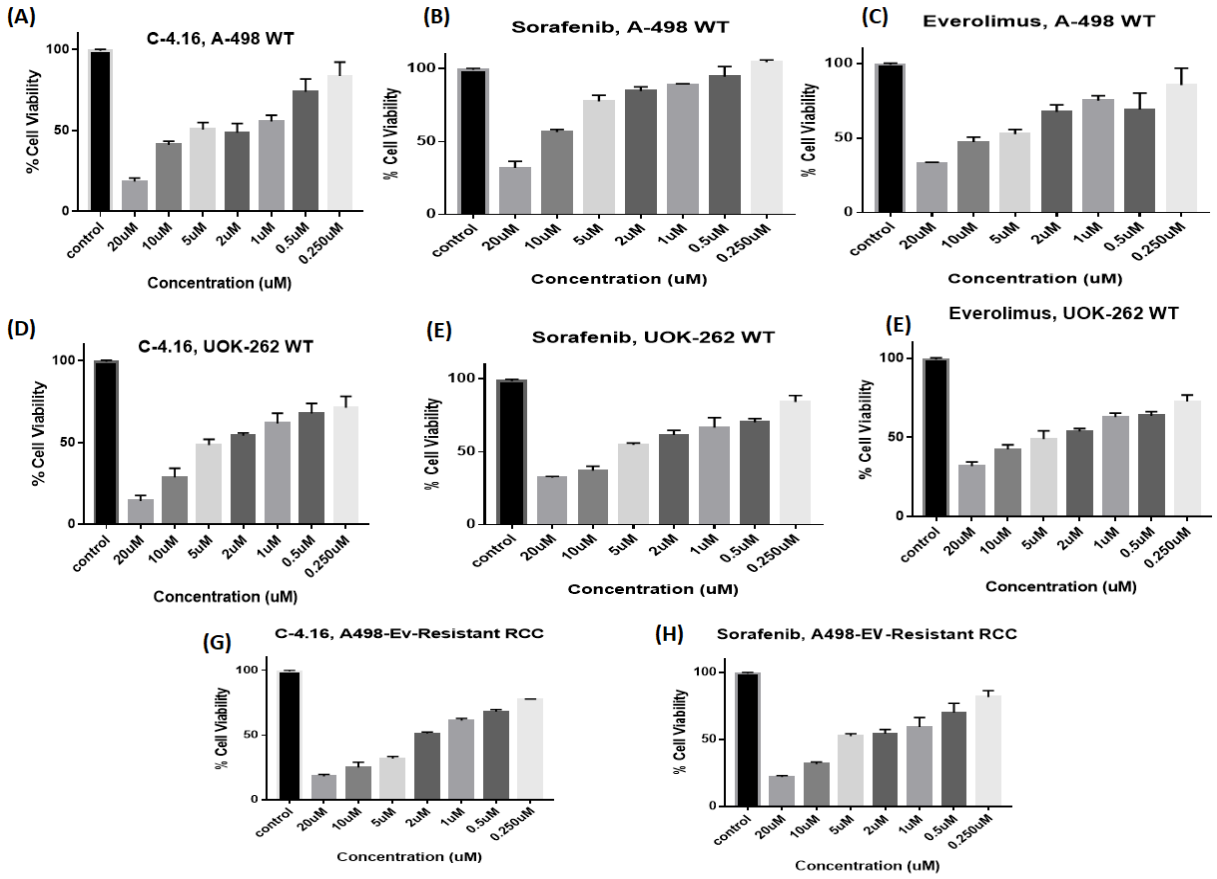

Figure 5.5. C-4.16 inhibits growth of RCC cell lines derived from WT and Everolimus-resistant cells. Cell cultures studies and in vitro cytotoxicity assay of C-4.16, sorafenib, Everolimus on (WT and Evr-Res) A498 and UOK-262 RCC cell lines. **(A, B, and C)** Cytotoxicity data indicates C-4.16 was more potent than FDA approved drugs (sorafenib and everolimus) in WT A498 and **(D, E, and F)** WT UOK262. Also, cell cultures studies result on EV-res A498 RCC cell lines **(G and H)** indicates that C-4.16 was more effective in inhibiting growth of Evr-res A498 RCC cell lines than sorafenib; however, Everolimus is not inhibiting the growth of Evr-res A498

and UOK262 RCC cell lines as previously published. The data in the GI_{50} columns represent mean of three independent experiments. Indicated parental and their respective drug resistant RCC cells were either untreated (Control) or treated with noted doses of C-4.16 and sorafenib for 48h.

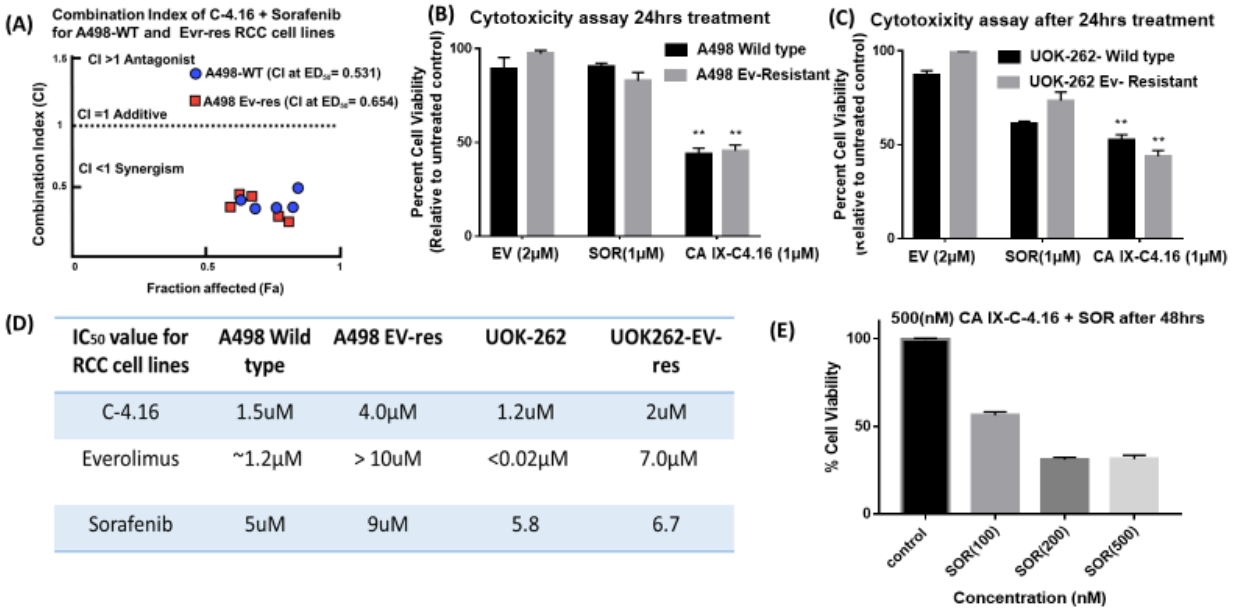

(D)

IC50 value for RCC cell lines	A498 Wild type	A498 EV-res	UOK-262	UOK262-EV-res
C-4.16	1.5uM	4.0μM	1.2uM	2uM
Everolimus	~1.2μM	> 10uM	<0.02μM	7.0μM
Sorafenib	5uM	9uM	5.8	6.7

Figure 5.6. High synergistic CI value of C-4.16 with sorafenib combination supports the hypothesis of selecting the combination to RCC treatment using hypoxia targeting OMs. (A) Combining very low doses of both drugs will lower the IC_{50} value significantly as in **(D)** which shows the combination index plot for C-4.16 plus sorafenib in the cells for both types A498 RCC cell lines indicates very strong synergism between sorafenib and C-4.16. **(B)** The results also show that CA IX-C-4.16 was more effective in inhibiting growth of A498 (WT and Ev-res) and to less extent **(C)** UOK262 (WT and Ev-res) RCC cell lines than sorafenib and Ev and support that C-4.16 was more potent than FDA approved drugs (sorafenib and everolimus). **(D)** We summarized IC_{50} value table for all drugs with all the above mentioned RCC cell lines. **(E)** In vitro cytotoxicity assay of CA IX-C4.16 (500 nM) in combination with different doses of sorafenib on Ev-res A498 RCC cell lines indicates that low dose of C-4.16-OMs sensitize sorafenib for inhibiting growth of RCC cell line.

5.4.7. Mechanism of C4.16 for overcoming drug resistance

In this study, we determined how induction of apoptosis and inhibition of oncogenic survival signaling would reinforce the synergistic cell killing and reversal of drug resistance in WT and Evr-res A498 cells when treated with CA IX C4.16+Sor. As shown in Figure 5.7. A, we

observed inhibition of AKT activation as indicated by downregulation of pAKT in C4.16 and Sor treatment compared to untreated control. We found that Evr-res RCC cells that were treated with C4.16 or Sor had a greater loss of AKT activities when compared with their WT cells treated with respective agents. Interestingly though, a combination of C4.16 and Sor completely abolished AKT activity (pAKT) in both the WT and resistant cells. Therefore, it is likely that superior RCC growth inhibition by C4.16 and Sor is in part due to suppression of oncogenic AKT activity. Moreover, C4.16 cytotoxicity was mediated by apoptosis induction (Figure 5.7 A) supporting our prior studies that have shown activation of apoptosis in C4.16 treated cells. Although, C4.16 or Sor induced caspase-3/7 activation, a significant upregulation of caspase-3/7 activity was noted in RCC cells treated with C4.16+Sor as compared to control (Figure 5.7 B). This finding was further supported by an increment of early and late apoptotic events in both WT and Evr-res A498 cells treated with CA IX-C4.16+Sor as compared to untreated control or CA IX-C4.16 (Figure 5.7 C). The fraction of cells that stained with Annexin V (+ve) or Annexin V (+ve) and 7-AAD (+ve) was higher in combination treatment than singular treatments as shown in Figure 5.7 D. In all the cases; combination always worked better than individual drugs in inhibiting RCC cells growth.

As shown previously, C4.16-dependent loss of RCC cell viability was due in part to reduced cyclin B1 levels, activation of pro-apoptotic, stress-activated protein kinases (SAPKs), and apoptosis [157]. Importantly, we also demonstrated that CARP-1 was a key player in inducing apoptosis and cell cycle arrest in the breast, lung and renal cancer cells [139,140]. The up-regulation of CARP-1 promotes activation of “apoptosis hallmarks,” such as caspase-mediated PARP cleavage, downregulation of PI3K/AKT signaling and loss of cyclin B1 in RCC [157]. To identify potent activators of CARP-1, a library of small molecules, namely CARP-1 functional mimetic (CFM) compounds were developed. An NCI-60 screening, as well as high throughput screening

using various cancer cell lines, including WT and drug-resistant Evr-res RCC, resulted in the identification of several potent analogs. Our current results suggest that C4.16 is a superior inhibitor of both WT and drug-resistant RCC even in comparison to the FDA approved drugs, such as Ever and Sor. As RCC is highly vascularized, the use of drugs to inhibit RTK, such as VEGFR or HGF signaling is used as first-line therapies. Alongside, mTOR inhibitors, such as Evr were approved as second-line single agent therapy. All these kinase inhibitors are approved for single agent therapy. However, tumors eventually become resistant to therapy including RKT/mTOR inhibitors. Our findings suggest that the NPs formulations of the inhibitors will be a worthwhile strategy to provide multiple benefits such as (i) amenable for i.v. injection leading to lowering of drug dose; (ii) higher stability and bioavailability; (iii) sustain drug release and reduced toxicity. Literature reports and clinical experience have revealed that inhibiting RCC proliferation with drugs combination specific to different targets is superior to monotherapy approaches [228]. However, such approaches tend to produce severe on-target and off-target toxicities [229]. To achieve the maximum therapeutic benefits and reduce the toxicity, we encapsulated anticancer drugs in CA IX-C4.16 NPs. This i.v. administrable NPs in combination with currently approved drugs is an excellent approach to precisely target the convergent pathways of RCC activity with resistant and tumor stroma features [230].

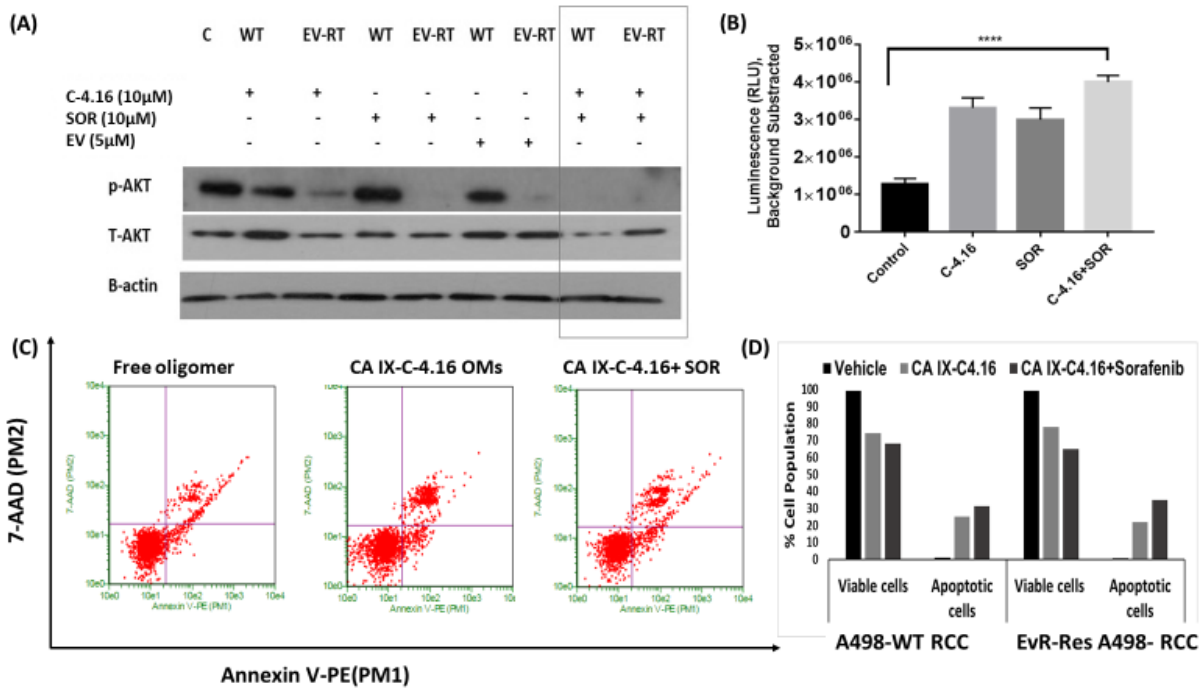

Figure 5.7. (A) Western Blot data indicates that C-4.16 stimulates apoptosis in WT and Ev-resistant RCC cells in part by upregulating pro-apoptotic CARP-1 and activating SAPKs as previously shown in [14], and in here P-AKT is indicated as the a protein which is affected much by combination of C4.16 and sorafenib. Indicated RCC cells were either untreated (Control, denoted as C), treated with C-4.16, Sorafenib, or Everolimus with (+) means presence of the combination and (-) indicates use only of single drug for noted dose and time. Cell lysates were analyzed by Western blotting (WB) as in Methods for levels activation (phosphorylation) and expression of both P-AKT and T-AKT in WT or Ev-res A498 RCC cells. **(B)** Up-regulation of caspase 3/7 with (C-4.16+SOR) treatment in Evr-res A498 cells indicates the C-4.16 mediated apoptosis to RCC cells as compared to sorafenib (SOR) treatment or combination (C-4.16+SOR). The results support (C-4.16+SOR) combination is more effective for RCC cell lines growth inhibition. **(C)** Free oligomer, CA IX-C-4.16 OMs and CA IX-C-4.16+ sorafenib with an increasing apoptosis measured by FACs using staining of Annexin V-FITC and PI in (A) A498 RCC (WT and Ev-res) cells are shown. Free oligomer (vehicle) were used as negative controls. Data represent mean □ SD, n=3 per group, **p<0.01 vs. control. **(D)** Histogram columns of both viable cells and apoptotic cells indicates that CA IX-C4.16 + sorafenib has more % apoptotic cell than CA IX- C4.16 alone which support our hypothesis of the synergism between these anticancer agents.

5.4.8. Reprogramming macrophages to modulate combination treatment:

To overcome the critical problem of current RCC treatment, we developed a tumor-penetrating nano-sized NP of spherical shape that can localize and penetrate tumor tissues efficiently and target

tumor hypoxia to deliver the combination drug cocktail to shut down vital tumorigenic signaling while simultaneously reprogramming macrophages for better therapeutic efficacy. Several studies have identified the key players that are responsible for drug resistance and immune evasion leading to the poor prognosis of RCC. These players are categorized based on their specific roles that include (i) RTK-mTOR that regulates critical tumorigenic signaling for tumor survival, immune suppression, and stroma formation, (ii) impairment of intrinsic and extrinsic apoptotic signaling is an essential player of drug resistance. Induction of CARP-1 protein has been well documented to induce apoptosis in cancer cells under the conditions of serum withdrawal or therapy stress. (iii) CA IX is a tumor hypoxia marker for the maintenance of extracellular acidosis and cancer stemness, thus facilitating tumor growth and metastases. More than seven clinical trials are underway to target CA IX in RCC and other solid tumors [NCT00059735, NCT00884520]. The delivery system we have engineered here will be a promising addition to clinical translation for better RCC treatment. Figure 5.8. A shows a schematic diagram as Raw264.7 cells were placed into the insert. Then, cells were polarized to M1-macrophage using IFN-γ and LPS, and to M2-macrophage using IL-4 recombinant protein. The change of morphology of Raw264.7 as shown in Figure 5.8. B supports the M1/M2 polarization of naïve Raw264.7 cells[231] followed by treatment with C4.16 and CA IX-C4.16+Sor for 24 h. The data in Figure 5.8. C clearly demonstrate the up-modulation of the tumoricidal M1-macrophage marker (CD86, iNOS) and down-modulation of the tumorigenic M2-macrophage marker (CD206, Arginase I) compared to untreated (UT) control and C4.16. The macrophage reprogramming ability of CA IX-targeting NP builds a rational of using (CA IX-C4.16+Sor) as a potent antitumor immune-stimulatory agent of RCC. The treatment of CA IX+Sor to Evr-res A498 cells cocultured with M1-macrophage resulted in the growth inhibition and change of morphology that could be due to tumoricidal M-1

macrophage mediated cell death of RCC cells as shown in Figure 5.8. D. Further to evaluate the macrophage induced RCC cell death, we analyzed up-modulation of caspase 3/7 in Evr-res A498 cell co-cultured with Raw 264.7 cell and treated with CA IX-C4.16+Sor or other treatments. The data from Figure 5.8. E clearly confirmed combination is significantly better in inducing apoptosis as compared to control or individual treatments. All these results demonstrate hypoxia targeting NP in combination with Sor is not only inducing chemotherapeutic effect but also reeducating macrophages to function as a tumoricidal agent, which could prove excellent for a combination of chemo-immune therapy to inhibit Evr-res RCC.

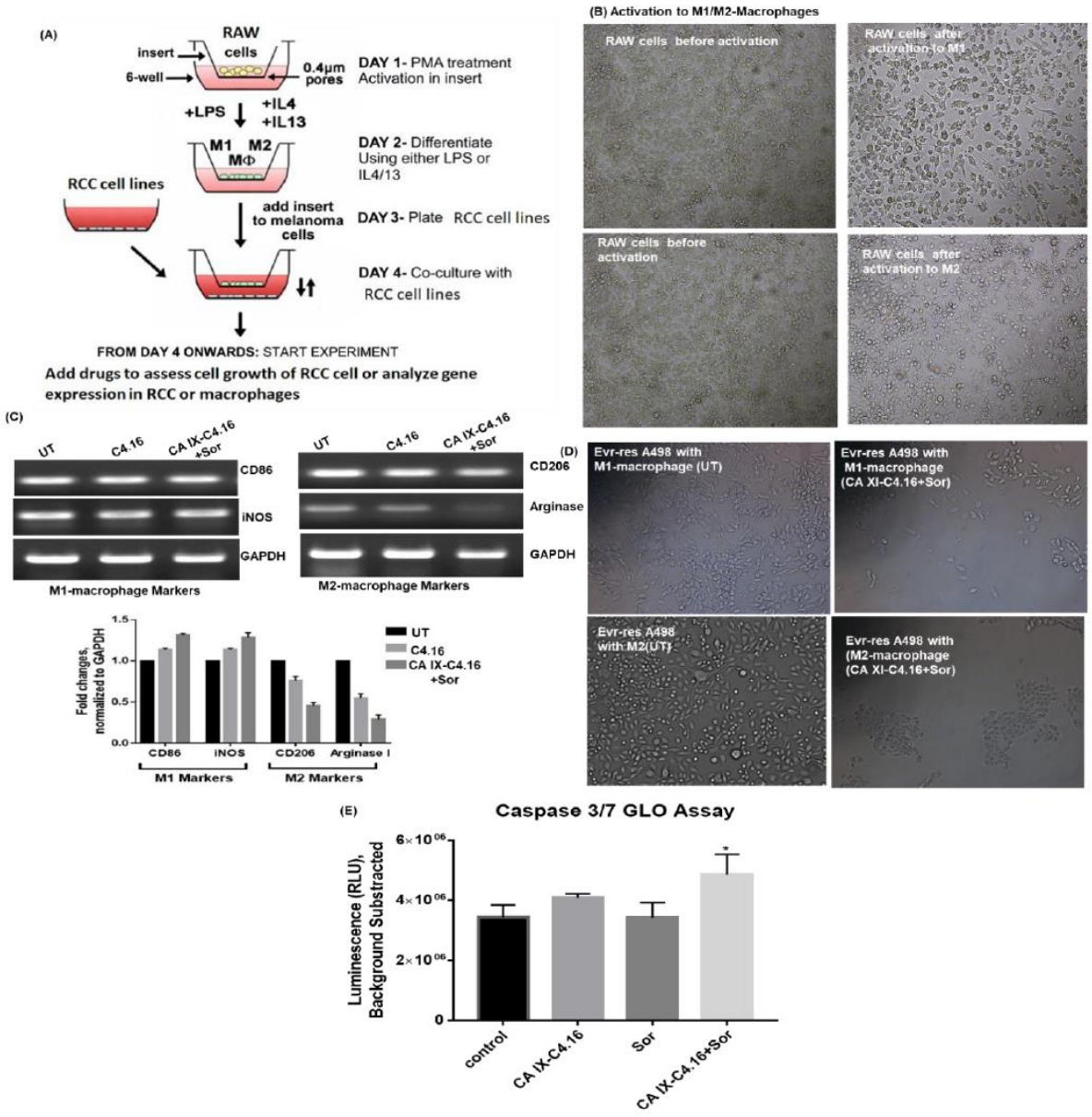

Figure 5.8. Reprogramming macrophages with CA IX-C4.16+Sorafenib treatment. (A) Schematic diagram of the procedure. Raw-264.7 cells were placed into the insert. Then, cells were polarized to M1-macrophage using IFN-□ and LPS, and to M2- macrophage using IL-4 recombinant protein. Scheme modified from the original protocol. (B) Change of morphology of M1 and M2 macrophages supports the polarization of Raw-264.7. (C) RT-PCR data clearly demonstrates the up-modulation of the tumoricidal M1-macrophage marker (CD86, iNOS) and down-modulation of the tumorigenic M2-macrophage marker (CD206, Arginase I) in CA IX-C4.16+Sor as compared to control and C4.16. The macrophage reprogramming ability of CA IX targeting NP builds a rational of using (CA IX-C-4.16+Sor) as a potent antitumor immune-stimulatory agent of RCC. (D) Change of morphology and reduction of Evr-res A498 density in M1-macrophage and Evr-res A498 co-cultured condition, treated with CA XI+Sor suggesting activated M1-

macrophage mediated RCC cell death. (E) Treatment of CA IX+Sor educate the Raw-264.7 in inducing caspase 3/7 mediated apoptosis of Evr-res A498.

5.4.9. Superior tumor core penetration and high tumor/liver uptake of CA IX oligomers in xenograft RCC model.

After optimizing the anticancer effect of CA IX-C4.16 at the cellular level, we performed NIR imaging in animals inoculated with RCC tumor model following administration of CA IX-S0456. The idea of performing NIR-imaging with CA IX-oligomer will provide several advantages including its use as (i) agent for tumor image guided RCC surgery in the clinic, as well as (ii) meaningful insights into the therapeutic outcome and safety of nanoformulation in RCC model. It is well known that clinically small molecule NIR imaging agents have excellent ability to distinguish the tumor lesion from healthy tissue in imaging-guided surgery as noted in NCT02317705 and NCT01778933 [232]. The results show CA IX-S0456 selectively home to the orthotopic subcutaneous Evr-res A498 tumor as compared to control (Figure 5.9. A and C). The bio-distribution (Bio-D) study in Figure 5.9. B validates the prominent tumor selectivity of CA IX-S0456 as compared other healthy organs such as liver and spleen. Imaging of the patient-derived RCC tumor xenograft (PDx) (Figure 5.9. C) showed favorable tumor localization of CA IX-S0456. The tumor selectivity of CA IX-S0456 in both drug resistant and PDx RCC model builds a foundation for widespread applicability of CA IX-S0456 in different RCC tumor model that builds a rational platform for further investigation towards clinical translation of this technology. In Figure 5.4, 3D spheroid uptake study of CA IX-rhodamine showed high localization of rhodamine in the core of the hypoxic Evr-res A498 spheroid. To ascertain core penetrating ability of CA IX-S0456 in a drug resistant tumor model, we performed a transverse section of the isolated tumor after the bio-D study. Figure 5.9. D confirmed that CA IX-S0446 is very efficient in penetrating the core of tumor that predominantly harbors hypoxia and drug resistant features.

As shown in Figure 5.9. E, more than 3-fold tumor/liver ROI in CA IX-oligomer compared to control demonstrates the feasibility of CA IX-S0456 in clinical translation as an image-guided surgery tool. The findings in Figure 5.9. F suggest the ROI is >2 fold in CA IX-S0456 treated tumor core as compared to tumor periphery. These results support a high binding affinity and specific tumor uptake, faster normal tissue clearance, and low non-specific organ uptake of CA IX-oligomer.

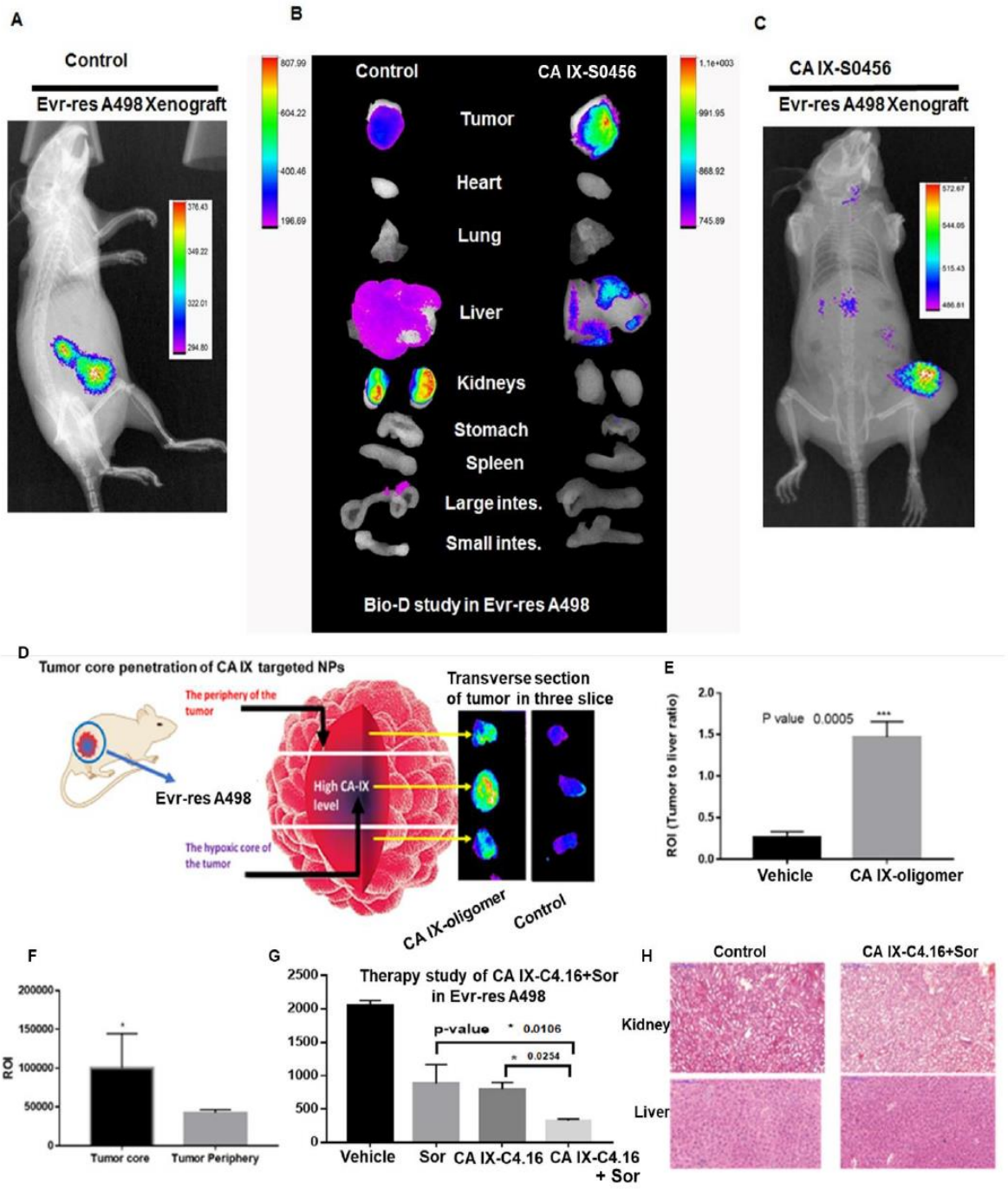

Figure 5.9. Superior tumor specificity of CA IX-oligomer and antitumor efficacy study of combination therapy in Evr-res A498 xenograft and RCC PDx model. (A and C) Superior tumor accumulation of CAIX oligomer (CA IX-S0456) as compared to control (S0456) in Evr-res A498 tumor xenograft model. (B) Bio distribution (Bio-D) study of CA IX-S0456 showed superior tumor specificity and low non-specific liver uptake in Evr-res A498 tumor bearing mice. The control, S0456 showed poor tumor accumulation with high off-target activity. ((D) Further to

demonstrate the tumor core penetration of NIR dye, isolated Evr-res A498 tumor was transversely sectioned, and brightest fluorescence intensity at the middle section confirmed of CA IX-S0456 has an excellent hypoxic tumor core penetration ability as compared to control. (E) Significantly high tumor/liver accumulation (more than 3-fold) of CA IX-oligomer solve the non-specificity effect of the oligomer. (F) Quantification of fluorescent ROI indicates CA IX-oligomer is significantly penetrating higher in tumor core contained as compared to its periphery. The results suggest the importance of CA IX-oligomer in selective tumor targetability of RCC tumor model. (G) Tumor growth inhibition of (CA IX-C4.16+Sor) is significantly higher compared to vehicle(control), Sor, and CA IX-C4.16 in Evr-res A498 xenograft tumor. Significant tumor growth suppression of combination therapy supports the rationale of using CA IX targeting nano-formulation as the delivery vehicle of potent drugs, C4.16. The data represented as average values from whole four animals in the respective group, bars, SE, significant where *$p<0.05$ vs. Control. (H) Histopathologic (H&E staining) examination to determine the toxicity of therapeutic drugs on livers and kidneys at the end of the experiments. Images indicate there is no significant sign of necrosis or loss of tissue architectural difference in vehicle control and CA IXC4.16+ Sor treated tissues.

5.3.10. Tumor growth inhibition and excellent safety of CA IX-C4.16+Sor in Evr-res tumor.

After confirming the in vitro anticancer activity, we finally examined the antitumor effect of CA IX-C4.16 NP in combination with Sor, to demonstrate the efficacy of combination regimen in reversing Evr-resistance in RCC. The CA IX-C4.16 NPs formulation inhibited the viability of WT and Evr-res A498 cells in vitro by stimulating various tumoricidal pathways including induction of apoptosis, downregulation of pAKT and up-modulation and education of M1-macrophages. As shown in Figure 5.9. G, CA IX-C4.16 significantly inhibited highly aggressive Evr-res A498 tumor in combination with Sor. The greater tumor growth inhibitory effect of CA IX-C4.16+Sor compared to control and individual treatments thus opens an avenue that CA IX-C4.16 nano-therapy can resurrect Sor as a more efficient anticancer therapeutic agent. Importantly, CA IX-C4.16+Sor did not cause any necrosis or morphological changes in tissue architecture of normal organs such as kidneys and liver (Figure 5.9. J). The superior tumor penetration of CAIX-oligomer and efficient antitumor effect of CA IX-C4.16+Sor in different RCC tumor model underscore a viable strategy for developing a smart therapy against drug resistant tumors

with high safety profile. The current findings can support the claim that CA IX-NPs loaded with anticancer payload can play a universal role in overcoming drug resistance and repurposing current drugs in a more efficient way.

5.4. Conclusions

In this study, we have demonstrated elevated expression of CA IX in RCC that qualifies its use as an excellent biomarker for targeted therapy and imaging. The combination of C4.16 and Sor have a superior synergistic cell killing in Evr-res RCC, which is due in part to activation of caspase 3/7 protein and complete eradication of oncogenic AKT activation. Combination of CA IX-C4.16 with Sor showed targeted delivery of payload in hypoxic tumor resulting in induction of sequential anticancer effects including, the resurrection of apoptosis, reversal of drug resistance, and reprogramming of malfunction macrophages. This NP could have a direct impact on developing newer therapies for treating RCC. We found that CA IX-C4.16 NP is suitable for intravenous administration with superior tumor accumulation of CA IX-oligomer as compared to liver and demonstrated effective antitumor response in Evr-res A498 tumor. Due to small molecular size and ease of chemical functionalization, CA IX-oligomer can potentially be further explored for selective CA IX tumor targeting for the diagnostic use and RCC image-guided surgery in the clinical setting. The tumor spheroid uptake study has clearly demonstrated excellent tumor core penetrating ability of CA IX-targeting oligomer, which is a critical indicator of tumor stromal disruption leading to better therapy response and immune modulation. In conclusion, the synergistic therapeutic potential of CA IX-C4.16 and Sor combination and selective NIR imaging of the CA IX anchored oligomer portend their promising potential towards developing better therapeutics and diagnostic tools for clinical translation against deadliest drug resistant RCC.

6. CHAPTER 6. SUMMARY AND KEY FINDINGS

6.1. Aim 1

6.1.1. Summary

Current treatments for Renal Cell Carcinoma (RCC) include a combination of surgery, targeted therapy, and immunotherapy. Emergence of resistant RCCs contributes to failure of drugs and poor prognosis, and thus warrants development of new and improved treatment options for RCCs. Here we generated and characterized RCC cells that are resistant to Everolimus, a frontline mTOR-targeted therapy, and tested whether our novel class of CARP-1 functional mimetic (CFM) compounds inhibit parental and Everolimus-resistant RCC cells. CFMs inhibited RCC cell viability in a dose-dependent manner that was comparable to Everolimus treatments. The GI_{50} dose of Everolimus for parental A498 cells was ~1.2μM while it was <0.02μM for the parental UOK262 and UOK268 cells. The GI_{50} dose for Everolimus-resistant A498, UOK262, and UOK268 cells were ≥10.0μM, 1.8-7.0μM, and 7.0-≥10.0μM, respectively. CFM-4 and its novel analog CFM-4.16 inhibited viabilities of Everolimus resistant RCC cells albeit CFM-4.16 was more effective than CFM-4. CFM-dependent loos of RCC cell viabilities was due in part to reduced cyclin B1 levels, activation of pro-apoptotic, stress-activated protein kinases (SAPKs), and apoptosis. CFM-4.16 suppressed growth of resistant RCC cells in three-dimensional suspension cultures. These findings portent promising therapeutic potential of CFM-4.16 in treatment of RCCs.

6.1.2. Key Findings:

(1) CARP-1 functional mimetics (CFM 4.16) are a novel small molecule inhibitor of triple-negative breast cancers, non-small cell lung cancers, and renal cell carcinoma.

(2) CFMs induce Apoptosis by activating SAPKs and elevating CARP-1. CARP-1/CCAR1 interacts with RIPK1, pro-apoptotic adaptor protein FADD, cleaved caspase 8 and is likely a part of an intracellular, apoptosis-transducing subcomplex.

(3) CFMs attenuate biological properties of cancer cell motility, migration, and invasion.

6.2. Aim 2

6.2.1. Summary:

CFMs are hydrophobic compounds and they have poor aqueous solubility and their dose escalation for in-vivo studies remain challenging. In this study, we encapsulated CFM-4.16 in Vitamin-E TPGS-based-micellar-nano-formulation that resulted in its higher loading (30% w/w). This CFM-4.16 nanoformulations inhibited viability of parental and Everolimus-resistant RCC cells *in vitro* and suppressed growth of parental A498 RCC-cell-derived xenografts in part by stimulating apoptosis. These findings portent promising therapeutic potential of CFM-4.16 nanoformulations in treatment of RCCs. Here we investigated whether the SMA-TPGS nano-formulation of CFM-4.16 circumvents the solubility concerns of CFM compounds to permit its intravenous administration in conducting in vivo studies. Also, the aim is to demonstrate if SMA-TPGS-CFM-4.16 nanoformulation can produce cancer cells inhibition in different types of cancer. For this purpose, we will optimize and characterize novel SMA-TPGS polymeric Nano micelles which then will increase water solubility of drug loaded formulation; thus, it will allow intravenous (i.v.) administration of the SMA-TPGS-CFM-4.16. Specifically, we aimed to achieve an increased serum bioavailability of CFM-4.16 due to administration using nano-formulation, increased nano-formulation accumulation and retention within the tumor by the EPR effect and therefore an increased localized CFM-4.16 concentration in tumor tissues relative to free drug and later

producing a marked antitumor response. In this regard, NSCLC, TNBC, and RCC cell lines were used to confirm the proof of concept for *in-vitro* effectiveness of nano micellar formulation of CFM analog. The TPGS-based nano-formulation of CFM-4.16 inhibits viability of RCC cells *in vitro* and their growth as xenografted tumors in immunocompromised mice.

6.2.2. Key Findings

CARP-1 functional mimetics (CFMs) are novel small molecule inhibitors of RCC. In addition, CFMs induce apoptosis by activating SAPKs and elevating CARP-1. In this study, we employed a nanotechnology to tackle the poor aqueous solubility of a potent CFM compound (CFM-4.16) which restricts its *in vivo* therapeutic efficacy. This SMA-TPGS-CFM-4.16 formulation maintained its nanoparticulate nature, homogenous polydispersity and high drug encapsulation efficacy. Since free CFM-4.16 or SMA-TPGS-CFM-4.16 elicited similar effects on cell viability, and levels of apoptosis would indicate that the anti-cancer effects of CFM-4.16 are retained in nanoformulation. Moreover, the physicochemical analyses indicate an optimum release of CFM-4.16 from nanoformulation. Together the physicochemical characteristics and biological activity of SMA-TPGS-CFM-4.16 seem promising for their use in future pre-clinical *in vivo* studies for the RCC tumor models.

6.3. Aim 3

6.3.1. Summary:

Drug resistance is one of the significant clinical burden in renal cell carcinoma (RCC). The development of drug resistance is attributed to many factors, including impairment of apoptosis, elevation of carbonic anhydrase IX (CA IX, a marker of tumor hypoxia), and infiltration of tumorigenic immune cells. To alleviate the drug resistance, we have used Sorafenib (Sor) in

combination with tumor hypoxia directed nanoparticle (NP) loaded with a new class of apoptosis inducer, CFM 4.16 (C4.16), namely CA IX-C4.16. The NP is designed to selectively deliver the payload to the hypoxic tumor (core), provoke superior cell death in parental (WT) and Everolimus-resistant (Evr-res) RCC and selectively downmodulate tumorigenic M2-macrophage. Copper-free 'click' chemistry was utilized for conjugating SMA-TPGS with Acetazolamide (ATZ, a CA IX-specific targeting ligand). The NP was further tagged with a clinically approved NIR dye (S0456) for evaluating hypoxic tumor core penetration and organ distribution. Imaging of tumor spheroid treated with NIR dye-labeled CA IX-SMA-TPGS revealed remarkable tumor core penetration that was modulated by CA IX-mediated targeting in hypoxic-A498 RCC cells. The significant cell killing effect with synergistic combination index (CI) of CA IX-C4.16 and Sor for Evr-Resistant A498 RCC cells suggests efficient reversal of Evr-resistance. The CA IX directed nanoplatform in combination with Sor has shown multiple benefits in overcoming drug resistance through (i) inhibition of p-AKT, (ii) upregulation of tumoricidal M1 macrophages resulting in induction of caspase 3/7 mediated apoptosis of Evr-res A498 cells in macrophage-RCC co-culturing condition, (iii) significant in vitro and in vivo Evr-res A498 tumor growth inhibition as compared to individual therapy, and (iv) untraceable liver and kidney toxicity in mice. Near-infrared (NIR) imaging of CA IX-SMA-TPGS-S0456 in Evr-res A498 and patient derived tumor xenograft (PDx) RCC model exhibited significant accumulation of NP in tumor core with >3-fold higher tumor/liver uptake as compared to control. In conclusion, this proof-of-concept study demonstrates versatile tumor hypoxia directed nanoplatform that can work in synergy with existing drugs for reversing drug-resistance in RCC accompanied with re-education of tumor-associated macrophages.

6.3.2. Key Findings

In this study, we have demonstrated elevated expression of CA IX in RCC that qualifies its use as an excellent biomarker for targeted therapy and imaging. The combination of C4.16 and Sor have a superior synergistic cell killing in Evr-res RCC, which is due in part to activation of caspase 3/7 protein and complete eradication of oncogenic AKT activation. Combination of CA IX-C4.16 with Sor showed targeted delivery of payload in hypoxic tumor resulting in induction of sequential anticancer effects including, the resurrection of apoptosis, reversal of drug resistance, and reprogramming of malfunction macrophages. This NP could have a direct impact on developing newer therapies for treating RCC. We found that CA IX-C4.16 NP is suitable for intravenous administration with superior tumor accumulation of CA IX-oligomer as compared to liver and demonstrated effective antitumor response in Evr-res A498 tumor. The tumor spheroid uptake study has clearly demonstrated excellent tumor core penetrating ability of CA IX-targeting oligomer, which is a critical indicator of tumor stromal disruption leading to better therapy response and immune modulation against deadliest drug resistant RCC.

APPENDIX

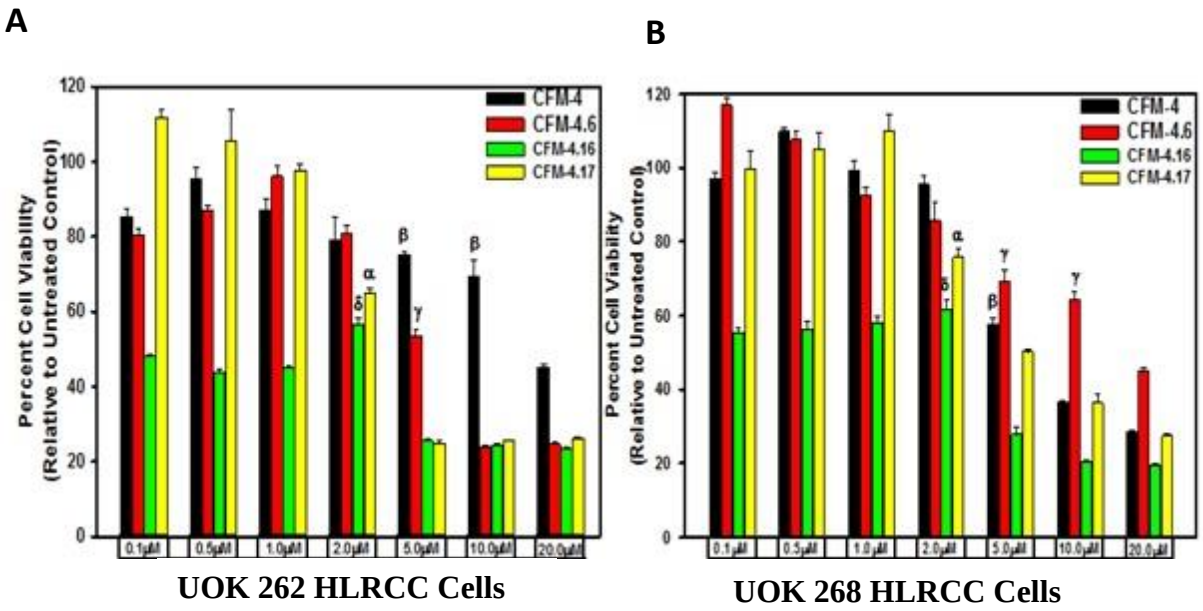

Appendix Figure 7.1. CFMs inhibit RCC cell growth. We treated noted cell lines either with DMSO (Control), with various CFMs (A, B) for indicated dose and time. We determined cell viability by MTT assay. The data in the histograms represent means of three independent experiments with 4-6 replicates for each treatment; bars, S.E. A-D, @,#,&,*, E-F, α,β,γ,δ, statistically significant inhibition (p = <0.05) relative to DMSO-treated respective controls. Adapted from [1].

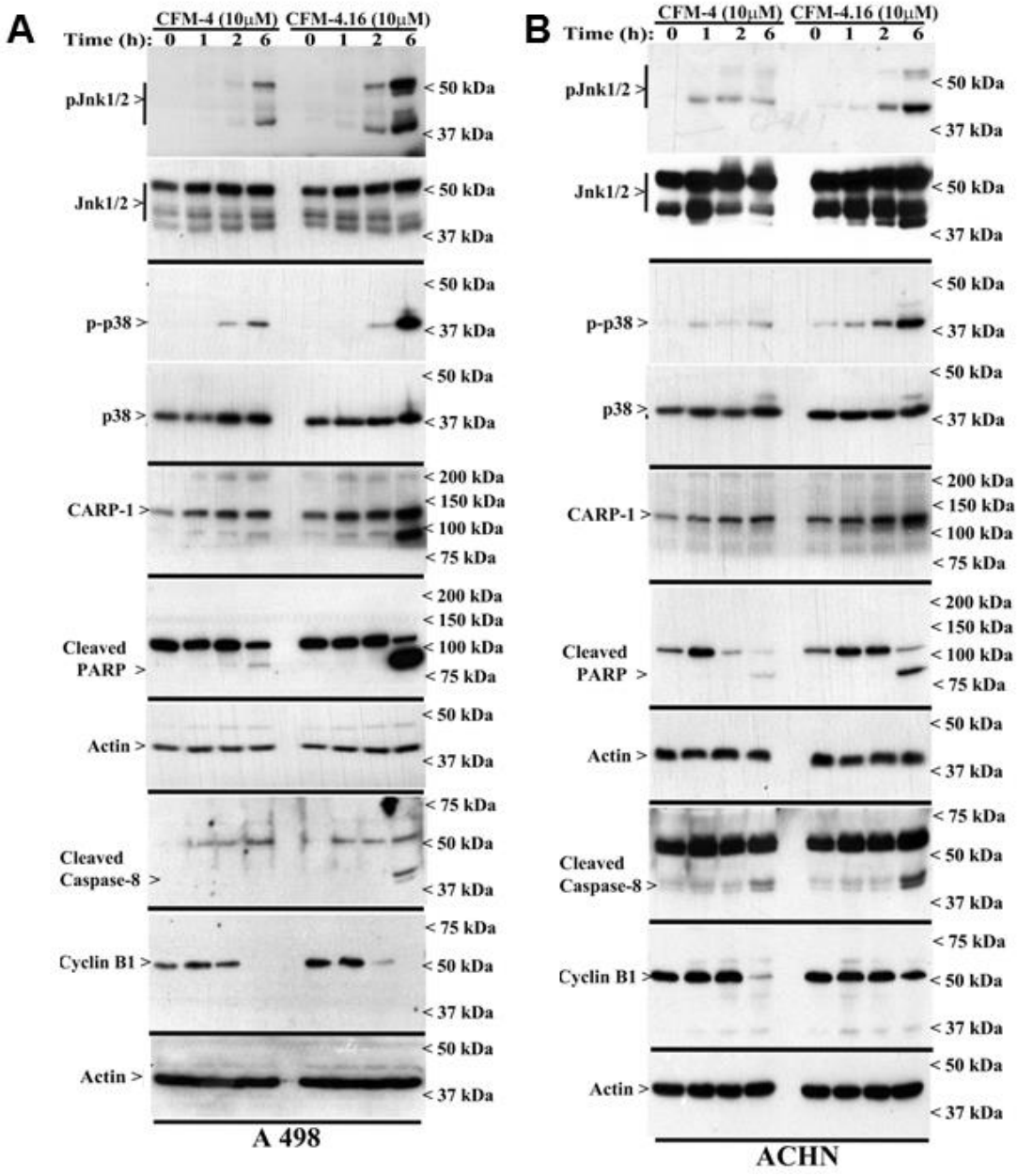

Appendix Figure 7.2. CFM-4. 16 stimulates apoptosis in parental and Everolimus-resistant RCC cells in part by upregulating pro-apoptotic CARP-1 and activating SAPKs. **(A, B)** Indicated RCC cells were either untreated (Control, denoted as 0), treated with CFM-4, or CFM-4.16 for noted dose and time. Cell lysates were analyzed by western blotting (WB) as in Methods for levels of CARP-1, cyclin B1, cleaved PARP and caspase-8, and activation (phosphorylation) of pro-apoptotic p38 and JNK1/2 SAPKs. The western blot membranes were probed with anti-actin antibodies to assess protein loading. Adapted from [1].

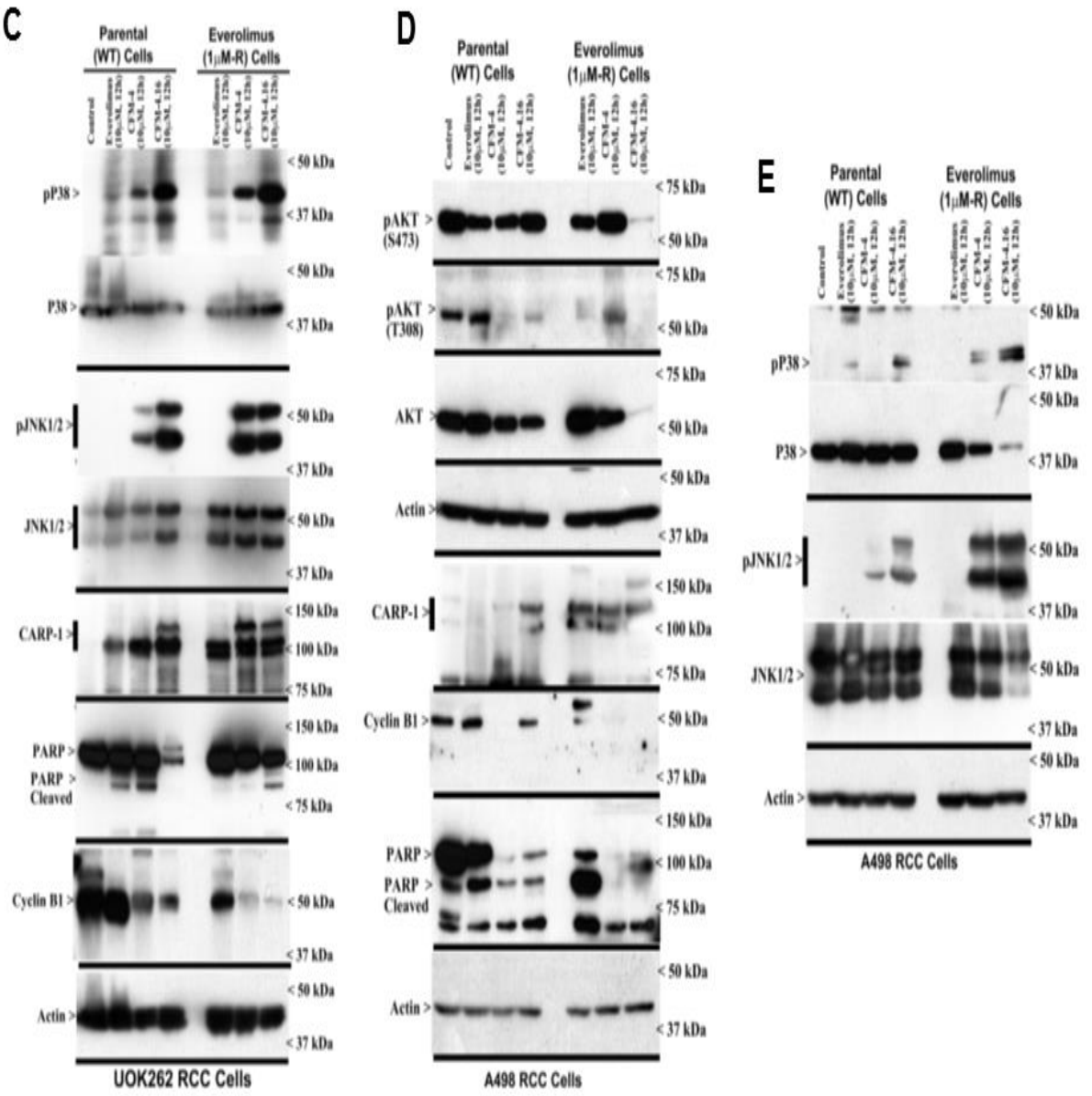

Appendix Figure 7.2. (continued) CFM-4. 16 stimulates apoptosis in parental and Everolimus-resistant RCC cells in part by upregulating pro-apoptotic CARP-1 and activating SAPKs. **(C-E)** Parental or Everolimus-resistant RCC cells were either untreated (Control), treated with Everolimus, CFM-4, or CFM-4.16 for noted dose and time. Cell lysates were analyzed by Western blotting (WB) for expression and/or activation of Akt, SAPKs, Cyclin B1, PARP, and CARP-1. The western blot membranes in panels C-E were probed with anti-actin antibodies to assess protein loading. Adapted from [1].

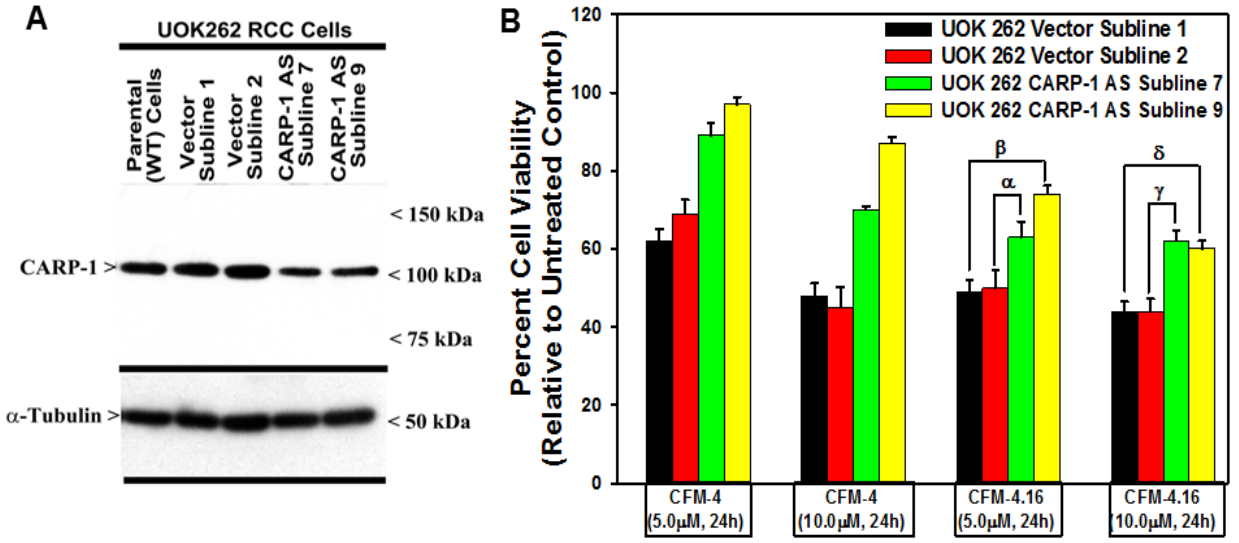

Appendix Figure 7.3. Knockdown of CARP-1 blocks CFM-4.16 effects. (A) Cells were either untransfected, transfected with the pcDNA3/Hygro vector plasmid or plasmid expressing CARP-1 antisense, and stable, hygromycin-resistant cells were generated and characterized as detailed in methods. Cell lysates from indicated stable cell lines were subjected to WB analysis as in figure 3 for levels of CARP-1 and α-tubulin. (B) The Indicated vector or CARP-1 antisense expressing RCC sublines were either untreated (Control) or treated with noted doses of CFM-4, or CFM-4.16 for 24h. Cell viability was determined by MTT assay. The histogram columns represent means of three independent experiments; bars, S.E. α, β, γ, δ, p = <0.05 relative to the vector expressing subline treated with CFM-4.16 only. Adapted from [1].

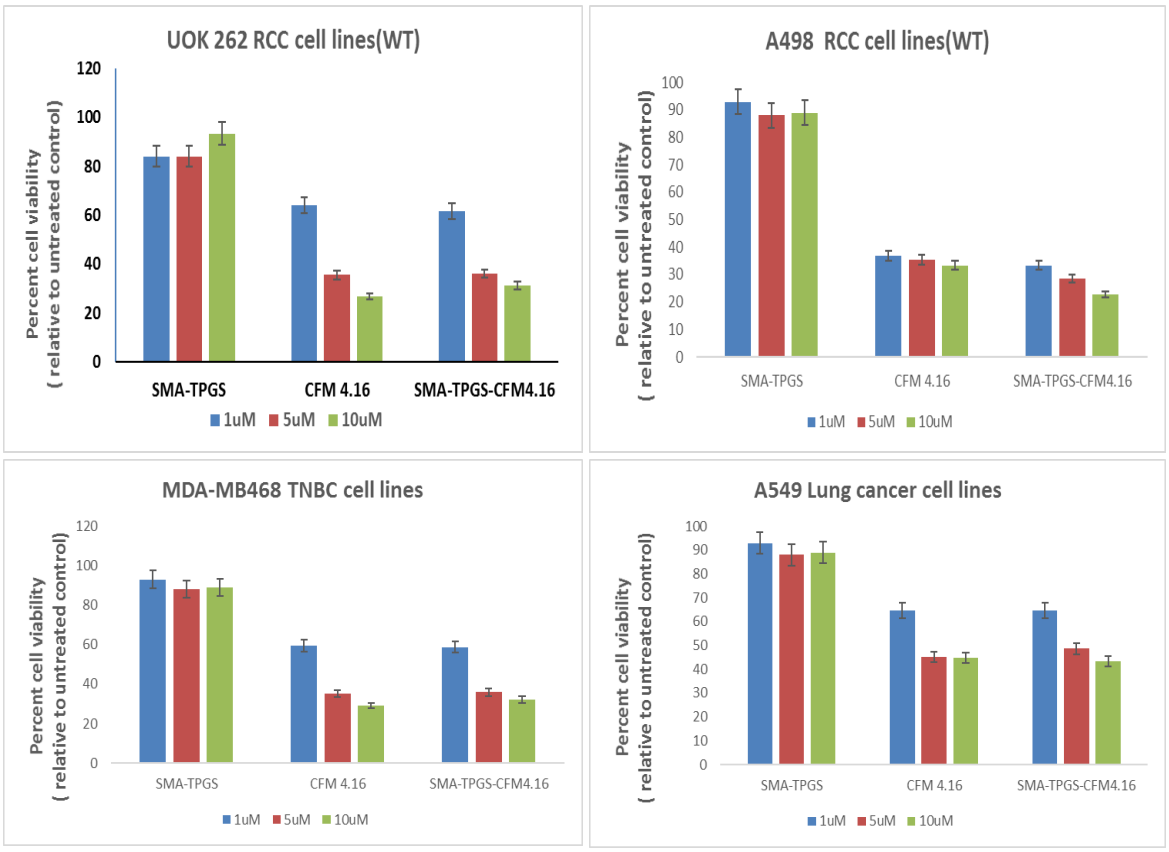

Appendix Figure 7.4. Triple negative cancer cells (MDA-MB468), lung cancer cells (A549) and renal cancer cells (A 498 and UOK 262) were treated with the indicated doses for 24 hours. The number of viable cells were then determined by MTT assay as described.

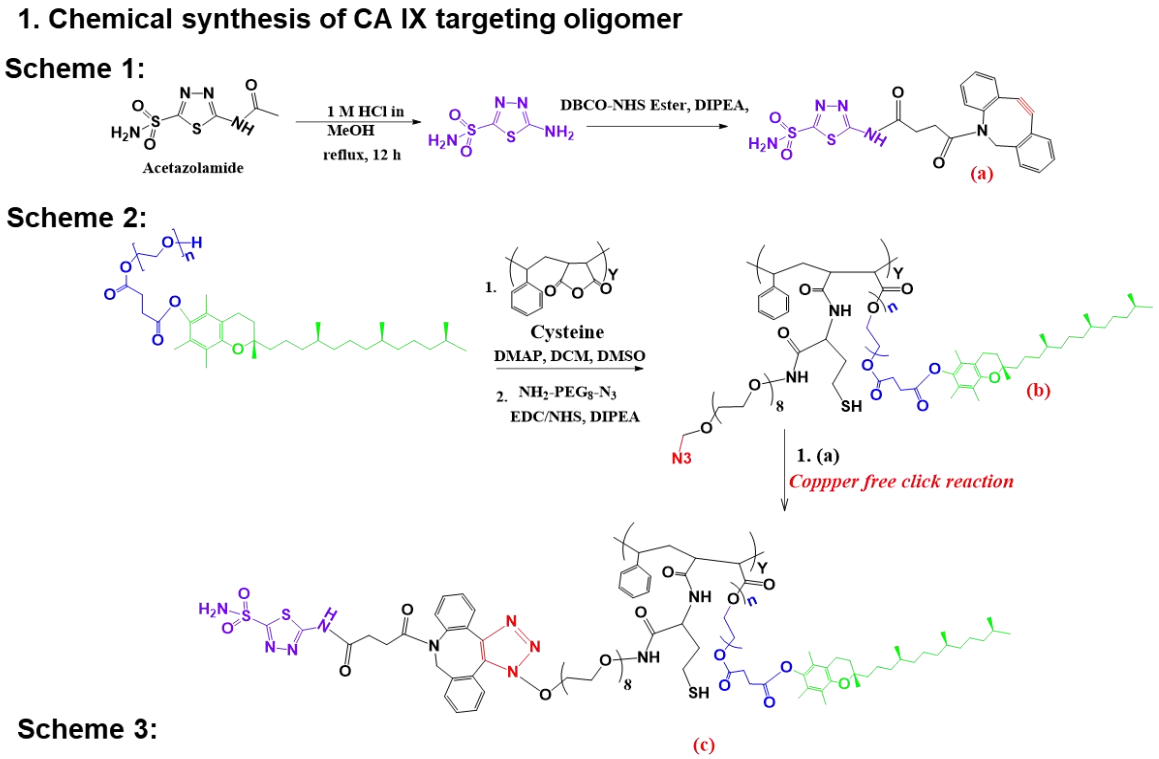

Appendix Figure 7.5. Scheme 1 and 2 indicate the general procedure for acetazolamide-oligomer fragment synthesis. Scheme 3 indicates the preparation of OMs with C-4.16 and mechanism of CA IX receptor mediated internalization of OMs in RCC.

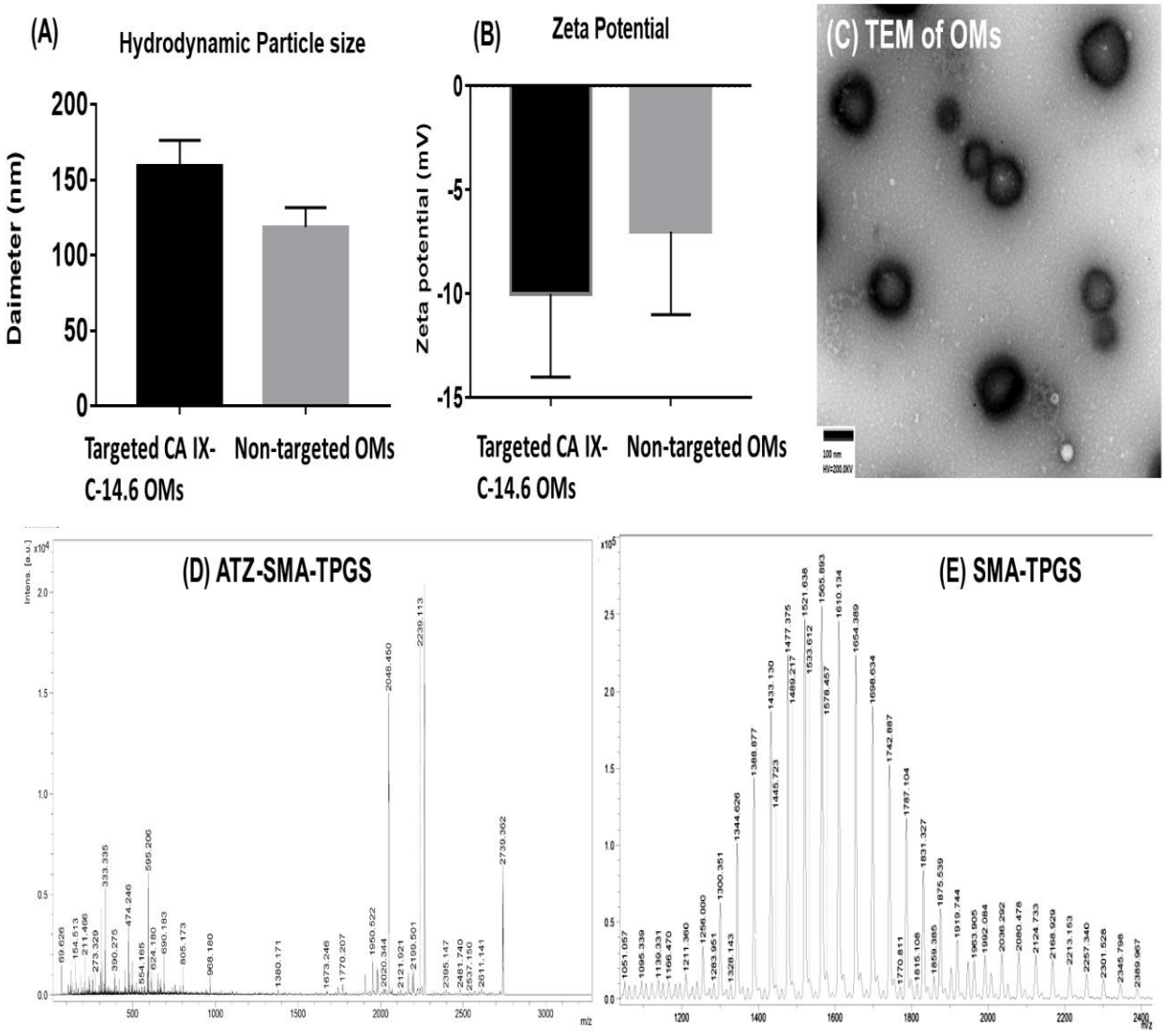

Appendix Figure 7.6. Oligomicelles formulation and characterization. **(A)** Hydrodynamic size of targeted CA IX-C4.16 OMs and non-targeted SMA-TPGS-C-4.16 OMs and (**B)** Zeta potential by Dynamic Light Scattering (DLS) are shown. **(C)** The morphology of representative OMs is characterized by TEM as shown. Scale bar = 100 nm. **(D and E)** MALDI-MS analysis of ATZ-SMA-TPGS and SMA-TPGS are shown. The increment of m/z value in ATZ-SMA-TPGS (m/z 2239.1) compared to SMA-TPGS(m/z1565.6) oligomers indicates the successful conjugation of ATZ to the SMA-TPGS polymers.

IHC FOR CA-IX Expression of A498 Tumor-confocal microscopy

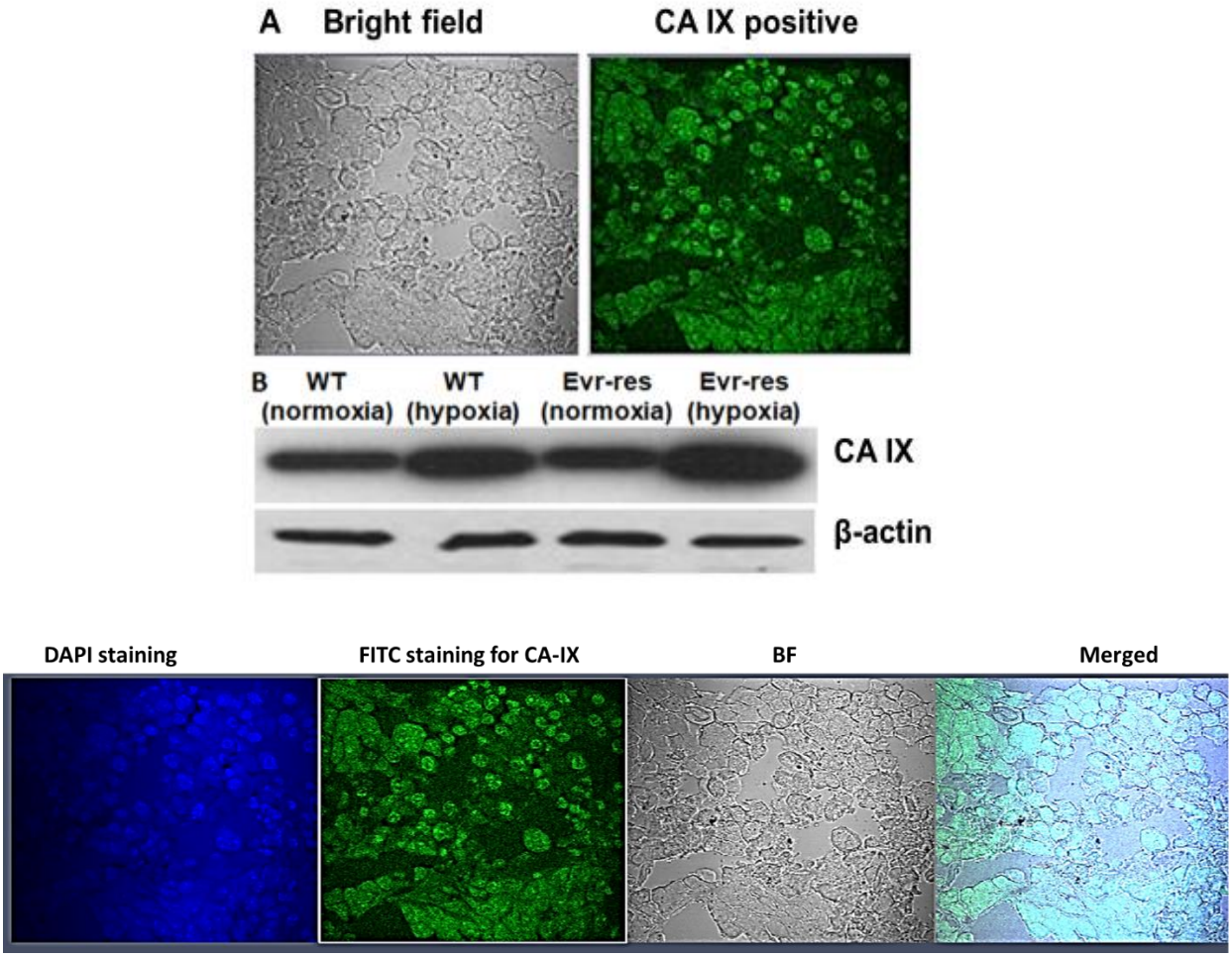

Appendix Figure 7.7. Overexpression of CA IX protein in A498 RCC cells and xenograft model. (A) Immunohistochemistry of CA IX positive A498 renal cell carcinoma tumor xenografts collected from tumor tissue section is shown. The intense bright green fluorescence indicates the rationale of choosing CA IX as an excellent RCC targeted therapy. **(B)** Western blot detection of CA IX protein in A498 and EV-A498 RCC cells lysates after normoxia (no cobalt chloride treatment) and hypoxia (treated with cobalt chloride for 72 hrs to induce hypoxia) are shown. The fold up-regulation of CA IX expression in hypoxic WT and EV-res A498 RCC cells than normoxia provides a solid foundation for delivering the payload into oxygen deprived regions and hypoxic core of RCC tumor.

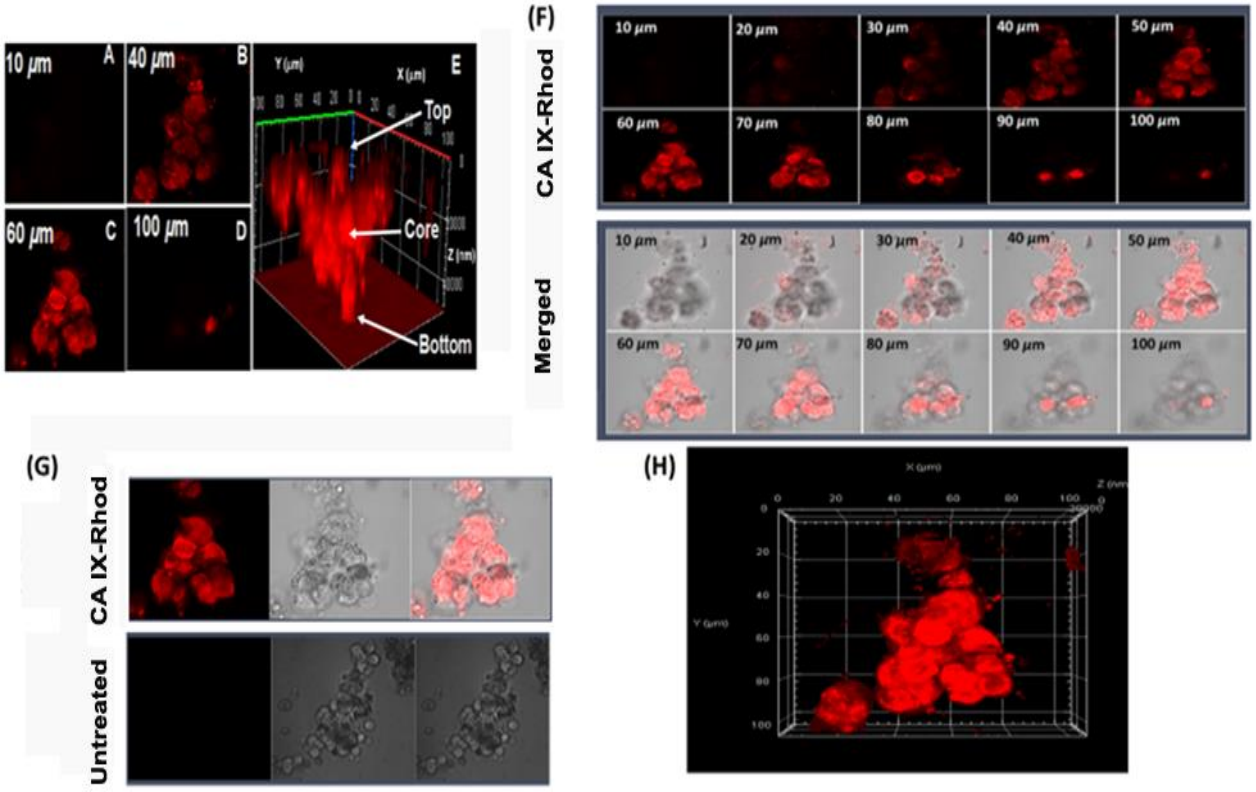

Appendix Figure 7.8. 3D spheroid uptake studies of hypoxia targeted-oligomer. Confocal microscope images of ATZ-oligomer conjugated with rhodamine B and treated with hypoxic A498 RCC cells -spheroid indicates tumor matrix penetration of CA IX targeted oligomicelles. The untreated and treated spheres were then photographed as noted in methods section. Z-stacking of the spheroid **(A-D)** clearly indicates that fluorescence intensity is superior in 40-60 µm section. The highest fluorescence intensity at the center (as indicated by arrow) of 3D- plot **(E)** suggests that CA IX-Rhod oligomer is highly efficient to reach deep into the core of the tumor spheroid. **(F)** Z-stacking of the spheroid at different sections from 10-100□m with CA IX targeted formulations also reveals similar findings as noted for the 40-60 µm that had superior fluorescence intensity. Figure **(G)** shows the untreated control experiments in comparison with CA IX-Rhod oligomer and Figure (**H**) shows the overall shape of the spheroid from along the three dimensions (x, y, and z).

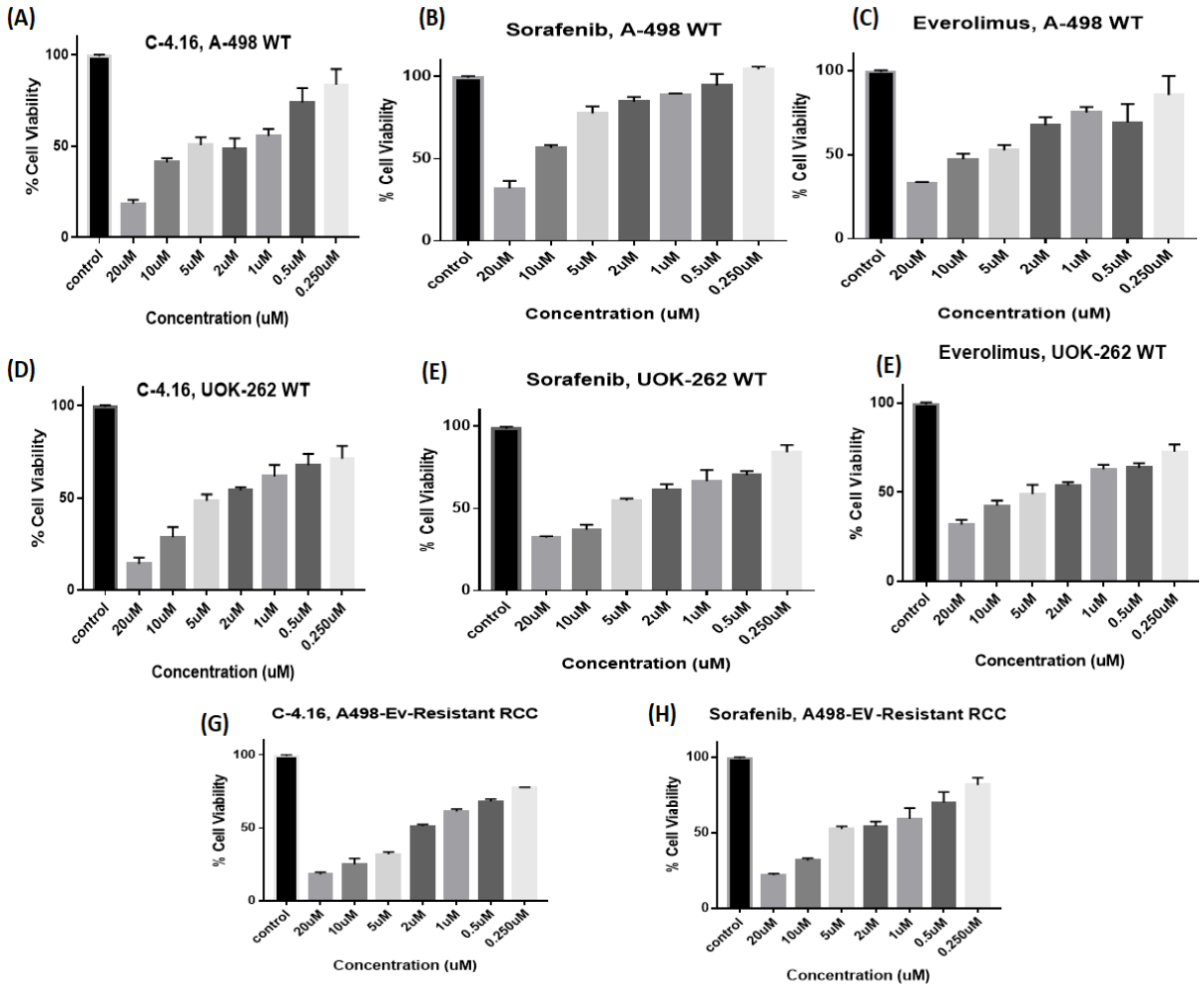

Appendix Figure 7.9. C-4.16 inhibits growth of RCC cell lines derived from WT and Everolimus-resistant cells. Cell cultures studies and in vitro cytotoxicity assay of C-4.16, sorafenib, Everolimus on (WT and Evr-Res) A498 and UOK-262 RCC cell lines. **(A, B, and C)** Cytotoxicity data indicates C-4.16 was more potent than FDA approved drugs (sorafenib and everolimus) in WT A498 and **(D, E, and F)** WT UOK262. Also, cell cultures studies results on EV-res A498 RCC cell lines **(G and H)** indicates that C-4.16 was more effective in inhibiting growth of Evr-res A498 RCC cell lines than sorafenib; however, Everolimus is not inhibiting the growth of Evr-res A498 and UOK262 RCC cell lines as previously published [14]. The data in the GI_{50} columns represent mean of three independent experiments. Indicated parental and their respective drug resistant RCC cells were either untreated (Control) or treated with noted doses of C-4.16 and sorafenib for 48h.

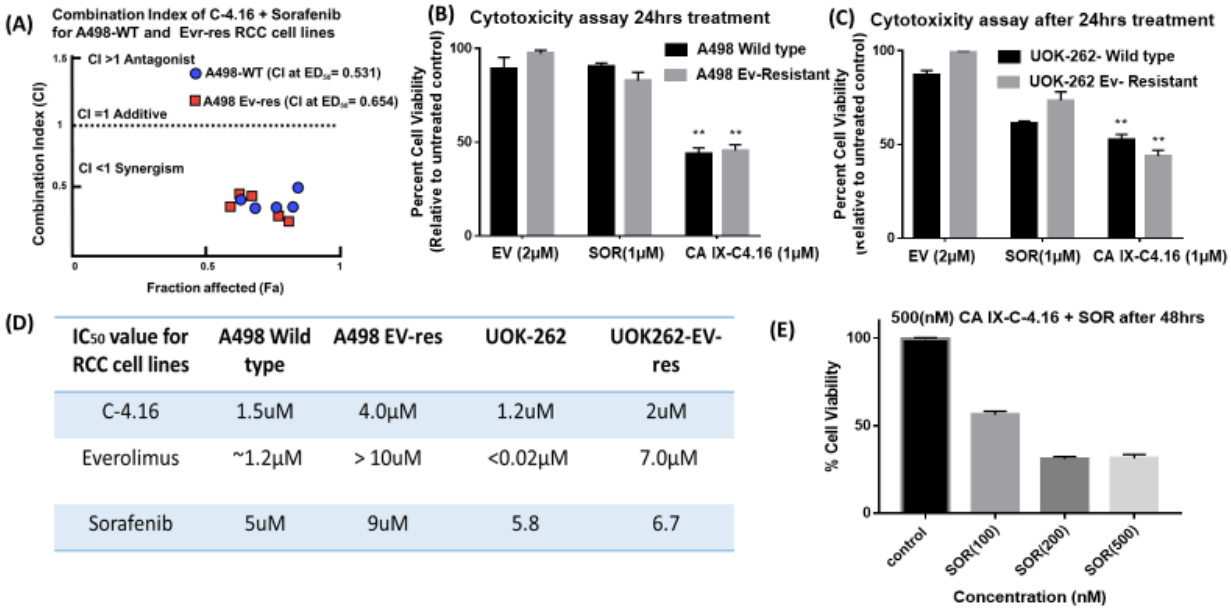

IC_{50} value for RCC cell lines	A498 Wild type	A498 EV-res	UOK-262	UOK262-EV-res
C-4.16	1.5uM	4.0μM	1.2uM	2uM
Everolimus	~1.2μM	> 10uM	<0.02μM	7.0μM
Sorafenib	5uM	9uM	5.8	6.7

Appendix Figure 7.10. High synergistic CI value of C-4.16 with sorafenib combination supports the hypothesis of selecting the combination to RCC treatment using hypoxia targeting OMs. (A) Combining very low doses of both drugs will lower the IC_{50} value significantly as in **(D)** which shows the combination index plot for C-4.16 plus sorafenib in the cells for both types A498 RCC cell lines indicates very strong synergism between sorafenib and C-4.16. **(B)** The results also show that CA IX-C-4.16 was more effective in inhibiting growth of A498 (WT and Ev-res) and to less extent **(C)** UOK262 (WT and Ev-res) RCC cell lines than sorafenib and Ev and support that C-4.16 was more potent than FDA approved drugs (sorafenib and everolimus). **(D)** We summarized IC_{50} value table for all drugs with all the above mentioned RCC cell lines. **(E)** In vitro cytotoxicity assay of CA IX-C4.16 (500 nM) in combination with different doses of sorafenib on Ev-res A498 RCC cell lines indicates that low dose of C-4.16-OMs sensitize sorafenib for inhibiting growth of RCC cell line.

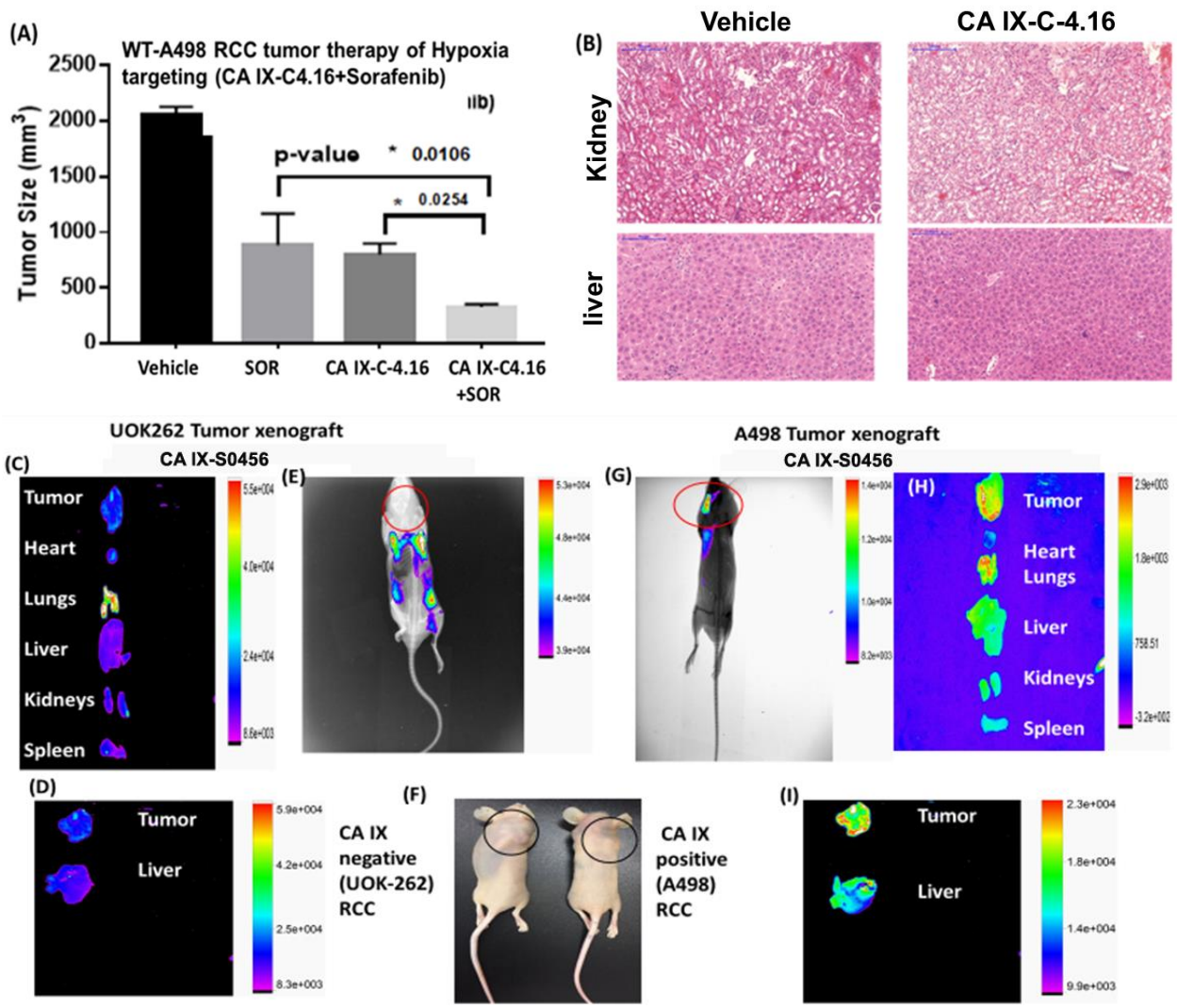
(A)
WT-A498 RCC tumor therapy of Hypoxia targeting (CA IX-C4.16+Sorafenib)
IIb)
Tumor Size (mm3)
2500
2000
1500
1000
500
0
p-value * 0.0106
* 0.0254
Vehicle
SOR
CA IX-C-4.16
CA IX-C4.16 +SOR
(B)
Vehicle
CA IX-C-4.16
Kidney
liver
UOK262 Tumor xenograft
CA IX-S0456
(C)
Tumor
Heart
Lungs
Liver
Kidneys
Spleen
(E)
(D)
Tumor
Liver
(F)
CA IX negative (UOK-262) RCC
CA IX positive (A498) RCC
A498 Tumor xenograft
CA IX-S0456
(G)
(H)
Tumor
Heart
Lungs
Liver
Kidneys
Spleen
(I)
Tumor
Liver

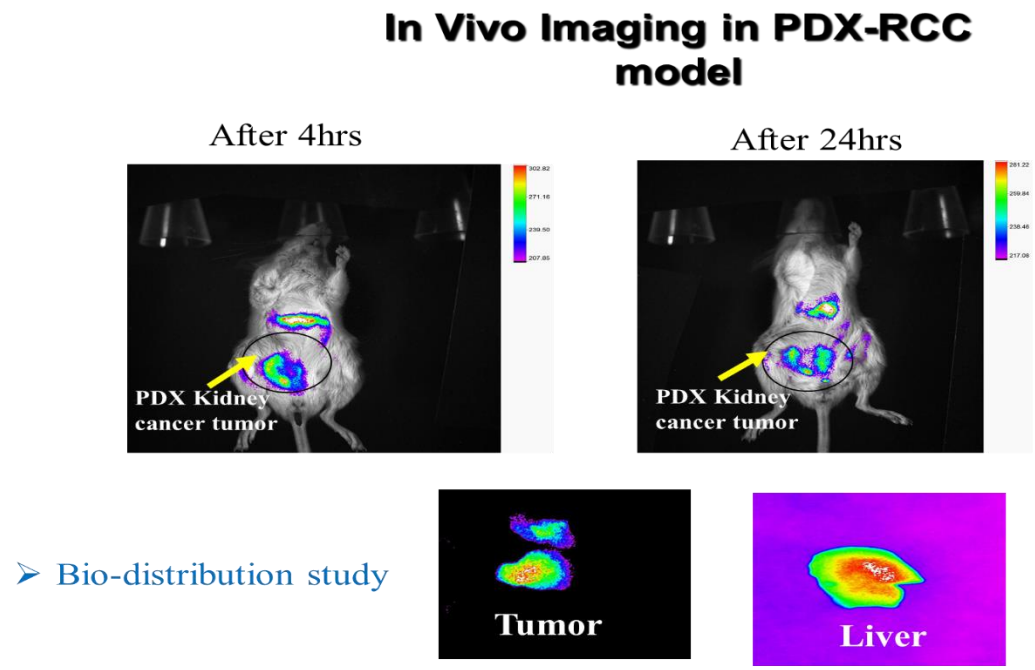

Appendix Figure 7.11. Antitumor efficacy study of combination therapy and NIR imaging of CA IX targeted oligomer in RCC xenografts tumor. (A) Tumor growth inhibition effect of (CA IX-C-4.16+SOR) is significantly higher compared to vehicle(control), SOR, and CA IX-C-4.16 in A498 xenograft tumor. Significant tumor growth suppression of combination therapy supports the rational of using CA IX targeting nano-formulation as delivery vehicle of potent drugs, C-4.16. The data represent as average values from total four animals in respective group, bars, SE, significant where *$p<0.05$ vs Control. **(B)** Histopathologic (H&E staining) examination to determine the toxicity of therapeutic drugs on livers and kidneys at the end of the experiments. Images indicate there is no significant sign of necrosis, or loss of tissue architectural difference in vehicle control and CA IX-C-4.16 treated tissues. **(C-F)** CA IX negative (UOK262) tumor treated with CA IX-S0456 oligomers shows high off-target effect and low tumor specificity. **(E)** UOK 262 and A498 tumor were inoculated on the circled parts. **(F-I)** CA IX positive (A498) tumor treated with hypoxia targeted-NIR oligomer shows high tumor targetability and low non-specific healthy organ uptake after 24 hrs of post injection suggesting the importance of CA IX for selective tumor imaging for RCC tumor model after 24 hrs indicates high fluorescence intensity at the tumor compared to liver and other organs.

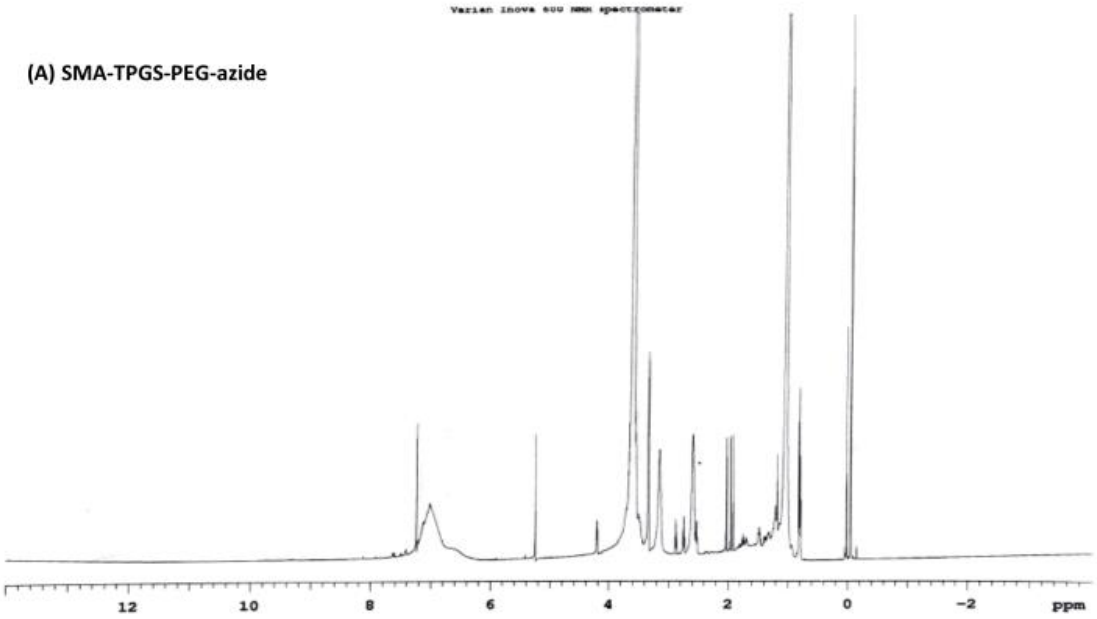
(A) SMA-TPGS-PEG-azide
12
10
8
6
4
2
0
−2
ppm

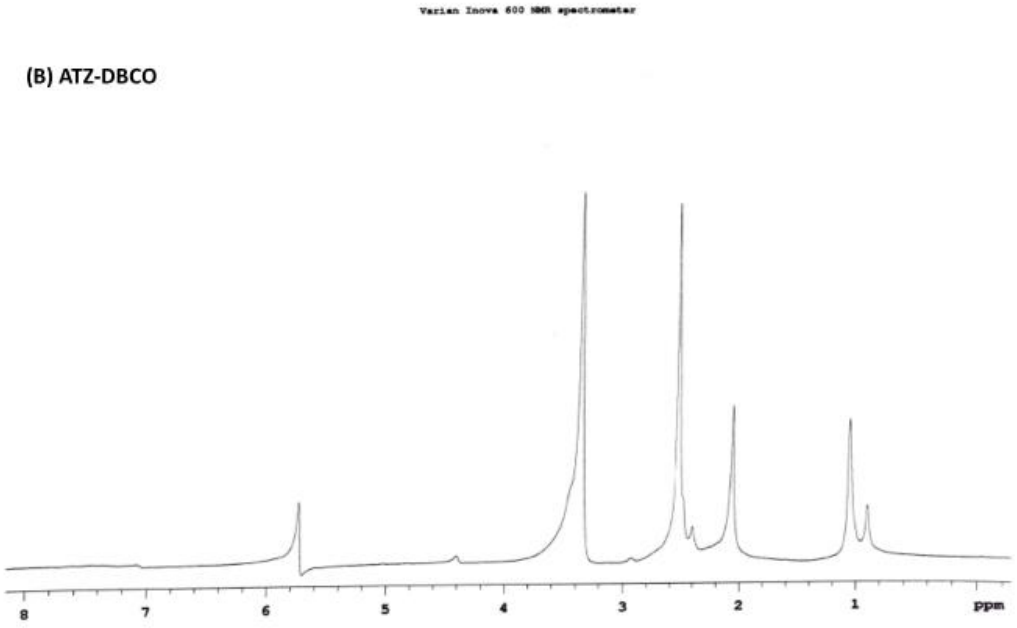
(B) ATZ-DBCO
8
7
6
5
4
3
2
1
ppm

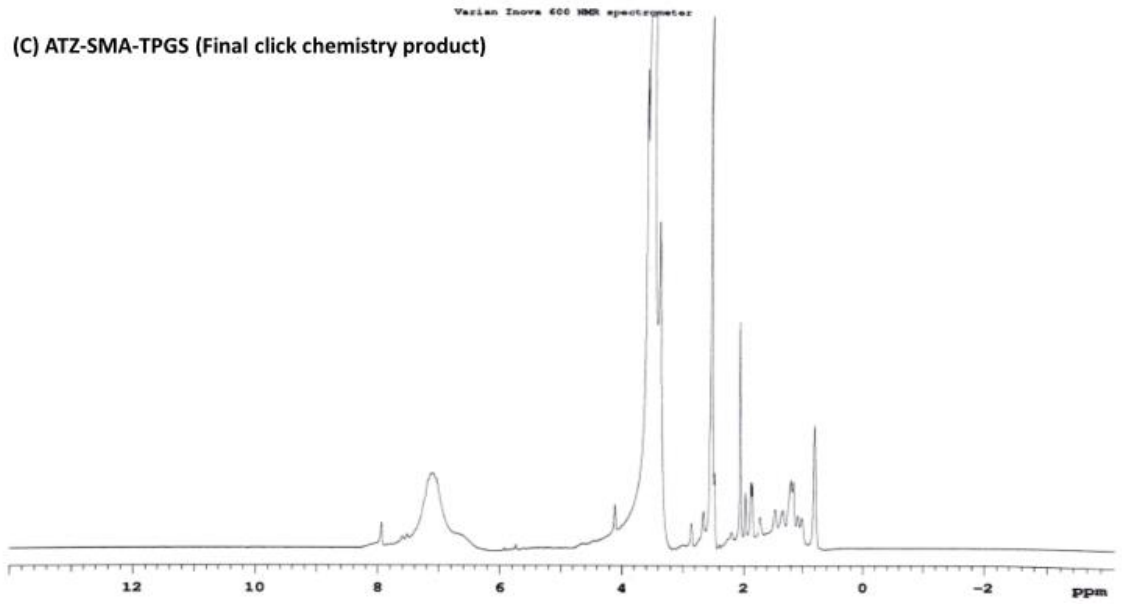

Appendix Figure 7.12. Compounds were characterized by ^{1}H-NMR to assure chemical identity (**Supplementary, S1 A-C**). SMA-TPGS-PEG-Azid and ATZ-DBCO conjugates indicates the successful conjugation of ATZ to the SMA-TPGS polymers. ^{1}H-NMR results confirmed the triazole ring formation as some characteristic peaks were found such as H-triazole ring around 7.9 ppm, O-CH2 of triazole ring around 5.2 ppm, and CH2-N3 peak around 4.2 ppm.

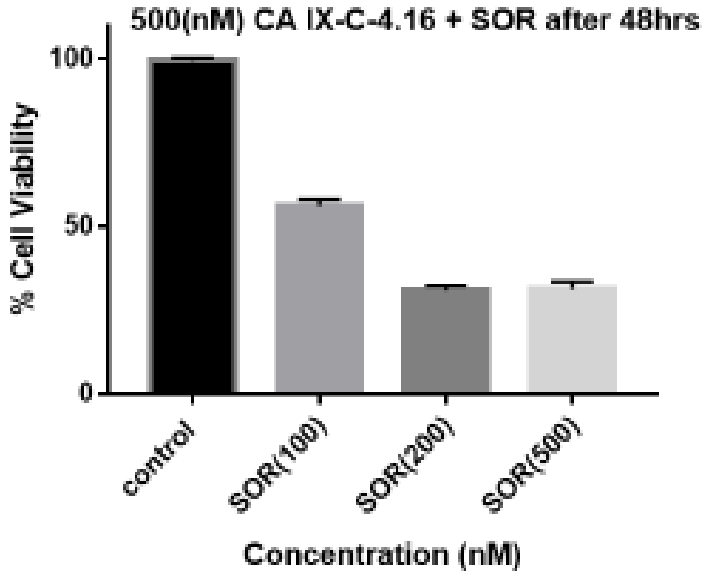

Appendix Figure 7.13. In vitro cytotoxicity assay of CA IX-C4.16 (500 nM) in combination with different doses of sorafenib on Ev-res A498 RCC cell lines indicates that low dose of CA IX-C4.16 NPs sensitize sorafenib for inhibiting growth of RCC cell line.

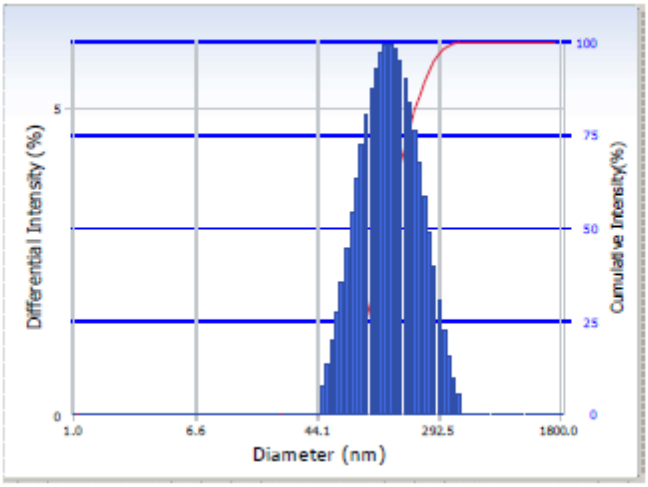

Diameter	(d)	: 122.5	(nm)
Polydispersity Index	(P.I.)	: 0.163	
Diffusion Const.	(D)	: 4.017e-008	(cm²/sec)
Residual		: 5.791e-003	(O.K)

PARTICLE SIZE DISTRIBUTION

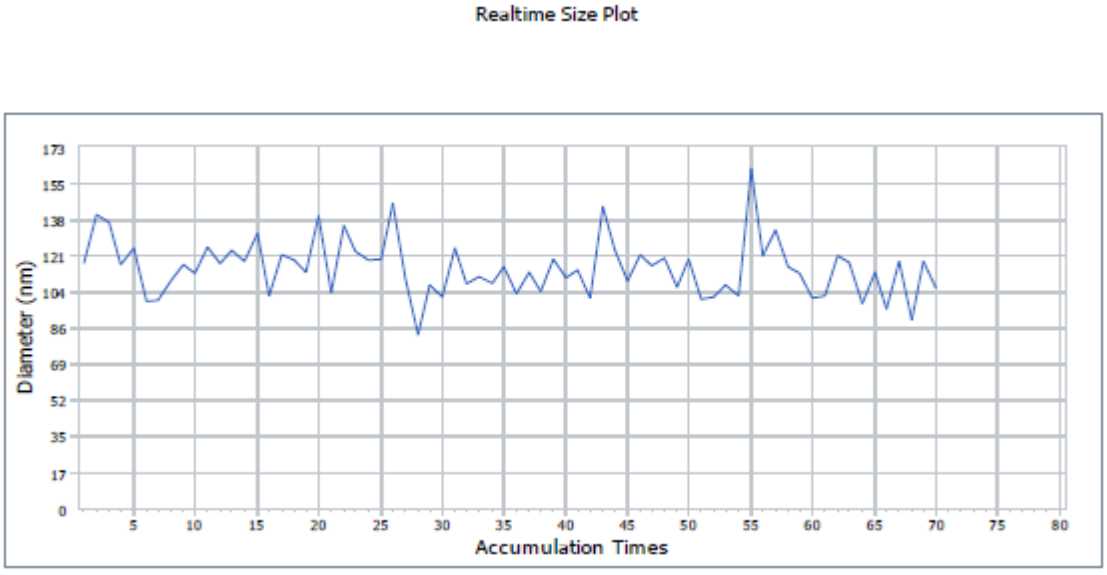

Appendix Figure 7.14. Particle size of NFs and the particle size distribution from DLS.

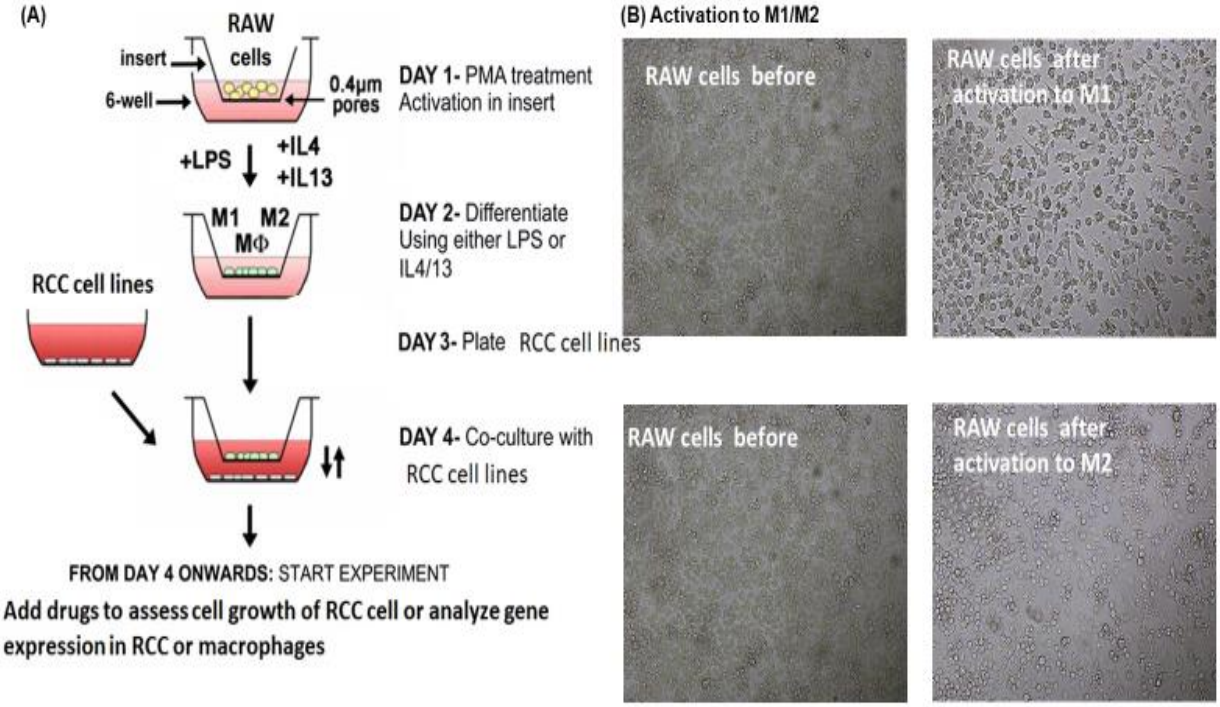

Appendix Figure 7.15. M1/M2 Activation procedure.

REFERENCE

1. Cheriyan, V. T. *et al.* A CARP-1 functional mimetic loaded vitamin E-TPGS micellar nano-formulation for inhibition of renal cell carcinoma. *Oncotarget* **5,** (2017).
2. Cohen, H. T. & Mcgovern, F. J. Renal-Cell Carcinoma. *N. Engl. J.Med* **353,** 2477–2490 (2005).
3. Jemal, A. *et al.* Cancer statistics, 2003. *CA. Cancer J. Clin.* **53,** 5–26 (2003).
4. Hollingsworth, J. M., Miller, D. C., Daignault, S. & Hollenbeck, B. K. Rising incidence of small renal masses: a need to reassess treatment effect. *J. Natl. Cancer Inst.* **98,** 1331–1334 (2006).
5. Chow, W.-H. & Devesa, S. S. Contemporary epidemiology of renal cell cancer. *Cancer J.* **14,** 288–301 (2008).
6. Chow, W.-H., Devesa, S. S., Warren, J. L. & Fraumeni Jr, J. F. Rising incidence of renal cell cancer in the United States. *Jama* **281,** 1628–1631 (1999).
7. Siegel, R. L., Miller, K. D. & Jemal, A. Cancer statistics, 2018. *CA. Cancer J. Clin.* **68,** 7–30 (2018).
8. Hsieh, J. J. *et al.* Renal cell carcinoma. *Nat. Rev. Dis. Prim.* **3,** 17009 (2017).
9. Data, M. Cancer Statistics, 2016. **66,** 7–30 (2016).
10. Crispen, P. L., Boorjian, S. A., Lohse, C. M., Leibovich, B. C. & Kwon, E. D. Predicting disease progression after nephrectomy for localized renal cell carcinoma: the utility of prognostic models and molecular biomarkers. *Cancer* **113,** 450–460 (2008).
11. Srigley, J. R. *et al.* The International Society of Urological Pathology (ISUP) vancouver classification of renal neoplasia. *Am. J. Surg. Pathol.* **37,** 1469–1489 (2013).
12. Kovacs, G. *et al.* The Heidelberg classification of renal cell tumours. *J. Pathol. A J.*

Pathol. Soc. Gt. Britain Irel. **183,** 131–133 (1997).

13. oncology/hematology, R. M.-C. reviews in & 2003, undefined. Prognostic factors and clinical trials of new agents in patients with metastatic renal cell carcinoma. *croh-online.com*

14. De, P. *et al.* Trends in incidence, mortality, and survival for kidney cancer in Canada, 1986–2007. *Cancer Causes Control* **25,** 1271–1281 (2014).

15. Levi, F. *et al.* The changing pattern of kidney cancer incidence and mortality in Europe. *BJU Int.* **101,** 949–958 (2008).

16. Gandaglia, G., Ravi, P., Abdollah, F., Abd-El, A.-E.-R. M. & others. Contemporary incidence and mortality rates of kidney cancer in the United States. *Can. Urol. Assoc. J.* **8,** 247 (2014).

17. Quinn, M. & Babb, P. Patterns and trends in prostate cancer incidence, survival, prevalence and mortality. Part I: international comparisons. *BJU Int.* **90,** 162–173 (2002).

18. Abdollah, F. *et al.* Incidence, survival and mortality rates of stage-specific bladder cancer in United States: a trend analysis. *Cancer Epidemiol.* **37,** 219–225 (2013).

19. Kim, M. M. *et al.* Improvement in prostate cancer survival over time: a 20-year analysis. *Cancer J.* **18,** 1–8 (2012).

20. Landis, S. H., Murray, T., Bolden, S. & Wingo, P. A. Cancer statistics, 1999. *CA. Cancer J. Clin.* **49,** 8–31 (1999).

21. Lopez-Beltran, A., Scarpelli, M., Montironi, R. & Kirkali, Z. 2004 WHO classification of the renal tumors of the adults. *Eur. Urol.* **49,** 798–805 (2006).

22. Humphrey, P. A., Moch, H., Cubilla, A. L., Ulbright, T. M. & Reuter, V. E. The 2016 WHO classification of tumours of the urinary system and male genital organs—part B:

prostate and bladder tumours. *Eur. Urol.* **70,** 106–119 (2016).

23. Linehan, W. M., Walther, M. M. & Zbar, B. The genetic basis of cancer of the kidney. *J. Urol.* **170,** 2163–2172 (2003).

24. Shuch, B. *et al.* Understanding pathologic variants of renal cell carcinoma: distilling therapeutic opportunities from biologic complexity. *Eur. Urol.* **67,** 85–97 (2015).

25. Linehan, W. M. *et al.* Genetic basis of cancer of the kidney: disease-specific approaches to therapy. *Clin. Cancer Res.* **10,** 6282S--6289S (2004).

26. Chen, F. *et al.* Multilevel genomics-based taxonomy of renal cell carcinoma. *Cell Rep.* **14,** 2476–2489 (2016).

27. Motzer, R. J., Bander, N. H. & Nanus, D. M. Renal-cell carcinoma. *N. Engl. J. Med.* **335,** 865–875 (1996).

28. Iafrate, M. *et al.* The Hereditary Renal Cancer Syndromes. *Urol. J.* **71,** 15–20 (2004).

29. Zbar, B. *et al.* Familial renal carcinoma: clinical evaluation, clinical subtypes and risk of renal carcinoma development. *J. Urol.* **177,** 461–465 (2007).

30. Rini, B. I., Campbell, S. C. & Escudier, B. Renal cell carcinoma. *The Lancet* **373,** 1119–1132 (2009).

31. Kroeger, N. *et al.* Metastatic non--clear cell renal cell carcinoma treated with targeted therapy agents: characterization of survival outcome and application of the International mRCC Database Consortium criteria. *Cancer* **119,** 2999–3006 (2013).

32. Vera-Badillo, F. E. *et al.* Systemic therapy for non--clear cell renal cell carcinomas: a systematic review and meta-analysis. *Eur. Urol.* **67,** 740–749 (2015).

33. Motzer, R., Jonasch, E., Agarwal, N., … C. B.-… C. C. & 2015, undefined. Kidney cancer, version 3.2015. *jnccn.org*

34. Escudier, B. *et al.* Renal cell carcinoma: ESMO Clinical Practice Guidelines for diagnosis, treatment and follow-up. *Ann. Oncol.* **27,** v58--v68 (2016).

35. Sankin, A., Hakimi, A. A., Hsieh, J. J. & Molina, A. M. Metastatic non-clear cell renal cell carcinoma: an evidence based review of current treatment strategies. *Front. Oncol.* **5,** 67 (2015).

36. Gerlinger, M. *et al.* Intratumor Heterogeneity and Branched Evolution Revealed by Multiregion Sequencing. *N. Engl. J. Med.* **366,** 883–892 (2012).

37. Gerlinger, M. *et al.* Genomic architecture and evolution of clear cell renal cell carcinomas defined by multiregion sequencing. *Nat. Genet.* **46,** 225 (2014).

38. Sankin, A. *et al.* The impact of genetic heterogeneity on biomarker development in kidney cancer assessed by multiregional sampling. *Cancer Med.* **3,** 1485–1492 (2014).

39. Griffin, N., Gore, M. E. & Sohaib, S. A. Imaging in metastatic renal cell carcinoma. *Am. J. Roentgenol.* **189,** 360–370 (2007).

40. Störkel, S. *et al.* Classification of renal cell carcinoma. *Cancer* **80,** 987–989 (1997).

41. Zbar, B. Von Hippel-Lindau disease and sporadic renal cell carcinoma. *Cancer Surv.* **25,** 219–232 (1995).

42. Linehan, W. M., Lerman, M. I. & Zbar, B. Identification of the von Hippel-Lindau (VHL) gene: its role in renal cancer. *Jama* **273,** 564–570 (1995).

43. Schmidt, L. *et al.* Germline and somatic mutations in the tyrosine kinase domain of the MET proto-oncogene in papillary renal carcinomas. *Nat. Genet.* **16,** 68 (1997).

44. Weirich, G. *et al.* Familial renal oncocytoma: clinicopathological study of 5 families. *J. Urol.* **160,** 335–340 (1998).

45. Linehan, W., Srinivasan, R., urology, L. S.-N. reviews & 2010, undefined. The genetic

basis of kidney cancer: a metabolic disease. *nature.com*

46. Iliopoulos, O., Kibel, A., Gray, S. & Kaelin Jr, W. G. Tumour suppression by the human von Hippel-Lindau gene product. *Nat. Med.* **1,** 822 (1995).

47. Zhuang, Z. *et al.* von Hippel-Lindau disease gene deletion detected in microdissected sporadic human colon carcinoma specimens. *Hum. Pathol.* **27,** 152–156 (1996).

48. Iliopoulos, O., Ohh, M. & Kaelin, W. G. pVHL19 is a biologically active product of the von Hippel--Lindau gene arising from internal translation initiation. *Proc. Natl. Acad. Sci.* **95,** 11661–11666 (1998).

49. Blankenship, C., Naglich, J. G., Whaley, J. M., Seizinger, B. & Kley, N. Alternate choice of initiation codon produces a biologically active product of the von Hippel Lindau gene with tumor suppressor activity. *Oncogene* **18,** 1529 (1999).

50. Schoenfeld, A., Davidowitz, E. J. & Burk, R. D. A second major native von Hippel--Lindau gene product, initiated from an internal translation start site, functions as a tumor suppressor. *Proc. Natl. Acad. Sci.* **95,** 8817–8822 (1998).

51. Gnarra, J. R. *et al.* Mutations of the VHL tumour suppressor gene in renal carcinoma. *Nat. Genet.* **7,** 85 (1994).

52. Lee, S. *et al.* Transcription-dependent nuclear-cytoplasmic trafficking is required for the function of the von Hippel-Lindau tumor suppressor protein. *Mol. Cell. Biol.* **19,** 1486–1497 (1999).

53. Ye, Y. *et al.* Subcellular localization of the von Hippel-Lindau disease gene product is cell cycle-dependent. *Int. J. cancer* **78,** 62–69 (1998).

54. Lee, S. *et al.* Nuclear/cytoplasmic localization of the von Hippel-Lindau tumor suppressor gene product is determined by cell density. *Proc. Natl. Acad. Sci.* **93,** 1770–1775 (1996).

55. Duan, D. R. *et al.* Characterization of the VHL tumor suppressor gene product: localization, complex formation, and the effect of natural inactivating mutations. *Proc. Natl. Acad. Sci.* **92,** 6459–6463 (1995).

56. Kim, W. & Kaelin, W. G. The von Hippel--Lindau tumor suppressor protein: new insights into oxygen sensing and cancer. *Curr. Opin. Genet. Dev.* **13,** 55–60 (2003).

57. George, D. J. & Kaelin Jr, W. G. The von Hippel--Lindau protein, vascular endothelial growth factor, and kidney cancer. *N. Engl. J. Med.* **349,** 419–421 (2003).

58. Bonifacino, J. S. & Weissman, A. M. Ubiquitin and the control of protein fate in the secretory and endocytic pathways. *Annu. Rev. Cell Dev. Biol.* **14,** 19–57 (1998).

59. Semenza, G. L. HIF-1 mediates metabolic responses to intratumoral hypoxia and oncogenic mutations. *J. Clin. Invest.* **123,** 3664–3671 (2013).

60. Masson, N. & Ratcliffe, P. J. Hypoxia signaling pathways in cancer metabolism: the importance of co-selecting interconnected physiological pathways. *Cancer Metab.* **2,** 3 (2014).

61. Kaelin Jr, W. G. Von hippel-lindau disease. *Annu. Rev. Pathol. Mech. Dis.* **2,** 145–173 (2007).

62. Wang, G. L. & Semenza, G. L. Purification and characterization of hypoxia-inducible factor 1. *J. Biol. Chem.* **270,** 1230–1237 (1995).

63. Tanimoto, K., Makino, Y., Pereira, T. & Poellinger, L. Mechanism of regulation of the hypoxia-inducible factor-1$α$ by the von Hippel-Lindau tumor suppressor protein. *EMBO J.* **19,** 4298–4309 (2000).

64. Wang, G. L., Jiang, B.-H., Rue, E. A. & Semenza, G. L. Hypoxia-inducible factor 1 is a basic-helix-loop-helix-PAS heterodimer regulated by cellular O2 tension. *Proc. Natl.*

Acad. Sci. **92,** 5510–5514 (1995).

65. Berra, E. *et al.* HIF prolyl-hydroxylase 2 is the key oxygen sensor setting low steady-state levels of HIF-1$α$ in normoxia. *EMBO J.* **22,** 4082–4090 (2003).

66. Chan, D. A., Sutphin, P. D., Yen, S.-E. & Giaccia, A. J. Coordinate regulation of the oxygen-dependent degradation domains of hypoxia-inducible factor 1$α$. *Mol. Cell. Biol.* **25,** 6415–6426 (2005).

67. Ivan, M. *et al.* Biochemical purification and pharmacological inhibition of a mammalian prolyl hydroxylase acting on hypoxia-inducible factor. *Proc. Natl. Acad. Sci.* **99,** 13459–13464 (2002).

68. Bruick, R. K. & McKnight, S. L. A conserved family of prolyl-4-hydroxylases that modify HIF. *Science (80-.).* **294,** 1337–1340 (2001).

69. Semenza, G. L. Hypoxia-inducible factor 1 (HIF-1) pathway. *Sci. Stke* **2007,** cm8--cm8 (2007).

70. Jaakkola, P. *et al.* Targeting of HIF-$α$ to the von Hippel-Lindau ubiquitylation complex by O2-regulated prolyl hydroxylation. *Science (80-.).* **292,** 468–472 (2001).

71. Yu, F., White, S. B., Zhao, Q. & Lee, F. S. HIF-1$α$ binding to VHL is regulated by stimulus-sensitive proline hydroxylation. *Proc. Natl. Acad. Sci.* **98,** 9630–9635 (2001).

72. Ivan, M. *et al.* HIF$α$ targeted for VHL-mediated destruction by proline hydroxylation: implications for O2 sensing. *Science (80-.).* **292,** 464–468 (2001).

73. Richard, S., Gardie, B., Couvé, S. & Gad, S. Von Hippel--Lindau: how a rare disease illuminates cancer biology. in *Seminars in cancer biology* **23,** 26–37 (2013).

74. Herman, J. G. *et al.* Silencing of the VHL tumor-suppressor gene by DNA methylation in renal carcinoma. *Proc. Natl. Acad. Sci.* **91,** 9700–9704 (1994).

75. Kim, W. Y. & Kaelin, W. G. Role of VHL gene mutation in human cancer. *J. Clin. Oncol.* **22,** 4991–5004 (2004).

76. Banks, R. E. *et al.* Genetic and epigenetic analysis of von Hippel-Lindau (VHL) gene alterations and relationship with clinical variables in sporadic renal cancer. *Cancer Res.* **66,** 2000–2011 (2006).

77. Reuter, V. E. & Tickoo, S. K. Differential diagnosis of renal tumours with clear cell histology. *Pathology* **42,** 374–383 (2010).

78. Hakimi, A. A. *et al.* An integrated metabolic atlas of clear cell renal cell carcinoma. *Cancer Cell* **29,** 104–116 (2016).

79. Lee, C.-H. *et al.* Bevacizumab monotherapy as salvage therapy for advanced clear cell renal cell carcinoma pretreated with targeted drugs. *Clin. Genitourin. Cancer* **14,** 56–62 (2016).

80. Dis., W. K. J.-A. R. P. M. & 2007, undefined. Von hippel-lindau disease. *annualreviews.org*

81. Kapitsinou, P. P. & Haase, V. H. The VHL tumor suppressor and HIF: insights from genetic studies in mice. *Cell Death Differ.* **15,** 650 (2008).

82. Wei, E. Y. & Hsieh, J. J. A river model to map convergent cancer evolution and guide therapy in RCC. *Nat. Rev. Urol.* **12,** 706 (2015).

83. Creighton, C. J. *et al.* Comprehensive molecular characterization of clear cell renal cell carcinoma. *Nature* **499,** 43–49 (2013).

84. Escudier, B., Szczylik, C., Porta, C. & Gore, M. Treatment selection in metastatic renal cell carcinoma: expert consensus. *Nat. Rev. Clin. Oncol.* **9,** 327–337 (2012).

85. Sosman, J. & Puzanov, I. Combination Targeted Therapy in Advanced Renal Cell

Carcinoma *. (2009). doi:10.1002/cncr.24234

86. Alsaab, H. *et al.* No TitlePD-1 and PD-L1 Checkpoint Signaling Inhibition for Cancer Immunotherapy: Mechanism, Combinations, and Clinical Outcome. *Front. Pharmacol* (2017). doi:https://doi.org/10.3389/fphar.2017.00561

87. Tsui, K. *et al.* Is adrenalectomy a necessary component of radical nephrectomy? UCLA experience with 511 radical nephrectomies. *J. Urol.* **163,** 437–441 (2000).

88. Sandock, D. S., Seftel, A. D. & Resnick, M. I. Adrenal metastases from renal cell carcinoma: role of ipsilateral adrenalectomy and definition of stage. *Urology* **49,** 28–31 (1997).

89. Berdjis, N. *et al.* Impact of resection margin status after nephron-sparing surgery for renal cell carcinoma. *BJU Int.* **97,** 1208–1210 (2006).

90. Simcsek, A. *et al.* Impact of preoperative radiological and postoperative pathological findings on survival of patients after radical nephrectomy performed with the indication of renal cell carcinoma. *Turkish J. Urol.* **41,** 1 (2015).

91. Patel, P. H., Chaganti, R. S. K. & Motzer, R. J. Targeted therapy for metastatic renal cell carcinoma. *Br. J. Cancer* **94,** 614 (2006).

92. Stephenson, A. J. *et al.* Guidelines for the surveillance of localized renal cell carcinoma based on the patterns of relapse after nephrectomy. *J. Urol.* **172,** 58–62 (2004).

93. Gofrit, O. N. *et al.* Renal Cell Carcinoma: Evaluation of the 1997 TNM System and Recommendations for Follow--Up after Surgery. *Eur. Urol.* **39,** 669–675 (2001).

94. Ficarra, V. *et al.* The ‘Stage, Size, Grade and Necrosis’ score is more accurate than the University of California Los Angeles Integrated Staging System for predicting cancer-specific survival in patients with clear cell renal cell carcinoma. *BJU Int.* **103,** 165–170

(2009).

95. Motzer, R. J., Bacik, J. & Mazumdar, M. Prognostic factors for survival of patients with stage IV renal cell carcinoma: Memorial Sloan-Kettering Cancer Center experience. *Clin. Cancer Res.* **10,** 6302S--6303S (2004).

96. Minguet, J., Smith, K. H., Bramlage, C. P. & Bramlage, P. Targeted therapies for treatment of renal cell carcinoma: Recent advances and future perspectives. *Cancer Chemotherapy and Pharmacology* **76,** 219–233 (2015).

97. Amato, R. J. Chemotherapy for renal cell carcinoma. *Semin.Oncol.* **27,** 177–186 (2000).

98. Bukowski, R. M. *et al.* Interferon-$γ$ and CXC chemokine induction by interleukin 12 in renal cell carcinoma. *Clin. cancer Res.* **5,** 2780–2789 (1999).

99. Bukowski, R. M. Cytokine therapy for metastatic renal cell carcinoma. in *Seminars in urologic oncology* **19,** 148–154 (2001).

100. Rosenberg, S. A. *et al.* A progress report on the treatment of 157 patients with advanced cancer using lymphokine-activated killer cells and interleukin-2 or high-dose interleukin-2 alone. *N. Engl. J. Med.* **316,** 889–897 (1987).

101. Motzer, R. J. *et al.* Overall survival and updated results for sunitinib compared with interferon alfa in patients with metastatic renal cell carcinoma. *J. Clin. Oncol.* **27,** 3584 (2009).

102. Rini, B. I. & Atkins, M. B. Resistance to targeted therapy in renal-cell carcinoma. *The Lancet Oncology* **10,** 992–1000 (2009).

103. Juengel, E. *et al.* Sulforaphane inhibits proliferation and invasive activity of everolimus-resistant kidney cancer cells in vitro. **7,** 85208–85219 (2016).

104. Mandriota, S. J. *et al.* HIF activation identifies early lesions in VHL kidneys: evidence for

site-specific tumor suppressor function in the nephron. *Cancer Cell* **1,** 459–468 (2002).

105. Iliopoulos, O. & Kaelin Jr, W. G. The molecular basis of von Hippel-Lindau disease. *Mol. Med.* **3,** 289 (1997).

106. Maranchie, J. K. *et al.* The contribution of VHL substrate binding and HIF1-$α$ to the phenotype of VHL loss in renal cell carcinoma. *Cancer Cell* **1,** 247–255 (2002).

107. Gnarra, J. R. *et al.* Post-transcriptional regulation of vascular endothelial growth factor mRNA by the product of the VHL tumor suppressor gene. *Proc. Natl. Acad. Sci.* **93,** 10589–10594 (1996).

108. Escudier, B. *et al.* Sorafenib in advanced clear-cell renal-cell carcinoma. *N. Engl. J. Med.* **356,** 125–134 (2007).

109. Trump, D. L. Randomized phase II study of multiple dose levels of CCI-779, a novel mammalian target of rapamycin kinase inhibitor, in patients with advanced refractory renal cell carcinoma. Atkins MB, Hidalgo M, Stadler WM, Logan TF, Dutcher JP, Hudes GR, Park Y, Liou SH, Marshall B, Boni JP, Dukart G, Sherman ML, Department of Medicine, Division of Hematology/Oncology, Beth Israel Deaconess Medical Center, Boston, MA.: J Clin Oncol 2004; 22: 909--18. in *Urologic Oncology: Seminars and Original Investigations* **22,** 431–432 (2004).

110. Heng, D. Y. C. *et al.* A population-based study evaluating the impact of sunitinib on overall survival in the treatment of patients with metastatic renal cell cancer. *Cancer* **115,** 776–783 (2009).

111. Oosterwijk-Wakka, J. C. *et al.* Effect of tyrosine kinase inhibitor treatment of renal cell carcinoma on the accumulation of carbonic anhydrase IX-specific chimeric monoclonal antibody cG250. *BJU Int.* **107,** 118–125 (2011).

112. Bellmunt, J. *et al.* Sequential Targeted Therapy After Pazopanib Therapy in Patients With Metastatic Renal Cell Cancer : Ef fi cacy and Toxicity. *Clin. Genitourin. Cancer* **12,** 262–269 (2014).

113. Calvo, E., Schmidinger, M., Heng, D. Y. C., Grünwald, V. & Escudier, B. Improvement in survival end points of patients with metastatic renal cell carcinoma through sequential targeted therapy. *Cancer Treat. Rev.* **50,** 109–117 (2016).

114. Motzer, R. J. *et al.* Efficacy of everolimus in advanced renal cell carcinoma: a double-blind, randomised, placebo-controlled phase III trial. *Lancet* **372,** 449–56 (2008).

115. Ishibashi, K. *et al.* Overriding TKI resistance of renal cell carcinoma by combination therapy with IL-6 receptor blockade. *Oncotarget* **8,** 55230 (2017).

116. Roulin, D. *et al.* Targeting renal cell carcinoma with NVP-BEZ235 , a dual PI3K / mTOR inhibitor , in combination with sorafenib. *Mol. Cancer* **10,** 90 (2011).

117. Alsaab, H., Sau, S. & Alzhrani, R. PD-1 and PD-L1 Checkpoint Signaling Inhibition for Cancer Immunotherapy: Mechanism, Combinations, and Clinical Outcome. *Front.* (2017).

118. Llovet, J. M. *et al.* Sorafenib in advanced hepatocellular carcinoma. *N. Engl. J. Med.* **359,** 378–390 (2008).

119. Cheng, A.-L. *et al.* Efficacy and safety of sorafenib in patients in the Asia-Pacific region with advanced hepatocellular carcinoma: a phase III randomised, double-blind, placebo-controlled trial. *Lancet Oncol.* **10,** 25–34 (2009).

120. Motzer, R. J. *et al.* Sunitinib versus interferon alfa in metastatic renal-cell carcinoma. *N. Engl. J. Med.* **356,** 115–124 (2007).

121. Pavía-Jiménez, A., Tcheuyap, V. T. & Brugarolas, J. Establishing a human renal cell carcinoma tumorgraft platform for preclinical drug testing. *Nat. Protoc.* **9,** 1848–59

(2014).

122. Mcdonald, P. C. & Dedhar, S. Carbonic Anhydrase IX (CAIX) as a Mediator of Hypoxia-Induced Stress Response in Cancer Cells. 255–269 (2014). doi:10.1007/978-94-007-7359-2

123. Waheed, A. *et al.* Carbonic anhydrase inhibitor suppresses invasion of renal cancer cells in vitro. (2000).

124. Jiang, Y. D., Ren, F. & Zheng, S. B. Value of MN/CAIX in the diagnosis of renal cell carcinoma. *Nan fang yi ke da xue xue bao= J. South. Med. Univ.* **32,** 412–414 (2012).

125. López, C. M. *et al.* Prognostic factors in patients with advanced renal cell carcinoma. *Clin. Genitourin. Cancer* **10,** 262–270 (2012).

126. Liao, S.-Y., Aurelio, O. N., Jan, K., Zavada, J. & Stanbridge, E. J. Identification of the MN/CA9 protein as a reliable diagnostic biomarker of clear cell carcinoma of the kidney. *Cancer Res.* **57,** 2827–2831 (1997).

127. Peña, C., Lathia, C., Shan, M., Escudier, B. & Bukowski, R. M. Biomarkers predicting outcome in patients with advanced renal cell carcinoma: results from sorafenib phase III TARGET. *Clin. cancer Res.* clincanres--3343 (2010).

128. Choueiri, T. K. *et al.* Carbonic anhydrase IX as a potential biomarker of efficacy in metastatic clear-cell renal cell carcinoma patients receiving sorafenib or placebo: analysis from the treatment approaches in renal cancer global evaluation trial (TARGET). in *Urologic Oncology: Seminars and Original Investigations* **31,** 1788–1793 (2013).

129. Choueiri, T. K. *et al.* Carbonic anhydrase IX and pathological features as predictors of outcome in patients with metastatic clear-cell renal cell carcinoma receiving vascular endothelial growth factor-targeted therapy. *BJU Int.* **106,** 772–778 (2010).

130. Minn, I. *et al.* [Cu] XYIMSR-06 : A dual-motif CAIX ligand for PET imaging of clear cell renal cell carcinoma. **7,** (2016).

131. Muselaers, C. H. J. *et al.* Anhydrase IX Monoclonal Antibody Girentuximab. 1035–1041 doi:10.2967/jnumed.114.137356

132. McDonald, P. C., Winum, J.-Y., Supuran, C. T. & Dedhar, S. Recent developments in targeting carbonic anhydrase IX for cancer therapeutics. *Oncotarget* **3,** 84–97 (2012).

133. Krall, N., Pretto, F., Mattarella, M. & Neri, D. Tc-Labeled Ligand of Carbonic Anhydrase IX Selectively Targets Renal Cell Carcinoma In Vivo. 943–950 doi:10.2967/jnumed.115.170514

134. Manuscript, A. *NIH Public Access*. **2012,** (2015).

135. Brouwers, A. H. Carbonic Anhydrase IX Expression in Clear Cell Renal Cell Carcinoma and Normal Tissues : Experiences From (Radio) Immunotherapy Carbonic Anhydrase IX Expression in Clear Cell Renal Cell Carcinomas Negatively Correlates With the Proportion of the Granular Cell Component. **26,** 3808–3809 (2017).

136. Svastova, E. *et al.* Carbonic anhydrase IX interacts with bicarbonate transporters in lamellipodia and increases cell migration via its catalytic domain. *J. Biol. Chem.* **287,** 3392–3402 (2012).

137. Rishi, A. K. *et al.* Cell cycle- and apoptosis-regulatory protein-1 is involved in apoptosis signaling by epidermal growth factor receptor. *J. Biol. Chem.* **281,** 13188–13198 (2006).

138. Rishi, A. K. *et al.* Identification and characterization of a cell cycle and apoptosis regulatory protein-1 as a novel mediator of apoptosis signaling by retinoid CD437. *J. Biol. Chem.* **278,** 33422–33435 (2003).

139. Puliyappadamba, V. T. *et al.* Antagonists of Anaphase-promoting Complex (APC)-2-Cell

Cycle and Apoptosis Regulatory Protein (CARP)-1 interaction are novel regulators of cell growth and apoptosis. *J. Biol. Chem.* **286,** 38000–38017 (2011).

140. Muthu, M., Cheriyan, V. T. & Rishi, A. K. CARP-1/CCAR1: a biphasic regulator of cancer cell growth and apoptosis. *Oncotarget* **6,** 6499–510 (2015).

141. Kim, J. H. *et al.* CCAR1, a Key Regulator of Mediator Complex Recruitment to Nuclear Receptor Transcription Complexes. *Mol. Cell* **31,** 510–519 (2008).

142. Ou, C.-Y., Chen, T.-C., Lee, J. V, Wang, J.-C. & Stallcup, M. R. Coregulator CCAR1 Positively Regulates Adipocyte Differentiation through the Glucocorticoid Signaling Pathway. *J. Biol. Chem.* **In press,** (2014).

143. Lehman, N. L. *et al.* Oncogenic Regulators and Substrates of the Anaphase Promoting Complex/Cyclosome Are Frequently Overexpressed in Malignant Tumors. *Am. J. Pathol.* **170,** 1793–805 (2007).

144. Peters, J. M. The anaphase-promoting complex: Proteolysis in mitosis and beyond. *Molecular Cell* **9,** 931–943 (2002).

145. Ashour, A. E. *et al.* CARP-1 Functional Mimetics: A Novel Class of Small Molecule Inhibitors of Medulloblastoma Cell Growth. *PLoS One* **8,** (2013).

146. Krusch, M. *et al.* The Kinase Inhibitors Sunitinib and Sorafenib Differentially Affect NK Cell Antitumor Reactivity In Vitro. (2017). doi:10.4049/jimmunol.0902404

147. Ángel, J., Ángel, M., González-larriba, J. L., León, L. & Pablo, J. Sorafenib in renal cell carcinoma. **80,** 314–322 (2011).

148. Beljanski, V., Knaak, C., Zhuang, Y. & Smith, C. D. Combined anticancer effects of sphingosine kinase inhibitors and sorafenib. **2,** 1132–1142 (2011).

149. 02-03-2017 combination study.

150. Kidney Cancer: Latest Research | Cancer.Net. Available at: http://www.cancer.net/cancer-types/kidney-cancer/latest-research. (Accessed: 13th April 2016)

151. Fox, M. E., Szoka, F. C. & Fr??chet, J. M. J. Soluble polymer carriers for the treatment of cancer: The importance of molecular architecture. *Acc. Chem. Res.* **42,** 1141–1151 (2009).

152. Mayol, L. *et al.* Amphiphilic hyaluronic acid derivatives toward the design of micelles for the sustained delivery of hydrophobic drugs. *Carbohydr. Polym.* **102,** 110–116 (2014).

153. Iyer, A. K., Khaled, G., Fang, J. & Maeda, H. Exploiting the enhanced permeability and retention effect for tumor targeting. *Drug Discov. Today* **11,** 812–818 (2006).

154. Greish, K. Enhanced permeability and retention effect for selective targeting of anticancer nanomedicine: are we there yet? *Drug Discov. Today Technol.* **9,** e161–e166 (2012).

155. Iyer, A. K. *et al.* Polymeric micelles of zinc protoporphyrin for tumor targeted delivery based on EPR effect and singlet oxygen generation. *J. Drug Target.* **15,** 496–506 (2007).

156. Matsumura, Y. & Maeda, H. A New Concept for Macromolecular Therapeutics in Cancer Chemotherapy: Mechanism of Tumoritropic Accumulation of Proteins and the Antitumor Agent Smancs. *Cancer Res.* **46,** 6387–6392 (1986).

157. Cheriyan, V. T. *et al.* A CARP-1 functional mimetic loaded vitamin E-TPGS micellar nano-formulation for inhibition of renal cell carcinoma. (2017).

158. Jamal, S. *et al.* CARP-1 functional mimetics are a novel class of small molecule inhibitors of malignant pleural mesothelioma cells. *PLoS One* **9,** 1–14 (2014).

159. Cheriyan, V. T. *et al.* CARP-1 functional mimetics are novel inhibitors of drug-resistant triple negative breast cancers. *Oncotarget* **2,** (2016).

160. Muthu, M. *et al.* Identification and Testing of Novel CARP-1 Functional Mimetic Compounds as Inhibitors of Non-Small Cell Lung and Triple Negative Breast Cancers. *J.*

Biomed. Nanotechnol. **11,** 1608–1627 (2015).

161. Kesharwani, P., Banerjee, S., Padhye, S., Sarkar, F. H. & Iyer, A. K. Parenterally administrable nano-micelles of 3, 4-difluorobenzylidene curcumin for treating pancreatic cancers. *Colloids Surfaces B Biointerfaces* **132,** 138–45 (2015).

162. Kesharwani, P., Banerjee, S., Padhye, S., Sarkar, F. H. & Iyer, A. K. Hyaluronic Acid Engineered Nanomicelles Loaded with 3,4-Difluorobenzylidene Curcumin for Targeted Killing of CD44+ Stem-Like Pancreatic Cancer Cells. *Biomacromolecules* **16,** 3042–3053 (2015).

163. Lv, P. C., Roy, J., Putt, K. S. & Low, P. S. Evaluation of a Carbonic Anhydrase IX-Targeted Near-Infrared Dye for Fluorescence-Guided Surgery of Hypoxic Tumors. *Mol. Pharm.* **13,** 1618–1625 (2016).

164. Brouwers, A. H. Carbonic Anhydrase IX Expression in Clear Cell Renal Cell Carcinoma and Normal Tissues : Experiences From (Radio) Immunotherapy Carbonic Anhydrase IX Expression in Clear Cell Renal Cell Carcinomas Negatively Correlates With the Proportion of the Granula. **26,** 3808–3809 (2017).

165. Pavlovich, C. P. & Schmidt, L. S. Searching for the hereditary causes of renal-cell carcinoma. *Nat. Rev. Cancer* **4,** 381 (2004).

166. Voss, M. H., Molina, A. M. & Motzer, R. J. mTOR inhibitors in advanced renal cell carcinoma. *Hematol. Oncol. Clin. North Am.* **25,** 835–852 (2011).

167. Harper, J. W., Burton, J. L. & Solomon, M. J. The anaphase-promoting complex: it's not just for mitosis any more. *Genes Dev.* **16,** 2179–2206 (2002).

168. Ashour, A. E. *et al.* CARP-1 functional mimetics: a novel class of small molecule inhibitors of medulloblastoma cell growth. *PLoS One* **8,** e66733 (2013).

169. Cheriyan, V. T., Muthu, M., Patel, K., Sekhar, S. & Rishi, A. K. CARP-1 functional mimetics are novel inhibitors of drug-resistant triple negative breast cancers. **7,**

170. Yang, Y. *et al.* A novel fumarate hydratase-deficient HLRCC kidney cancer cell line, UOK268: A model of the Warburg effect in cancer. *Cancer Genet.* **205,** 377–390 (2012).

171. Neuzillet, C. *et al.* State of the art and future directions of pancreatic ductal adenocarcinoma therapy. *Pharmacol. Ther.* (2015). doi:10.1016/j.pharmthera.2015.08.006

172. Zhang, Z., Tan, S. & Feng, S. S. Vitamin E TPGS as a molecular biomaterial for drug delivery. *Biomaterials* **33,** 4889–4906 (2012).

173. Wang, Y. *et al.* Enhanced tumor delivery of gemcitabine via PEG-DSPE/TPGS mixed micelles. *Mol. Pharm.* **11,** 1140–1150 (2014).

174. Duhem, N., Danhier, F. & Préat, V. Vitamin E-based nanomedicines for anti-cancer drug delivery. *J. Control. Release* **182,** 33–44 (2014).

175. Neophytou, C. M. & Constantinou, A. I. Drug Delivery Innovations for Enhancing the Anticancer Potential of Vitamin E Isoforms and Their Derivatives. *Biomed Res. Int.* **2015,** 1–16 (2015).

176. Seymour, L. W. *et al.* A novel dosage approach for evaluation of SMANCS [poly-(styrene-co-maleyl-half-n-butylate) - neocarzinostatin] in the treatment of primary hepatocellular carcinoma. *Int. J. Oncol.* **12,** 1217–23 (1998).

177. Maeda, H. SMANCS and polymer-conjugated macromolecular drugs: Advantages in cancer chemotherapy. *Adv. Drug Deliv. Rev.* **46,** 169–185 (2001).

178. Maeda, H., Sawa, T. & Konno, T. Mechanism of tumor-targeted delivery of macromolecular drugs, including the EPR effect in solid tumor and clinical overview of the prototype polymeric drug SMANCS. *J. Control. Release* **74,** 47–61 (2001).

179. Dabholkar, R. D., Sawant, R. M., Mongayt, D. A., Devarajan, P. V. & Torchilin, V. P. Polyethylene glycol–phosphatidylethanolamine conjugate (PEG–PE)-based mixed micelles: Some properties, loading with paclitaxel, and modulation of P-glycoprotein-mediated efflux. *Int. J. Pharm.* **315,** 148–157 (2006).

180. Zhang, Z. & Feng, S. Nanoparticles of poly (lactide)/ vitamin E TPGS copolymer for cancer chemotherapy : Synthesis , formulation , characterization and in vitro drug release. **27,** 262–270 (2006).

181. Amjad, M. W., Kesharwani, P., Amin, M. C. I. M. & Iyer, A. K. Recent advances in the design, development, and targeting mechanisms of polymeric micelles for delivery of siRNA in cancer therapy. *Prog. Polym. Sci.* **64,** 154–181 (2017).

182. Iyer, A. K., Greish, K., Fang, J., Murakami, R. & Maeda, H. High-loading nanosized micelles of copoly(styrene-maleic acid)-zinc protoporphyrin for targeted delivery of a potent heme oxygenase inhibitor. *Biomaterials* **28,** 1871–81 (2007).

183. Amjad, M. W. *et al. In Vivo* Antitumor Activity of Folate-Conjugated Cholic Acid-Polyethylenimine Micelles for the Codelivery of Doxorubicin and siRNA to Colorectal Adenocarcinomas. *Mol. Pharm.* **12,** 4247–4258 (2015).

184. Kesharwani, P., Banerjee, S., Padhye, S., Sarkar, F. H. & Iyer, A. K. Parenterally administrable nano-micelles of 3,4-difluorobenzylidene curcumin for treating pancreatic cancer. *Colloids Surfaces B Biointerfaces* **132,** 138–145 (2015).

185. Luong, D. *et al.* Folic acid conjugated polymeric micelles loaded with a curcumin difluorinated analog for targeting cervical and ovarian cancers. *Colloids Surfaces B Biointerfaces* **157,** 490–502 (2017).

186. Iyer, A. K., Greish, K., Fang, J., Murakami, R. & Maeda, H. High-loading nanosized

micelles of copoly(styrene-maleic acid)-zinc protoporphyrin for targeted delivery of a potent heme oxygenase inhibitor. *Biomaterials* **28,** 1871–1881 (2007).

187. Daruwalla, J. *et al.* Evaluation of the effect of SMA-pirarubicin micelles on colorectal cancer liver metastases and of hyperbaric oxygen in CBA mice. *J. Drug Target.* **15,** 487–95

188. Harmonisation, I. C. on. Ich Harmonised Tripartite Guideline Validation of Analytical Procedures : *ICH Harmon. Tripart. Guidel. Valid. Anal. Proced. TEXT Methodol. Q2(R1) step4* (2005). doi:10.1017/CBO9781107415324.004

189. Wu, Y. *et al.* D-α-tocopherol polyethylene glycol succinate-based derivative nanoparticles as a novel carrier for paclitaxel delivery. *Int. J. Nanomedicine* **10,** 5219–35 (2015).

190. Maeda, H., Wu, J., Sawa, T., Matsumura, Y. & Hori, K. Tumor vascular permeability and the EPR effect in macromolecular therapeutics: a review. *J. Control. Release* **65,** 271–84 (2000).

191. Greish, K., Sawa, T., Fang, J., Akaike, T. & Maeda, H. SMA-doxorubicin, a new polymeric micellar drug for effective targeting to solid tumours. *J. Control. Release* **97,** 219–30 (2004).

192. Khadka, P. *et al.* Pharmaceutical particle technologies: An approach to improve drug solubility, dissolution and bioavailability. *Asian J. Pharm. Sci.* **9,** 304–316 (2014).

193. Sau, S. *et al.* Multifunctional nanoparticles for cancer immunotherapy: A groundbreaking approach for reprogramming malfunctioned tumor environment. *J. Control. Release* (2018).

194. Fröhlich, E. The role of surface charge in cellular uptake and cytotoxicity of medical nanoparticles. *Int. J. Nanomedicine* **7,** 5577–91 (2012).

195. Muthu, M. S., Kutty, R. V., Luo, Z., Xie, J. & Feng, S. S. Theranostic vitamin E TPGS micelles of transferrin conjugation for targeted co-delivery of docetaxel and ultra bright gold nanoclusters. *Biomaterials* **39,** 234–248 (2015).

196. Lin, C. *et al.* Pulmonary delivery of triptolide- loaded liposomes decorated with anti-carbonic anhydrase IX antibody for lung cancer therapy. *Sci. Rep.* 1–12 (2017). doi:10.1038/s41598-017-00957-4

197. Xu, Y. *et al.* Preparation of intravenous injection nanoformulation of VESylated gemcitabine by co-assembly with TPGS and its anti-tumor activity in pancreatic tumor-bearing mice. *Int. J. Pharm.* **495,** 792–797 (2015).

198. Feng, S. S. *et al.* Chemotherapeutic engineering: Vitamin E TPGS-emulsified nanoparticles of biodegradable polymers realized sustainable paclitaxel chemotherapy for 168 h in vivo. *Chem. Eng. Sci.* **62,** 6641–6648 (2007).

199. Maeda, H. Macromolecular therapeutics in cancer treatment: The EPR effect and beyond. *Journal of Controlled Release* **164,** 138–144 (2012).

200. Cairns, P. Renal cell carcinoma. *Cancer Biomarkers* **9,** 461–473 (2011).

201. Guo, H. *et al.* The PI3K/AKT Pathway and Renal Cell Carcinoma. *Journal of Genetics and Genomics* **42,** 343–353 (2015).

202. Strese, S., Fryknäs, M., Larsson, R. & Gullbo, J. Effects of hypoxia on human cancer cell line chemosensitivity. *BMC Cancer* **13,** 331 (2013).

203. Smaldone, M. C. & Maranchie, J. K. Clinical implications of hypoxia inducible factor in renal cell carcinoma. *Urol. Oncol.* **27,** 238–245 (2009).

204. Zarrabi, K., Fang, C. & Wu, S. New treatment options for metastatic renal cell carcinoma with prior anti-angiogenesis therapy. *J. Hematol. Oncol.* **10,** 38 (2017).

205. Hillen, F. & Griffioen, A. W. Tumour vascularization: Sprouting angiogenesis and beyond. *Cancer and Metastasis Reviews* **26,** 489–502 (2007).

206. Bhise, K. *et al.* Nanomedicine for cancer diagnosis and therapy: advancement, success and structure--activity relationship. *Ther. Deliv.* **8,** 1003–1018 (2017).

207. Wickens, J. M. *et al.* Recent advances in hyaluronic acid-decorated nanocarriers for targeted cancer therapy. *Drug Discov. Today* (2016).

208. Sau, S., Alsaab, H. O., Kashaw, S. K., Tatiparti, K. & Iyer, A. K. Advances in antibody--drug conjugates: a new era of targeted cancer therapy. *Drug Discov. Today* (2017).

209. Alsaab, H. *et al.* Folate Decorated Nanomicelles Loaded with a Potent Curcumin Analogue for Targeting Retinoblastoma. *Pharmaceutics* **9,** 15 (2017).

210. Escudier, B. *et al.* Sorafenib in Advanced Clear-Cell Renal-Cell Carcinoma. *N. Engl. J. Med.* **356,** 125–134 (2007).

211. Zhang, L. *et al.* Resistance of renal cell carcinoma to sorafenib is mediated by potentially reversible gene expression. *PLoS One* **6,** (2011).

212. Kawakami, K. *et al.* 356 SECRETED FRIZZLED-RELATED PROTEIN-5 (SFRP-5) IS EPIGENETICALLY DOWNREGULATED AND FUNCTIONS AS A TUMOR SUPPRESSOR IN RENAL CELL CANCER. *J. Urol.* **183,** e141 (2010).

213. Yang, Y. *et al.* Metabolic Reprogramming for Producing Energy and Reducing Power in Fumarate Hydratase Null Cells from Hereditary Leiomyomatosis Renal Cell Carcinoma. *PLoS One* **8,** (2013).

214. Almansour, A. I. *et al.* Design, synthesis and antiproliferative activity of decarbonyl luotonin analogues. *Eur. J. Med. Chem.* **138,** 932–941 (2017).

215. Anjibabu, R., Sau, S., Reddy, B. J. M., Banerjee, R. & Reddy, B. V. S. Heteropoly acid

catalyzed synthesis of 8-methyl-2-aryl/alkyl-3- oxabicyclo[3.3.1]non-7-ene derivatives through (3,5)-oxonium-ene reaction. *Tetrahedron Lett.* **54,** 7160–7163 (2013).

216. Zhang, N. *et al.* Cobalt Chloride-induced Hypoxia Induces Epithelial-mesenchymal Transition in Renal Carcinoma Cell Lines. *Ann. Clin. Lab. Sci.* **47,** 40–46 (2017).

217. Shih, J.-W. *et al.* Long noncoding RNA LncHIFCAR/MIR31HG is a HIF-1$α$ co-activator driving oral cancer progression. *Nat. Commun.* **8,** 15874 (2017).

218. Dal Corso, A. & Neri, D. Linker stability influences the anti-tumor activity of acetazolamide-drug conjugates for the therapy of renal cell carcinoma. *J. Control. Release* **246,** 39–45 (2017).

219. Gawde, K. A. *et al.* Synthesis and characterization of folate decorated albumin bio-conjugate nanoparticles loaded with a synthetic curcumin difluorinated analogue. *J. Colloid Interface Sci.* **496,** 290–299 (2017).

220. Sau, S., Mondal, S. K., Kashaw, S. K., Iyer, A. K. & Banerjee, R. Combination of cationic dexamethasone derivative and STAT3 inhibitor (WP1066) for aggressive melanoma: a strategy for repurposing a phase I clinical trial drug. *Mol. Cell. Biochem.* 1–18 (2017).

221. Sahu, P., Kashaw, S. K., Jain, S., Sau, S. & Iyer, A. K. Assessment of penetration potential of pH responsive double walled biodegradable nanogels coated with eucalyptus oil for the controlled delivery of 5-fluorouracil: In vitro and ex vivo studies. *J. Control. Release* **253,** 122–136 (2017).

222. Shibata, T. *et al.* Transthiocarbamoylation of Proteins by Thiolated. (2011). doi:10.1074/jbc.M111.308049

223. Hoogstins, C. E. S. *et al.* A novel tumor-specific agent for intraoperative near-infrared fluorescence imaging: A translational study in healthy volunteers and patients with

ovarian cancer. *Clin. Cancer Res.* **22,** 2929–2938 (2016).

224. Pastorekova, S. Carbonic anhydrase IX is a clinically significant tissue and serum biomarker associated with renal cell carcinoma. *Oncol. Lett.* (2012). doi:10.3892/ol.2012.1001

225. Bao, B. *et al.* In vivo imaging and quantification of carbonic anhydrase IX expression as an endogenous biomarker of tumor hypoxia. *PLoS One* **7,** e50860 (2012).

226. Soyupak, B. *et al.* CA9 expression as a prognostic factor in renal clear cell carcinoma. *Urol. Int.* **74,** 68–73 (2005).

227. Uemura, H. *et al.* A phase I trial of vaccination of CA9-derived peptides for HLA-A24-positive patients with cytokine-refractory metastatic renal cell carcinoma. *Clin. cancer Res.* **12,** 1768–1775 (2006).

228. Hsieh, J. J. *et al.* Overcome tumor heterogeneity-imposed therapeutic barriers through convergent genomic biomarker discovery: a braided cancer river model of kidney cancer. in *Seminars in cell & developmental biology* **64,** 98–106 (2017).

229. Molina, A. M. *et al.* Phase 1 trial of everolimus plus sunitinib in patients with metastatic renal cell carcinoma. *Cancer* **118,** 1868–1876 (2012).

230. Hsieh, J. J. & Cheng, E. H. A braided cancer river connects tumor heterogeneity and precision medicine. *Clin. Transl. Med.* **5,** 42 (2016).

231. Zajac, E. *et al.* Angiogenic capacity of M1- and M2-polarized macrophages is determined by the levels of TIMP-1 complexed with their secreted proMMP-9. *Blood* **122,** 4054–4067 (2013).

232. Zhang, R. R. *et al.* Beyond the margins: real-time detection of cancer using targeted fluorophores. *Nat. Rev. Clin. Oncol.* **14,** 347–364 (2017).

ABSTRACT

TUMOR MULTICOMPONENT TARGETING POLYMER-LIPID HYBRID NANOPARTICLES TO OVERCOME DRUG RESISTANCE IN RENAL CELL CARCINOMA

by

HASHEM OBAID ALSAAB

August 2018

Advisor: Dr. Arun K. Iyer

Major: Pharmaceutical Sciences

Degree: Doctor of Philosophy

Renal Cell Carcinoma (RCC) contributes to more than 90% of the most common form of kidney tumor and remains one of the ten leading causes of cancer death in the United States. Although surgery remains an option for operable tumors, high metastatic index and resistance to radiation and chemotherapies prompted recent development of therapeutics that target the RCC angiogenesis and cell proliferation pathways. Eventually, new strategies with encouraging results have emerged that include immunotherapy, such as the programmed death-1 inhibitor (Nivolumab), cytokines, and a combination of chemo-immune therapy. Thus, developing alternative strategies with effective treatment options remains an urgent unmet need for therapy-resistant RCC. In this regard, combination treatment targeting different cancer survival pathway of tumor microenvironment can be advantageous. Along these lines, we have pursued different combination drug regimens, including inhibitors that target mTOR (everolimus) and RTK or VEGFR (cabozantinib or sorafenib), as possible treatment strategies. In addition, we explored the rational design of nanoparticles to selectively deliver a variety of therapeutic payloads to target hypoxic tumor microenvironment overexpressing carbonic anhydrase-IX (CA IX). Our strategy involved establishing a library of tumor penetrating nanocarriers carrying combination drug

payload of RTK-inhibitor with our own apoptosis inducer/CARP-1 protein functional mimetics (CFM-4.16). Nano-carriers were tailored to have varying composition and size that could: (i) efficiently reach the tumor core; (ii) target tumor multi-components including cancer epithelial cells and tumor-associated macrophages (TAM) for overcoming drug resistance in RCC. Specifically, the current work was focused on multimodal approaches, including (a) Optimization of hypoxia marker (CA IX) targeted polymer-lipid nano-formulation (PLNP) using copper-free 'click' chemistry; (b) In vitro and in vivo pre-clinical imaging and therapy of PLNP loaded with multiple drugs in inhibiting RCCs using mice bearing resistant RCCs and human cancer mimicking patient-derived xenografts (PDx). The results of antitumor efficacy and biodistribution of targeted PLNPs in animals bearing RCC xenograft and PDx models revealed selective accumulation of drugs at tumor sites resulting in greater tumor growth inhibition with reduced side effects. These findings portent promising therapeutic potentials for our newly developed hypoxia-targeted-PLNPs loaded with CFM-4.16 in combination with RTK-inhibitor for effective RCC therapy in the clinic.

AUTOBIOGRAPHICAL STATEMENT
HASHEM OBAID ALSAAB

EDUCATION

2015-2018 PhD, Pharmaceutical Sciences
Wayne State University, Detroit, MI,

2013-2015 MS, Pharmaceutical Sciences with Industrial Pharmacy option
University of Toledo, Toledo, OH

2004-2010 Doctor of Pharmacy Pharm.D. (Clinical Pharmacy)
King Abdul-Aziz University, Jeddah, KSA

AWARDS AND SCHOLARSHIPS

1- 2012- Saudi Arabian Cultural Mission (SACM) Scholarship to study Master's degree at the University of Toledo, Toledo OH, US.
2- 2014- SACM Travel Support to attend American Association of Pharmaceutical Scientists (AAPS) Meeting a in San Diego, CA, US.
3- 2015- Saudi Arabian Cultural Mission (SACM) Scholarship to study PhD degree at Wayne State University, Detroit MI, US.
4- 2017- SACM Travel Support to attend American Association of Pharmaceutical Scientists (AAPS) Meeting a in Denver, CO, US.
5- 2018- AAPS Travel award from Wayne State University to attend American Association of Cancer Research (AACR) Meeting in Chicago, IL, US.
6- 2018- A prestigious Frank O. Taylor Pharmacy Scholarship award. The scholarship was created to support students specializing in industrial pharmacy, and today is awarded to students in the pharmaceutical sciences. Eligibility – Students with an interest in pursuing a career in industrial pharmacy and who, in the opinion of the faculty, excel in both research productivity and didactic courses.

IMPORTANT PUBLICATIONS

1. Hashem O. Alsaab, et al. (2018). Tumor Hypoxia Directed Multimodal Nanotherapy for Overcoming Drug Resistance in Renal Cell Carcinoma and Reprogramming Macrophages. Biomaterials (under review).
2. Hashem O. Alsaab, et al. PD-1 and PD-L1 Checkpoint Signaling Inhibition for Cancer Immunotherapy: Mechanism, Combinations, and Clinical Outcome. *Frontiers in Pharmacology* 2017, 8:561.
3. Cheriyan, V. T.*, Alsaab, H. O.*, et al. (2017). A CARP-1 functional mimetic loaded vitamin E-TPGS micellar nano-formulation for inhibition of renal cell carcinoma. Oncotarget, 8(62), 104928. (* equal contribution).